UNIVERSITÀ POLITECNICA DELLE MARCHE

FACOLTÀ DI INGEGNERIA

Corso di Laurea magistrale in Biomedical Engineering

ELECTROCARDIOGRAPHIC ALTERNANS RELATED TO HEMODIALYSIS TREATMENT

Relatore:

Prof.ssa Laura Burattini

Tesi di Laurea di:

Chiara Leoni

Correlatore:

Dott.ssa Ilaria Marcantoni

A.A. **2019** / **2020**

ABSTRACT

Hemodialysis (HD) is a clinical procedure used to treat subjects suffering from chronic kidney failure, i.e. compromised renal function. Unluckily, HD patients are at a high risk of sudden cardiac death (SCD) due to the elevated incidence of arrhythmias and heart failure. Prevention of SCD is among the greatest concerns for public health, and indexes that can contribute to investigate SCD itself, based on the analysis of the electrocardiogram (ECG), have been introduced. One of the most popular indexes for the investigation of SCD is T-wave alternans (TWA), i.e. beat-to-beat fluctuations of the T wave in the ECG. TWA, however, represents only part of the total cardiac electrical activity: fluctuations related to the P wave, i.e. P-wave alternans (PWA), and to the QRS complex, i.e. QRS alternans (QRSA), should be investigated as well. As a consequence, a full coverage of the electrical activity of the heart was introduced in terms of ECG alternans (ECGA). ECGA was first defined as the prevalent nature of electrical alternans, i.e. PWA, QRSA or TWA. Nowadays, the interpretation of ECGA is changing: rather than being only regarded as the prevalent nature of alternans, ECGA should also be seen as an expression of PWA, QRSA and TWA. For these reasons, this thesis work aimed to validate an improved ECGA quantification method, based on the popular Heart-rate Adaptive Match filter (HRAMF), that should be able to measure PWA, QRSA and TWA devoid of reciprocal influence. Moreover, it aimed to investigate the effects that HD treatment may produce on ECGA, as well as understand if and how HD effectively increases SCD risk, and comprehend the relationship among PWA, QRSA and TWA. Previous studies performed on HD patients mainly focused on TWA only, and reported that TWA tends to increase before and during treatment, only to eventually decrease after HD. More recently, ECGA was also investigated on a single HD patient, although the quantification method applied could not guarantee that PWA, QRSA and TWA were computed in an independent manner. The new ECGA quantification method here proposed, instead, studied each type of alternans after making sure that all other ECG waves, that had to be excluded from the measurement, had been zeroed out. The method was applied on a continuous 24-hour Holter recording performed on a HD patient. The ECG recording was then divided into four macro-time periods (PRE-HD, before HD; IN-HD, during HD; POST-HD, after HD; NT-HD, night time after HD) to perform statistical comparisons. TWA showed increased amplitude values in PRE-HD (40 μV for lead V_5)

and IN-HD (38 μV for lead V_6), that corresponded to higher SCD risk periods, and started to decrease one hour after the end of the treatment. These findings, probably a direct consequence of treatment itself, were similar to previous literature results concerning TWA. PWA amplitude values, that were generally small, also decreased after treatment, reaching 0 μV. QRSA amplitude instead started to increase during IN-HD, where it reached amplitude values equal to 41 μV for lead aV_R, and was still high in POST-HD (54 μV for lead V_6). TWA was the prevalent alternans in several cases, especially in PRE-HD and NT-HD. As also QRSA showed the highest amplitude values in different leads during IN-HD and POST-HD, it was concluded that HD seems to majorly affect the ventricles of the heart. Amplitude values obtained in this study were much lower than those computed with previous methods, as the new method seemed to avoid overestimation produced by reciprocal alternans influences. Moreover, statistical differences (p<0.05) and weak correlation among all types of alternans and all time periods were found, proving that the new quantification method was indeed able to reliably and independently measure PWA, QRSA and TWA. Physiological influences not deriving from quantification, however, cannot be ruled out. It has been observed in literature, in fact, that changes happening at the level of one wave may produce changes on the other ECG waves. Moreover, QRSA and TWA may coexist, as both may derive from different electrolytes concentrations being simultaneously unbalanced.

TABLE OF CONTENTS

INTRODUCTION

Hemodialysis (HD) is a clinical procedure employed to treat patients affected by chronic kidney failure. Cases of chronic kidney failure have been increasing during the past few years, especially in western countries: in the United States only, 15% of adults (around 37 million people) are estimated to have renal failure. As kidney function is greatly compromised in this kind of disease, HD treatment intends to replace it, by filtering blood from wastes in an extracorporeal manner. However, it has been noticed that HD patients are at high risk of sudden cardiac death (SCD) due to the elevated incidence of arrhythmias and heart failure: these, in fact, make up for 40% of known causes of death among dialysis patients [1].

SCD, defined as death due to cardiac arrest or heart not beating sufficiently to maintain life, is, indeed, often associated with ventricular arrhythmias, e.g. ventricular fibrillation and sustained ventricular tachycardia. Prevention of SCD has become one of the greatest concerns for public health and, during the years, researchers dedicated themselves to find ways that could allow to identify patients at high risk of SCD. The analysis of the T wave of the electrocardiogram (ECG) by means of automatic methods soon proved, in this case, to be an ally: in particular, investigations performed on its beat-to-beat fluctuations, i.e. T-wave alternans (TWA), were able to evaluate cardiac consequences deriving from the presence of certain pathologies.

In the last couple of years, it was understood that, as TWA reflects only part of the electrical activity of ventricular heart cells, also alternans of other ECG waves, such as P-wave alternans (PWA) and QRS alternans (QRSA) should be investigated, as they represent fluctuations of the P wave and QRS complex, respectively. From these considerations, the concept of ECG alternans (ECGA), intended as the prevalent nature of electrical alternans that may affect the ECG, was born [2].

However, the interpretation of ECGA is currently changing. Not only ECGA should be regarded as the prevalent among the three types of alternans, i.e. PWA, QRSA and TWA, but also as an expression of all three. This obviously calls for a new and reliable quantification of the three alternans, stripped of possible reciprocal influence that may have affected alternans measurement in the past.

For these reasons, the aim of this thesis is to validate an improved quantification method for ECGA, where reciprocal influences among PWA, QRSA and TWA evaluations are removed. Validation of the new method will be performed by analyzing ECG recordings of a HD patient. ECGA will be investigated in order to verify if, as pointed out in literature, HD treatment actually increases the risk to develop arrhythmias in HD patients. The evaluation of PWA and QRSA, in addition to TWA, may contribute to better comprehend if such risk could mainly affect atrial or ventricular electrical activity, as well as understand if the evaluation of ECGA as an expression of PWA, QRSA and TWA could give further information with respect to the assessment of TWA alone. It could also provide details on the possible relationships among PWA, QRSA and TWA behaviors.

1. CHAPTER 1: CARDIOVASCULAR SYSTEM

The cardiovascular system is constituted by three components:

- *blood*, fluid that circulates in our body and carries substances to and away from the cells;
- *blood vessels*, conduits that allow the appropriate blood perfusion in the different parts of the body. Their distribution allows the distinction of systemic and pulmonary circulation;
- *heart*, a muscular pump that is devoted to driving the blood flow through the vessels.

According to these, the main function of the cardiovascular system seems to be the transport of substances, e.g. oxygen and nutrients, to all parts of the body by means of blood being pumped through the blood vessels by the heart. In reality, this system is involved in several other important functions:

- *Regulation* of blood flow for a better distribution of fluids, control of body temperature and acid–base homeostasis;
- *Protection* against infections, by demolition of pathogens, and blood loss, via coagulation;
- *Transport* of carbon dioxide towards the lungs, of hormones towards target cells and of wastes towards the kidneys in order to be removed from the organism.

Therefore, to fully understand how the cardiovascular system works and interacts with other apparatuses, in particular the kidneys in the endocrine system, it is fundamental to examine in depth its components, starting from the heart [3].

1.1. Anatomy of the heart

The heart is located in the mediastinum, inside the thoracic cavity, between the lungs and behind the sternum. It is about the size of a fist, with approximate weight of 300-350 g in males and 250-300 g in females. It is tilted leftwards, leaning for the most part in the left side of the body with respect to the anatomical median plane. This allows to distinguish a superior section, called *base*, corresponding to the point where major blood vessels are

attached, and an inferior section, named *apex*, laying on the diaphragm (Figure 1). Apex and base are 13 cm apart in adults.

The organ is enclosed in a protective sac, the *pericardium*, made of a superficial fibrous layer and a serous inner layer and filled with watery fluid that serves as lubricant during every beat. The serous inner sheet is attached to the heart wall, where it forms the first of three layers:

- *Epicardium*, outer layer mainly constituted by connective tissue. It also comprehends adipose tissue in certain areas, while other areas stay uncovered. Branches of some of the major blood vessels run immediately under it;
- *Endocardium*, layer similar to the epicardium, although it lacks adipose tissue. It covers the inner wall of the heart and extends to the vessels endothelium;
- *Myocardium*, thick layer ascribed to the rhythmic contraction and relaxation of the heart. It is mainly constituted by striate muscular fibers - despite being an involuntary muscle – disposed in the so-called Torrent Guasp Band, remnant of the embryonic stages of development. Such disposition allows the contraction and enhances blood ejection (Figure 2).

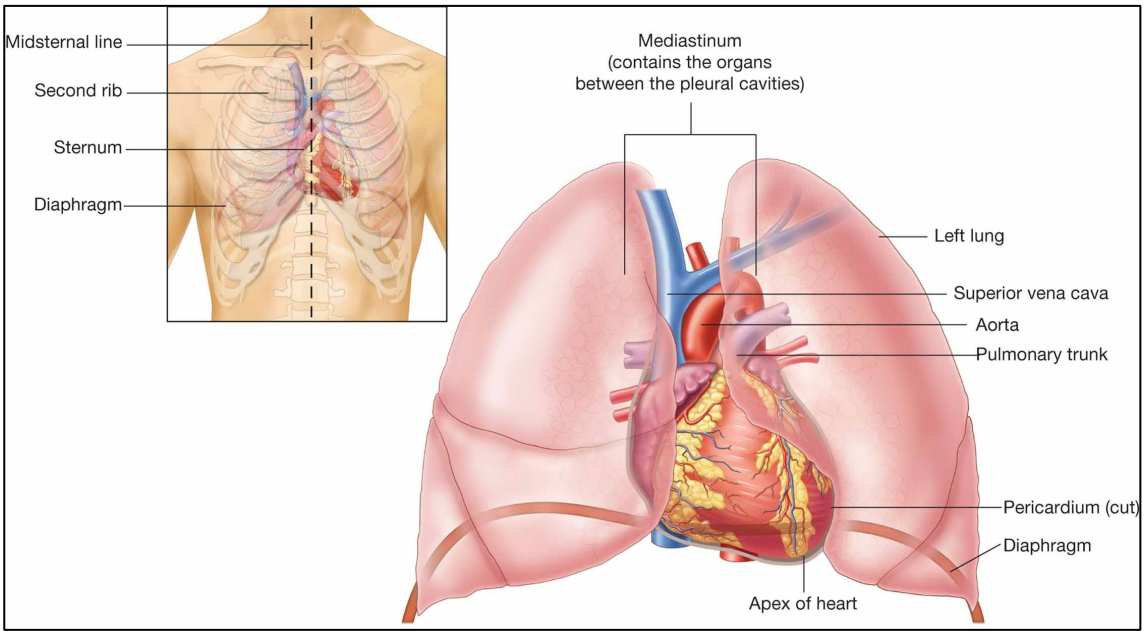

Figure 1. Heart location in the thoracic cavity. It is visible its position behind the sternum and above the diaphragm.

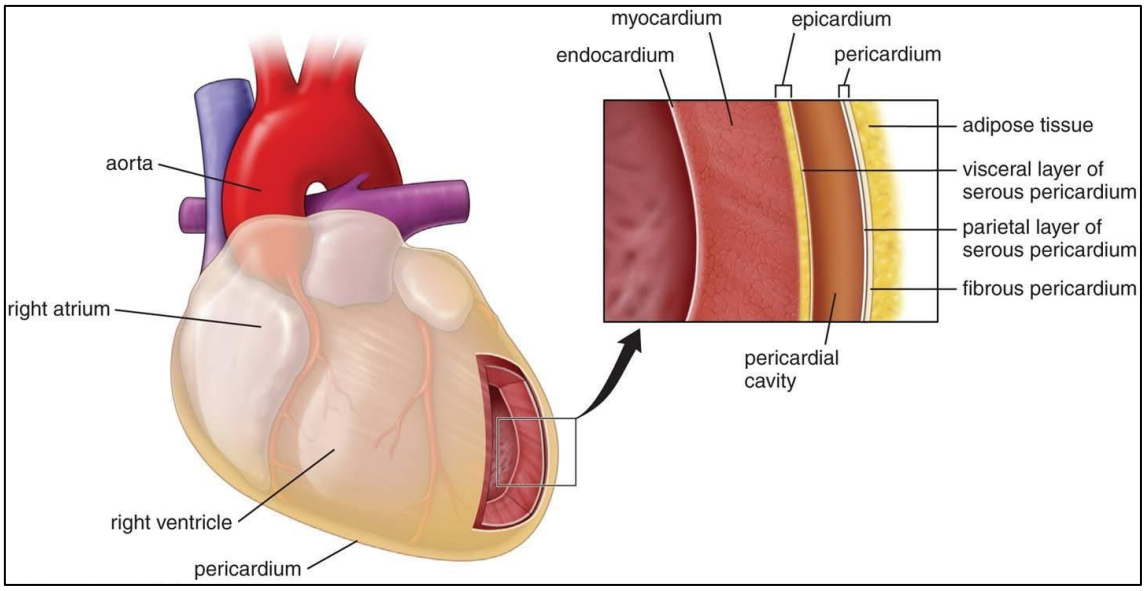

Figure 2. Representation of the heart wall divided into its different layers, with the pericardial cavity containing the lubricant fluid.

In particular, the cardiac muscle cells of the myocardium are arranged in layers that, during contraction, come together, exerting the needed pressure on blood. Differently from skeletal muscle cells, that rest for prolonged periods, heart cells contract about once every second, without resting, for a total of almost 3 billion times in average life. However, it is still thanks to similarities with both skeletal and smooth muscles that the cardiac muscle tissues can be excited and in turn convert chemical energy contained in ATP bonds into contractile force. The hydrolysis of ATP, in fact, drives the exchanges of ions between the cytosol and sarcoplasmic reticulum of the cells, with the sarcoplasmic reticulum being a large intracellular storage section of calcium. With the release of calcium from the sarcoplasmic reticulum into the cytosol, intracellular calcium concentrations increase, triggering contraction of the myocytes. The excitation is propagated by a network of cells, known as the conduction system, via gap junctions, that connect these cells with the cardiac muscle cells. Changes in the rate of excitation are indicated by sympathetic and parasympathetic innervations, with the latter belonging to the vagus nerve. Sympathetic fibers innervate the entire heart, releasing neurotransmitter norepinephrine and stimulating quick responses, while parasympathetic fibers innervate mainly special cells in the atria, releasing acetylcholine and slowing heart pace down [3].

Details on the conduction pathway will be however discussed in the next subchapters regarding heart's physiology.

The human heart can be then divided into two halves (right and left), each made of two cavities, *atrium* and *ventricle*.

- Right and left atria, with their thin walls, are separated by the interatrial septum and receive blood returning to the heart via the superior and inferior vena cava and pulmonary veins, respectively.
- Right and left ventricles, with thicker walls, are separated by the interventricular septum, and push blood into the pulmonary trunk and aorta, allowing oxygenation of blood and perfusion of all body tissues; the right ventricle occupies most of the anterior part of the heart, while the left ventricle is located posteriorly and forms the apex.

Atria and ventricles of each half of the heart are one-way connected by *atrioventricular (AV) valves*: they allow blood to flow from the atria to the ventricles but not backwards (from ventricles to atria). The right AV valve is made of three fibrous cusps and for that it is also known as the tricuspid valve; the left AV valve has two cusps and it is therefore called bicuspid valve. Chordae tendineae connect the valves to the papillary muscles, extensions of the ventricular wall that keep the valve cusps in place and avoid prolapse. *Semilunar valves* are also present: the pulmonary valve regulates blood flow from the right ventricle to the pulmonary trunk; the aortic valve regulates blood flow from the left ventricle into the aortic arch. Their function is indeed similar to that of the AV valves, although no chordae tendineae are present in this case (Figure 3) [3].

1.2. Physiology of the heart

Until now, we have seen the description of the anatomical aspects of the heart, i.e. the structures that altogether make up the heart and work together to perform their function. It is therefore important to investigate about the physiology of the heart itself: with physiology, we indicate the study of all the chemical and physical processes that structures in our body carry out to support life. Thus, we will describe the different

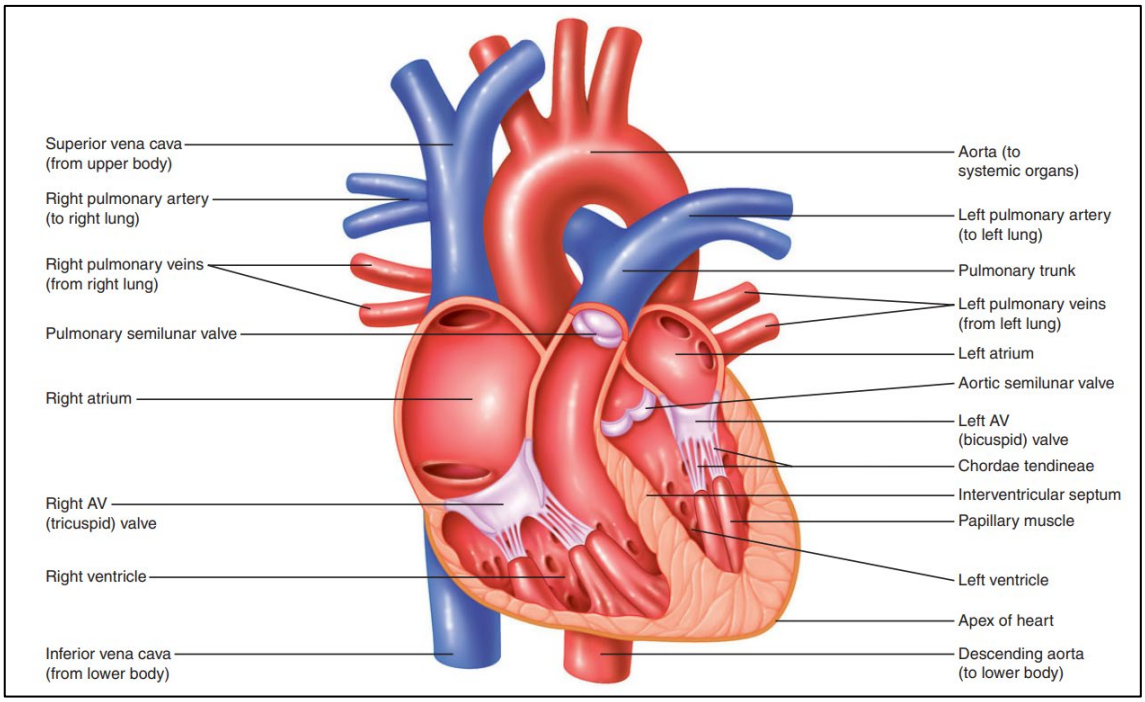

Figure 3. Cut section of the heart showing atria, ventricles and cardiac valves [4].

processes happening in our heart and, in particular, the mechanisms behind cardiac contraction.

1.2.1. Electrical function

The heart needs to contract in a very synchronized manner to guarantee that blood is adequately pumped in the circulatory system. Efficient pumping requires atrial contraction first, immediately followed by ventricular contraction. The contractile action is coordinated by the conduction system, which determines the order of contraction of the cardiac cells.

Conduction system

Cardiac muscle contractions, differently from skeletal muscles, are not triggered by central nervous system innervations, but are initiated by particular cells within the muscle itself. The ability to generate signals that trigger contraction autonomously and on a periodic basis is called autorhythmicity. This property is due to the action of a small percentage – close to 1% - of muscle cells that do not generate contractile force but

provide rhythm for the cardiac activity. These cells, that altogether form the conduction system, are the pacemaker cells, that initiate an impulse and establish the rhythm, and conduction fibers, that transmit impulses to the whole heart in a coordinated manner.

- *Pacemaker cells*. These cells spontaneously generate impulses (or excitations, stimuli) and therefore initiate contraction of the heart. They determine the rate of the heartbeat by firing APs regularly. Despite being located in almost all parts of the heart, they can be mainly found in two regions of the myocardium:
    1. The *sinoatrial node* (SA node), at the level of the connection between the upper wall of the right atrium and the superior vena cava;
    2. The *atrioventricular node* (AV node), near the tricuspid valve, in the interatrial septum.

    The rates at which SA node and AV node fire differ from each other. Generally, the SA node fires at a higher rate compared to the AV node and drives the depolarization of the cells, sending impulses to the AV node via conduction fibers. For this reason, the SA node is also considered the pacemaker of the heart.

- *Conduction fibers*. These cells are specialized into quickly conducting impulses generated by the pacemaker cells to the whole myocardium, therefore triggering muscle contraction. Theoretically, all cardiac cells are capable of transmitting excitation. As conduction fibers are larger in diameter compared to normal cardiac muscle fibers, though, these can transmit impulses much faster than the ordinary fibers (in certain areas of the conduction system, cardiac impulses can be transmitted with a velocity of 4 m/s).

Impulses generated by the pacemaker cells travel rapidly through the conduction fibers, in order to coordinate the cells activation and contraction. The spread of such excitation is first perceived by the atria, that consequently depolarize, contracting as a whole. Excitation then reaches the ventricles, which also depolarize and contract as a response to the stimulus. This transmission sequence is possible thanks to the connections called gap junctions, that allow the electrical stimuli to pass from one cell to another in the shape of ionic movements. Gap junctions are concentrated in the intercalated disks, structures that form the junctions between adjacent muscle fibers and contain several desmosomes to resist mechanical stress. This latter property is fundamental, considering that the

myocardium has to resist stretching, while the heart is filled with blood, and tension, due to muscle contraction during each heartbeat [4].

Transmission of an impulse normally occurs in five steps (Figure 4 and 5):

1. First, an impulse is generated by the SA node. Starting from the SA node, the stimulus travels towards the AV node by means of the internodal pathway, a series of fibers that pass through the atrial walls. The stimulus is also transmitted to the whole atria via interatrial pathways, allowing the contraction.

2. Once the signal arrives to the AV node, it is slightly delayed, as the AV node transmits impulses less rapidly than other cells in the conduction system. Precisely, the transmission is delayed of 0.1 s before it is allowed to move forward to the rest of the heart.

3. After the delay in the AV node, the stimulus can travel through the Bundle of His, a short bundle of muscle fibers that are concentrated in the upper part of the interventricular septum. The Bundle of His, together with the AV node, is the only electrical connection between atria and ventricles.

4. As soon as the impulse has been conducted through the His Bundle, which happens rather quickly considering the reduced length of the bundle, the signal splits into the right and left bundle branches, that transmit the stimulus to the right and left ventricles, respectively.

5. Finally, the impulse reaches a network of branches called Purkinje fibers, that spread from the apex of the heart to the rest of the ventricular myocardium, allowing depolarization to reach all myocardial cells in the ventricles.

As described so far, both SA node and AV node are capable of generating spontaneous impulses, but the pacemaking activity is usually dictated by the SA node. The AV node rarely guides electrical activity for two main reasons: the first one, already mentioned, is that the SA node fires at a higher frequency (70 bpm) than the AV node (50 bpm); the second one is that excitations coming from the SA node reach the ventricles via the AV node and, when this happens, the AV node goes through a refractory period, i.e. the AV node cannot generate its own impulses. As a consequence, the AV node rarely fires autonomously. If, however, the SA node slows down or fails to initiate an excitation, the

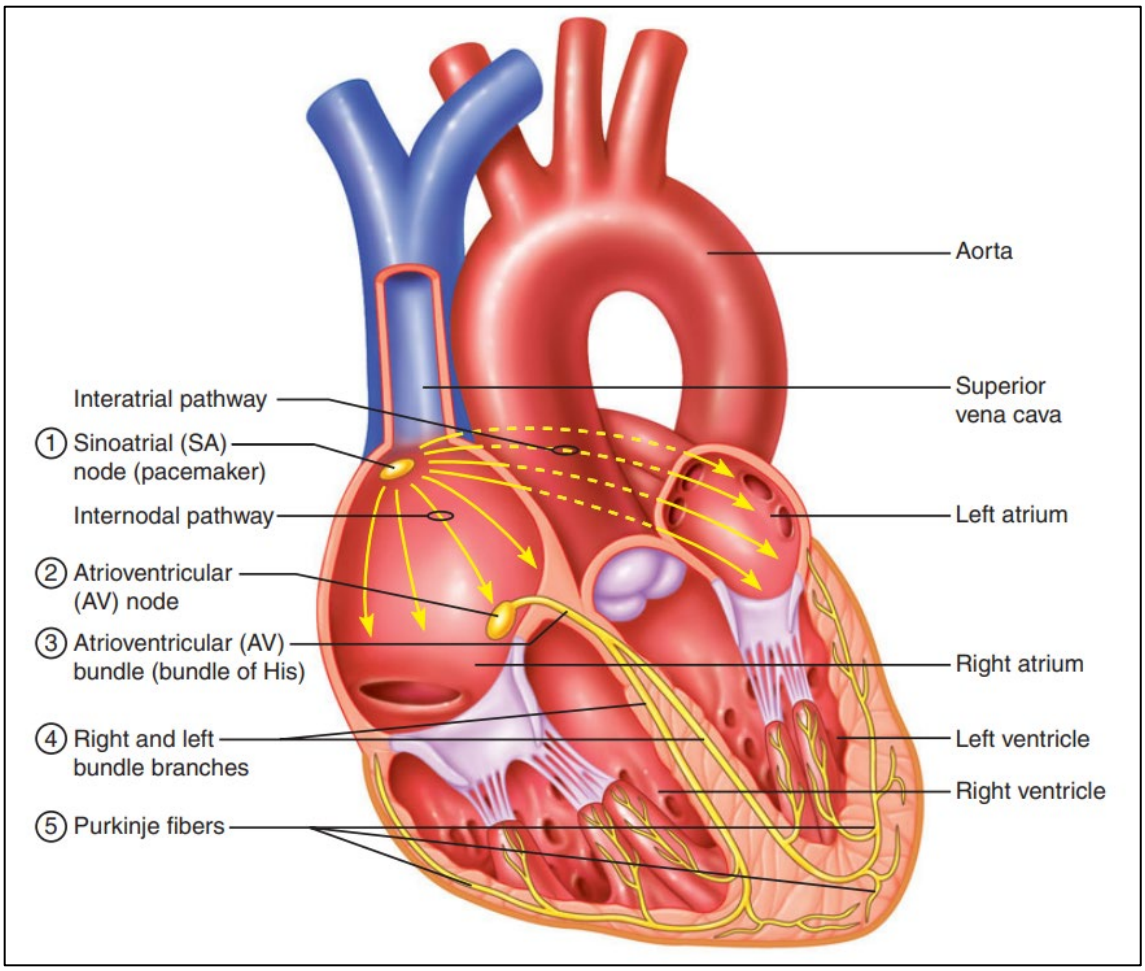

Figure 4. Conduction system of the heart. The numbers indicate the order in which the impulses propagate into the heart [4].

AV node takes over, generating an impulse that will travel through the conduction system and normally trigger ventricular contraction. If also this "emergency system" encounters problems, cells in the Purkinje fibers can take over as well, although the firing rate will be further reduced (30 – 40 bpm) [4].

After describing the path followed by these impulses, it is now worth examining the cellular mechanisms that are responsible for them.

Cardiac action potential

The impulse that is generated at the level of SA node and that propagates to the whole heart via the conduction system is called action potential (AP). Pacemaker cells and

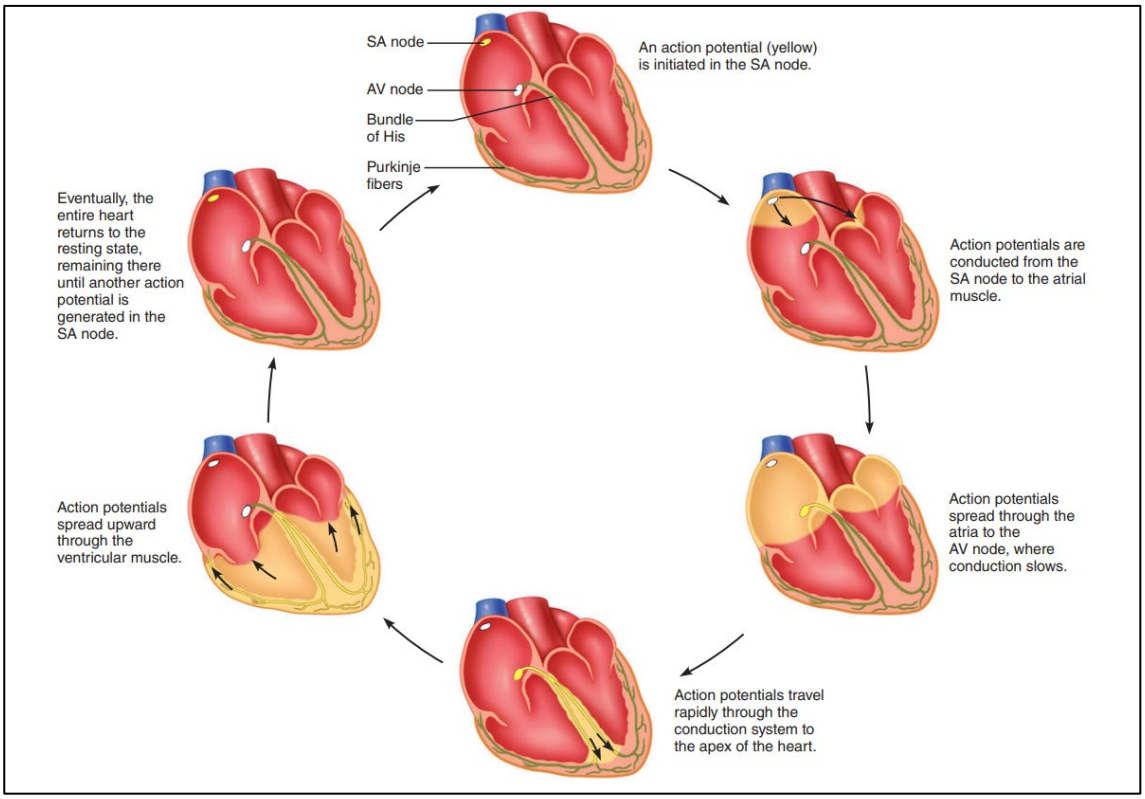

Figure 5. Propagation of the stimulus through the heart [4].

cardiac contractile cells present APs that differ in shape and duration, depending on the ionic currents that come into play.

- *AP in pacemaker cells*. As previously mentioned, pacemaker cells can regularly fire AP without external stimuli (only autonomic neurons exert influence on the firing rate). This is due to the fact that pacemaker cells do not have a steady resting potential, meaning that, immediately after an AP, pacemaker cells start to slowly depolarize and continue to do so until the membrane potential of the cell reaches the threshold needed to fire a new AP. In particular, the membrane potential, that is around -60 to -70 mV at resting condition, slowly increases with the shape of a "ramp" that will ultimately lead to an AP called pacemaker potential.

  The shape of the AP is dictated by permeability changes to sodium, potassium and calcium ions (Na^+, K^+, and Ca^{2+}, respectively). The slow depolarization that occurs at the beginning of the pacemaker potential is given by the closure of K^+ channels and opening of the "funny" current channels, named so because of their unusual characteristics (they open after cell repolarization, allowing Na^+ and K^+

to cross the cell membrane). This produces a net decrease of K^+ movement out of the cell and increase of Na^+ entering the cell, that in turn give rise to an initial depolarization. Funny channels stay open only for a short time, closing when membrane potential is at -55 mV, i.e. close to the threshold. At that point, transient Ca^{2+} channels (T-type channels) start to open, increasing Ca^{2+} current and depolarizing the cell even further. T-type channels, which remain open for a brief time too, trigger the opening of long-lasting Ca^{2+} channels (L-type channels), producing a large increase of Ca^{2+} and also Na^+ current and, in turn, of depolarization. The increased depolarization then triggers the opening of K^+ channels: the rise of K^+ current towards the cell brings the membrane potential down and stimulates the decrease of Ca^{2+} current, closing Ca^{2+} channels and finally leading to the repolarization of the membrane (Figure 6) [4].

- *AP in contractile cells*. AP from pacemaker cells arrives to the contractile cells by means of gap junctions. In these cells, however, the AP differs from that described for pacemaker cells, due to the dimension of the cells as well as the type and number of ion channels they own. In fact, unlike pacemaker cells, contractile cells have stable resting potential and a long-lasting AP that can be divided into five phases.

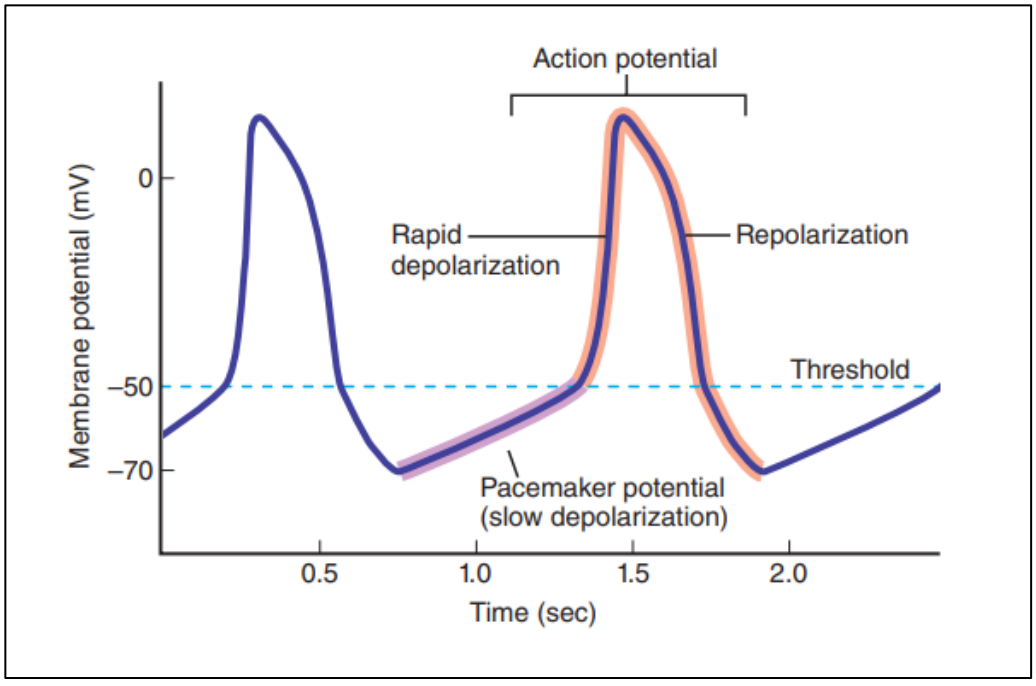

Figure 6. AP of a pacemaker cell [4].

- *Phase 0*. In this phase, depolarization of the cell membrane pushes the opening of voltage-gated (activated by changes in the electrical membrane potential) Na^+ channels, increasing Na^+ flow into the cell. As a consequence, the membrane becomes more positive, leading to the opening of more Na^+ channels and to a rapid rise of membrane potential up until +30 to +40 mV.
- *Phase 1*. Na^+ channels opened in phase 0 start to inactivate, reducing Na^+ inward current. This causes a fall of the membrane potential towards negative values, since, at the same time, K^+ flows out of the cell. Membrane potential however drops only a little, as voltage-gated K^+ channels start to close, decreasing K^+ outward current, and L-type Ca^{2+} channels open, allowing Ca^{2+} inward flow. Both changes allow to counteract the Na^+ channels inactivation.
- *Phase 2*. This phase is also known as the *plateau phase*. Here, most of K^+ channels stay closed, while Ca^{2+} channels activated in phase 1 stay open. The elevated Ca^{2+} current allows the maintenance of the membrane in the depolarized state.
- *Phase 3*. In phase 3, K^+ outward current starts to increase, as a group of K^+ channels slowly reopens. This ionic movement decreases the membrane potential to more negative values and pushes more K^+ channels to open. In the meantime, Ca^{2+} channels begin to close, reducing Ca^{2+} inward flow, and this leads to the repolarization of the membrane and termination of the AP.
- *Phase 4*. This final phase corresponds to the *resting potential*. Due to K^+ outward currents being greater than Ca^{2+} and Na^+ inward currents, the resting potential is equal to -90 mV, that approximately corresponds to the equilibrium potential of K^+ (Figure 7).

Once an AP is stimulated in contractile cells, this must be propagated to neighboring cardiac cells to produce a contraction: the mechanism behind this propagation is called excitation-contraction coupling and is based on depolarizing currents travelling through gap junctions between cells. These depolarizing currents will in turn cause Ca^{2+} channels

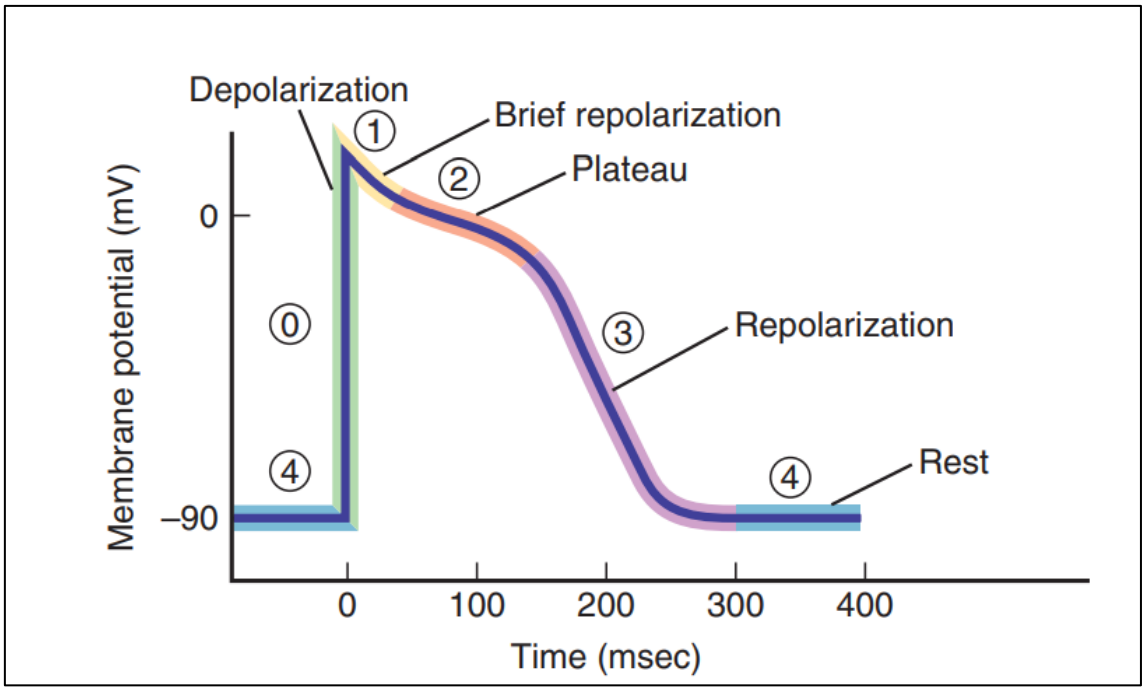

Figure 7. AP of a contractile cardiac cell. The numbers identify the different phases of the AP [4].

on the cells membrane to open and trigger mechanical contraction of the cardiac muscle cells [4].

1.2.2. Mechanical function

The heart pump, with all its components, goes through a number of events and changes during a single complete heartbeat. These aspects, such as contraction and pumping action exerted by the muscle fibers, valve opening and closure, atrial and ventricular pressure changes, define the so-called *cardiac cycle*.

As the cardiac cycle involves all the events of a heartbeat, including both ventricular contraction and relaxation, this can be divided into two major segments: *systole*, corresponding to ventricular contraction and constituting 30% of the cycle, and *diastole*, corresponding to ventricular relaxation and 70% of the cycle. Atria also undergo contraction and relaxation, but the aforementioned terms generally refer to ventricular events [4], [5].

The examination of the cardiac cycle starts from the diastole, in particular when atria and ventricles are completely relaxed, and consists of four phases:

1. *Ventricular filling*. Blood enters the atria via systemic and pulmonary veins, and then, through the AV valves, goes into the ventricles at its own pressure. This occurs because pressure in the veins is greater than in the atria. In the meantime, semilunar valves are closed due to ventricular pressure being lower than that of the aorta and pulmonary arteries;
2. *Isovolumetric contraction*. Ventricles start to contract (beginning of the systole). As a consequence, ventricular pressure increases and, when it exceeds atrial pressure, AV valves close. Semilunar valves also remain closed, as ventricular pressure is not high enough to open them. This means that blood volume inside the ventricles is constant, as no blood flows in or out of the ventricles, and contraction will not vary it;
3. *Ventricular ejection*. As ventricular pressure rises to a peak, surpassing aortic pressure, semilunar valves open, allowing ejection of blood into the aorta and pulmonary arteries. Afterwards, ventricular pressure falls again under the aortic pressure, meaning that semilunar valves will close once more, ending ejection (beginning of the diastole);
4. *Isovolumetric relaxation*. The ventricular myocardium is relaxing, and some blood is staying inside the ventricles. As the ventricular pressure is too low to keep the semilunar valves open, but too high to allow the opening of the AV valves, relaxation happens with constant blood volume in the ventricles (Figure 8).

It is immediately visible how the phases of the cardiac cycle are dictated by changes in pressure in the different parts of the heart. It is therefore necessary to also delve into such pressures [4], [5].

Ventricular pressure, during ventricular filling, stays low until the end of the phase, where we see a small but sudden increase due to the addition of blood coming from atrial contraction. It increases more rapidly during systole and then falls near to zero at the beginning of a new diastole, before starting to slowly increase again. *Atrial pressure* follows a similar trend during diastole, with the increase, in late diastole, indicating atrial

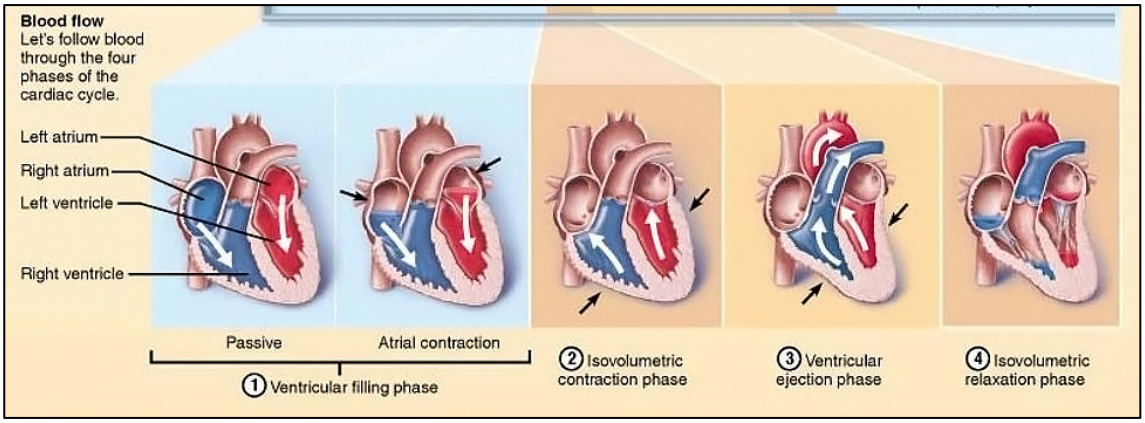

Figure 8. Phases of the cardiac cycle.

contraction. This short rise in pressure is however followed by a series of small increases that are of little significance for the whole cardiac cycle (Figure 9).

Aortic pressure, during diastole, slowly declines, as the volume of blood in the aorta keeps decreasing and is routed in the systemic blood vessels. The decline ends in a minimum called *diastolic pressure*. As systole begins, aortic pressure keeps falling since the aortic valve still has to open (ventricular pressure has to be higher than aortic pressure for that to happen). Once the aortic valve opens and blood can be ejected from the ventricles, aortic pressure starts rising, reflecting the increase of blood volume in the aorta. As soon as the flow of blood from the heart starts to slow down, aortic pressure reaches its maximum, i.e. *systolic pressure* and then decreases. The closure of the aortic valve at the end of the systole gives a particular curve in pressure, called *dicrotic notch* (Figure 9). Aortic pressure is often indicated by means of its average, i.e. *mean arterial pressure*.

For what concerns volumes instead, it is worth mentioning the changes that can be seen in *ventricular volume*, in particular left ventricular volume. The volume of blood in the ventricles increases towards the end of ventricular filling, rather quickly at first and then more slowly as time passes (Figure 9). When diastole ends, there is a small but abrupt increase in volume, representing blood being pushed into the ventricles after atrial contraction. The maximum value reached at this point is called *end-diastolic volume* (EDV). During isovolumetric contraction, there is no change in volume, but as soon as the aortic valve opens at the beginning of ventricular ejection, ventricular volume starts to decrease. This trend goes on, until the aortic valve closes again at the end of ejection,

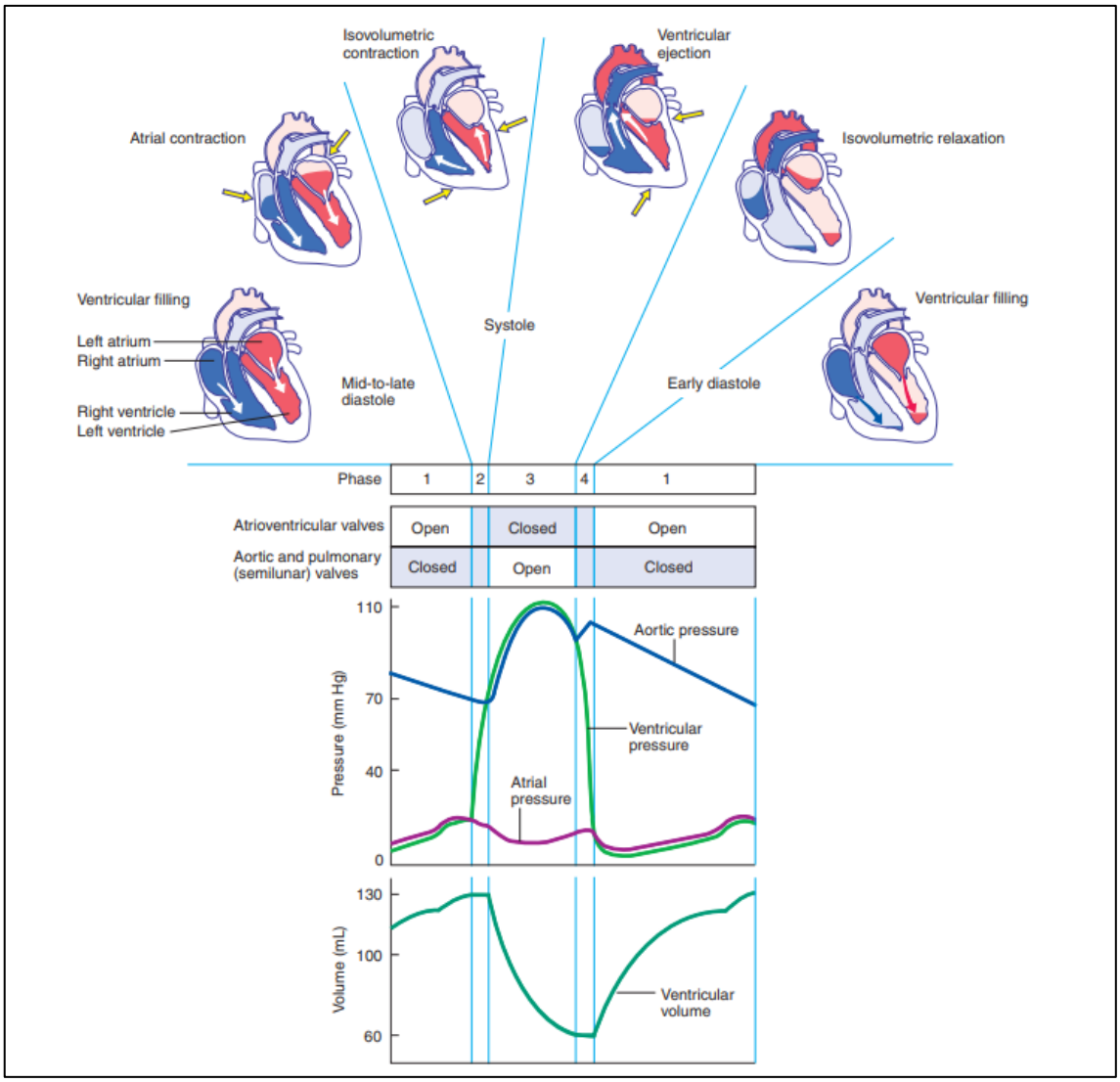

Figure 9. Evolution of the aortic, ventricular and atrial pressure, as well as ventricular volume, during the different phases of the cardiac cycle [4].

and ventricular volume reaches its minimum, i.e. *end-systolic volume* (ESV). The difference between EDV and ESV gives the *stroke volume* (SV), i.e. the volume of blood ejected during a heartbeat, normally close to 70 ml. Moreover, the ratio between SV and EDV will give the *ejection fraction* (EF), i.e. the fraction of EDV ejected in one beat.

Combining pressure and volume changes in the heart, we can obtain the *pressure-volume curve*, a plot that represents each phase of the cardiac cycle. The loop, generally reporting the pressure and volume changes of the left ventricle, starts with ventricular filling, where, due to the ongoing relaxation of the ventricle, ventricular pressure slightly decreases.

Pressure then slowly goes up together with ventricular volume, until contraction is initiated and the mitral valve closes. Isovolumetric contraction follows, as volume remains constant, until ventricular pressure exceeds that of the aorta and the aortic valve opens. Rapid ejection is initiated, and maximum pressure is reached. Then, ejection becomes slower and stops when ventricular pressure is lower than aortic pressure, which causes the closure of the aortic valve and prevents backflow of blood to the heart. Finally, the heart, with all its valves closed, relaxes with constant volume until ventricular pressure falls below atrial pressure and mitral valve opens again, restarting the loop (Figure 10) [4], [5].

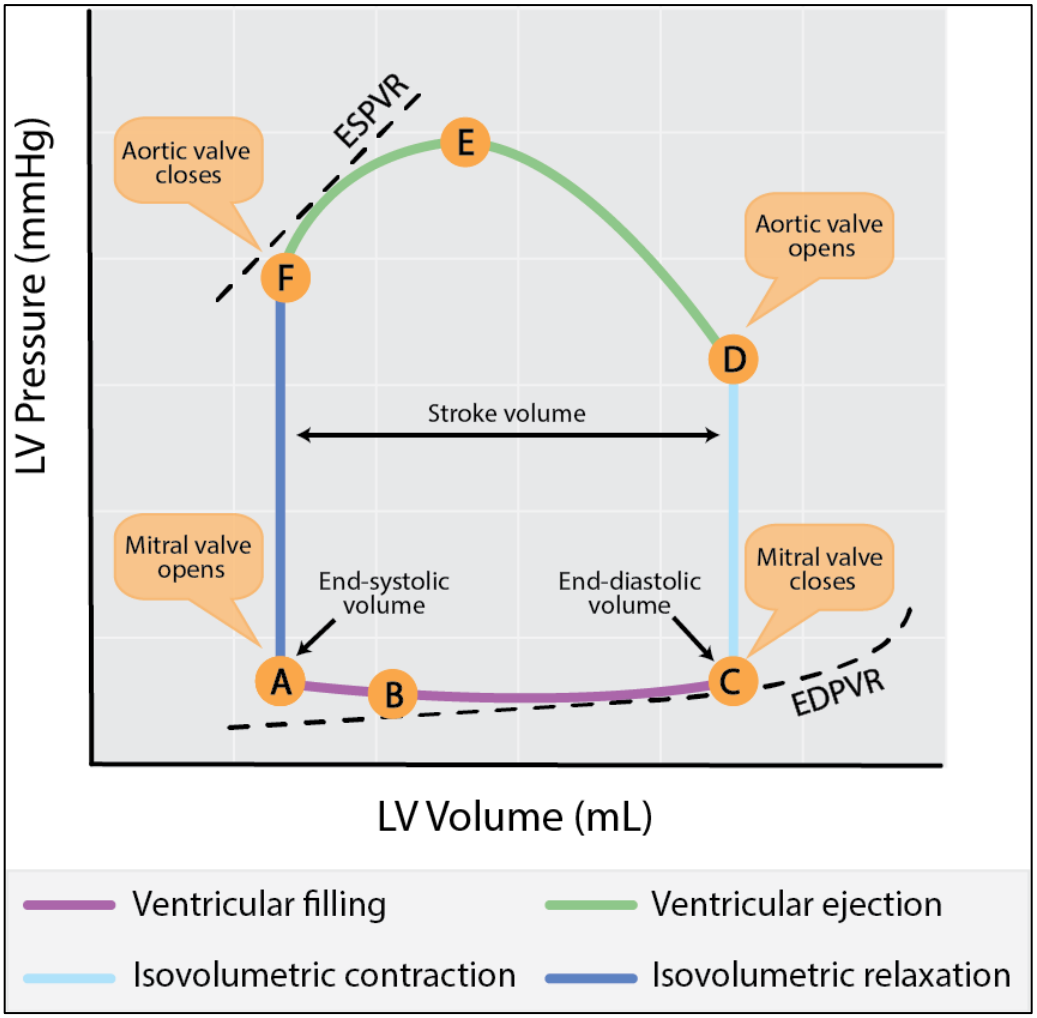

Figure 10. Pressure-volume loop of the left ventricle. The loop starts when the mitral valve opens, indicated with the letter A. Points B and E identify the minimum and maximum ventricular pressure, respectively. ESPVR: end-systolic pressure-volume relationship; EDPVR: end-diastolic pressure-volume relationship.

1.3. Systemic and pulmonary circulation

The action of the heart generally provides the overall driving force for the movement of blood, but it does not act entirely alone: the vascular system, in fact, has a major role for what concerns the regulation of blood pressure and the perfusion of the different tissues in our body. This is allowed by an intricate but very efficient system of vessels that, together with the heart, forms the totality of the cardiovascular system.

There are three main categories of blood vessels:

- *Arteries* (and arterioles), efferent vessels that carry blood away from the heart;
- *Veins* (and venules), afferent vessels carrying blood to the heart;
- *Capillaries*, thin vessels that connect smaller arteries to small veins.

The majority of blood vessels consists of a hollow interior, called lumen, where blood flow happens, surrounded by a layer of epithelium, i.e. the endothelium or *tunica intima*, which acts as a semipermeable membrane to substances entering and leaving blood. A second, thicker layer, *tunica media*, usually follows, made of smooth muscle cells and fibrous or elastic connective tissue, that determines the ability of the vessel to dilate or contract when needed. Finally, an external third layer, *tunica adventitia*, made of loose connective tissue and containing nerves, surrounds the internal layers [3].

Depending on the amount of endothelium, smooth muscle and connective tissue, vessels are easily distinguishable (Figure 11). In fact, arteries are generally constituted by a high amount of smooth muscle cells, that make these vessels highly elastic and thick. Veins are usually thin walled instead, allowing a greater amount of distention of the vessels themselves. Capillaries are also thin walled but completely lack external connective tissue, as these vessels are devoted to the exchange of substances between blood and tissues, by means of diffusion or bulk flow, thanks to the presence of pores: except for continuous capillaries, where endothelial cells are joined together by tight junctions and intercellular spaces are very narrow, fenestrated and discontinuous capillaries possess fenestrations of different sizes, that allow the exchange of big proteins [3], [5].

The different vessels, given their structure as well as connection between one another, grant the separation of oxygenated and deoxygenated blood into two circulatory systems,

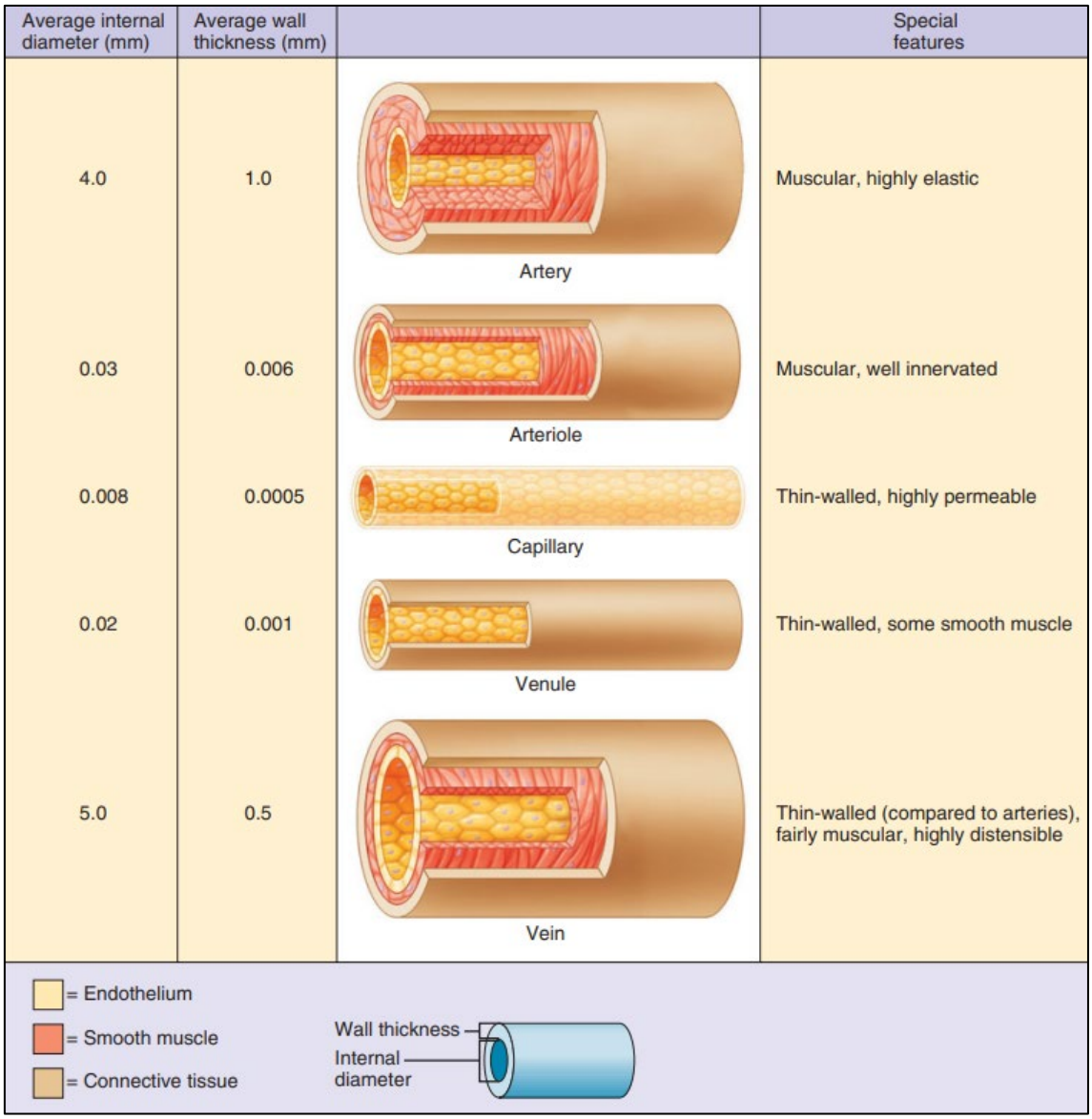

Figure 11. Structural differences of the distinct types of blood vessels [4].

which rhythm is instructed by the heart acting as a double pump: these are called pulmonary circulation and systemic circulation.

- *Pulmonary circulation*. Deoxygenated blood coming from the periphery of the body is conveyed by the superior and inferior vena cava to the right atrium. Blood then moves into the right ventricle and is pushed into the pulmonary trunk, a large artery that branches into two pulmonary arteries, supplying right and left lung respectively. Then, the two arteries keep branching into arterioles that connect with venules and veins by means of capillaries. Specifically, these capillaries are

contained in the alveoli, where blood exchanges carbon dioxide with oxygen introduced in the lungs by breathing. Newly oxygenated blood leaves the lungs via four pulmonary veins and reaches the left atrium, where systemic circulation can start.

- *Systemic circulation*. From the left atrium, blood flows into the left ventricle. When the left ventricle contracts, blood is pushed into the aorta. The aorta then branches into progressively smaller arteries and arterioles, reaching in parallel all parts of the body, except the lungs. In particular, the abdominal aorta divides into the hepatic and mesenteric arteries, that bring oxygenated blood to the liver and intestine, as well as the renal artery, that delivers blood to the kidneys for it to be filtered, via capillaries, from toxins and excessive electrolyte (minerals that carry electrical charge) concentrations. Capillaries again connect arterioles with venules, which, in systemic circulation, unite to form the superior and inferior venae cavae. Superior and inferior venae cavae collect deoxygenated blood from above and below the heart, respectively, and return such blood to the right atrium, where pulmonary circulation will be reinitiated (Figure 12).

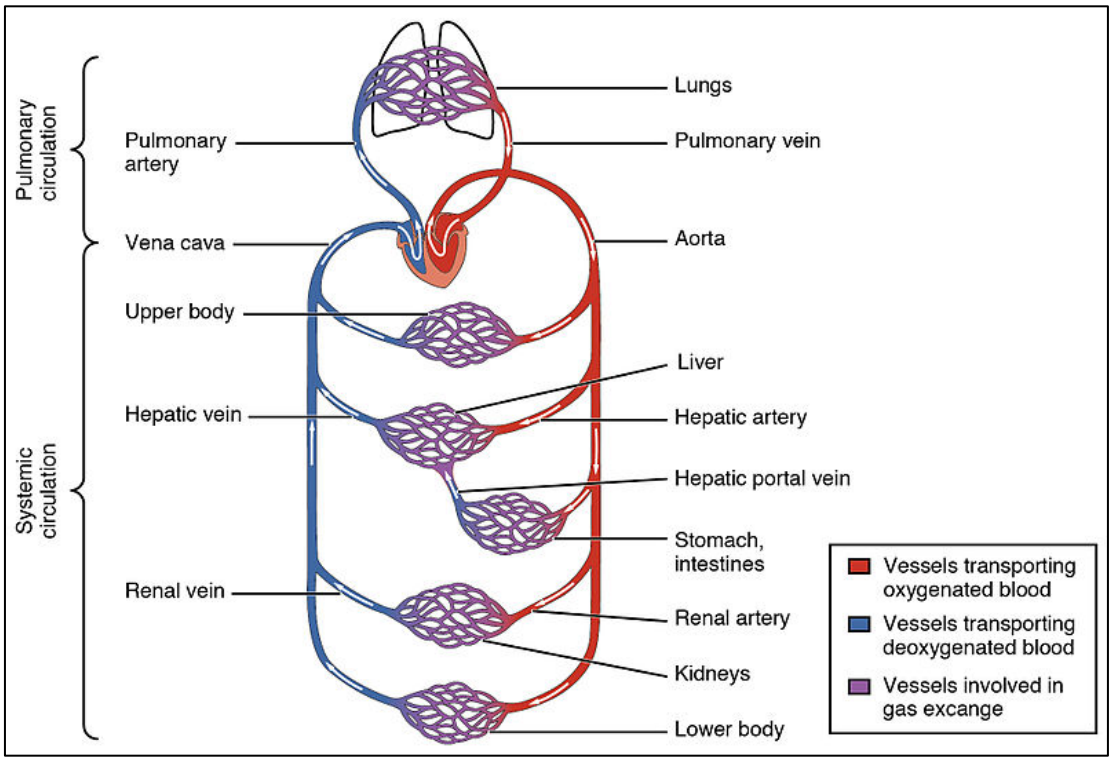

Figure 12. Pulmonary and systemic circulation pathways.

Pulmonary circulation is subjected to lower hemodynamic resistances compared to systemic circulation: this generally explains why the right heart is thin walled and guarantees sufficient time for blood to exchange carbon dioxide with oxygen. Higher resistance in systemic circulation instead ensures that all tissues receive a proper fraction of oxygenated blood, according to their specific needs, i.e. metabolic changes [3], [5].

2. CHAPTER 2: ELECTROCARDIOGRAM

After discussing the structure and electrical activity of the heart in the previous chapter, it is now necessary to speak about how such electrical activity can be observed. The most popular and noninvasive way to monitor cardiac electrical activity is the *electrocardiogram* (ECG or EKG, where EKG is the German form of the word, elektrokardiogramm) [4].

Noninvasive ECG was first measured in 1887 by Augustus Waller (1856-1922) by means of a capillary electrometer, i.e. a photographic film moving alongside a tube containing sulphuric acid and mercury in response to electric fields. Waller, however, despite his efforts, did not believe the ECG could be clinically useful.

Willem Einthoven (1860-1927), instead, recognized the importance of ECG recordings in determining whether problems exist in the electrical activity of the heart. In fact, at the beginning of the 20^{th} century, he developed the first high-quality ECG recorder, adapted from the string galvanometer, with improvements that could allow its application in clinical environments.

Nowadays, the ECG is measured by physicians by means of electrodes, mainly placed on the surface of the thorax.

2.1. Genesis

In Chapter 1.2.1. we have seen cardiac electric events at an intracellular level, i.e. APs. We also mentioned how an AP is transmitted from one cell to the neighboring one. Considering two cells, Na^+ channels in the first cell are open, so this cell will start to produce its own AP. The AP will then transmit, e.g. from left to right, via gap junctions from cell one to cell two, where Na^+ channels will open as well, increasing Na^+ influx. Indeed, cell two, affected by this intracellular current, will progressively become less negative and this creates a potential difference between the second and first cell. As cell one is still intracellularly more positive than cell two, cell one will also be externally more negative than cell two. As a consequence, external positive charges will start to flow from right to left, so towards more negative potential, that is above cell one. This net driving

force, given by the movement of positive charges from right to left creates an extracellular current (Figure 13). This extracellular current will give rise to a certain voltage that, if recorded, will be at the basis of the ECG.

These ionic movements are however extended to an increased number of cardiac cells, as, from cell two, the intracellular and extracellular currents will reach a third cell and so on. This gives rise, in the extracellular space, to the so-called depolarization wavefront, that moves from left to right and is considered positive at its head and negative at the tail. The extracellular current flows from positive to negative potential, taking all possible pathways. If we considered each pathway as a *dipole vector* (pointing from negative to positive potential) and vectorially summed them up, we would obtain the equivalent dipole vector, a total representation of the depolarization wavefront. Dipole vectors referring to the electrical activity of specific parts of the heart, when added together, will result in the so-called *heart vector*, popular concept in electrocardiography and vectorcardiography as it represents all the activity of the heart at a given moment.

In the meantime, while intracellular current propagates further from the first cells that showed AP, a repolarization wavefront can be observed as well. The first leftmost cells to depolarize, at a given moment, starts to repolarize with an outflow of K^+. As a result,

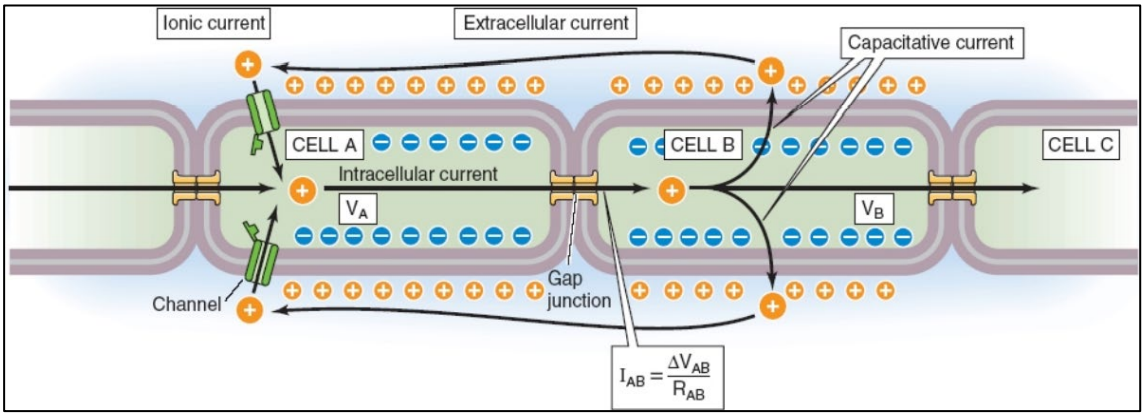

Figure 13. Movement of intracellular and extracellular currents. The intracellular current propagates from cell A to cell B, making the former more negative than the latter. External positive charges will be therefore attracted towards cell A, generating an extracellular current. V_A: intracellular potential of cell A; V_B: intracellular potential of cell B; I_{AB}: intracellular current between cells A and B; Δ_{AB}: potential difference between cells A and B; R_{AB}: resistance between cells A and B.

potentials are inverted: the head of the repolarization wavefront will be negative, while the tail will be positive. Extracellular currents will also be reversed.

If two electrodes, one positive (or right electrode) and one negative (or left electrode), were put on the body surface at a certain distance, they would be able to record these wavefronts in terms of potential difference. A depolarization wavefront moving from left to right would be displayed as a positive deflection, followed by a negative deflection corresponding to repolarization, in the ECG. Electrodes placed perpendicularly to the dipole vectors would instead record a potential difference equal to zero.

Using these two electrodes would allow to pick up the different electrical fields associated to the moving heart vector. For instance, it would be possible to measure how potentials vary during the course of cardiac activity, e.g. during ventricular depolarization. An increased number of electrodes will enable to obtain body surface potential maps (Figure 14) from which it is possible to easily construct the ECG, and the variations observed in terms of deflections will represent the ECG shape [6].

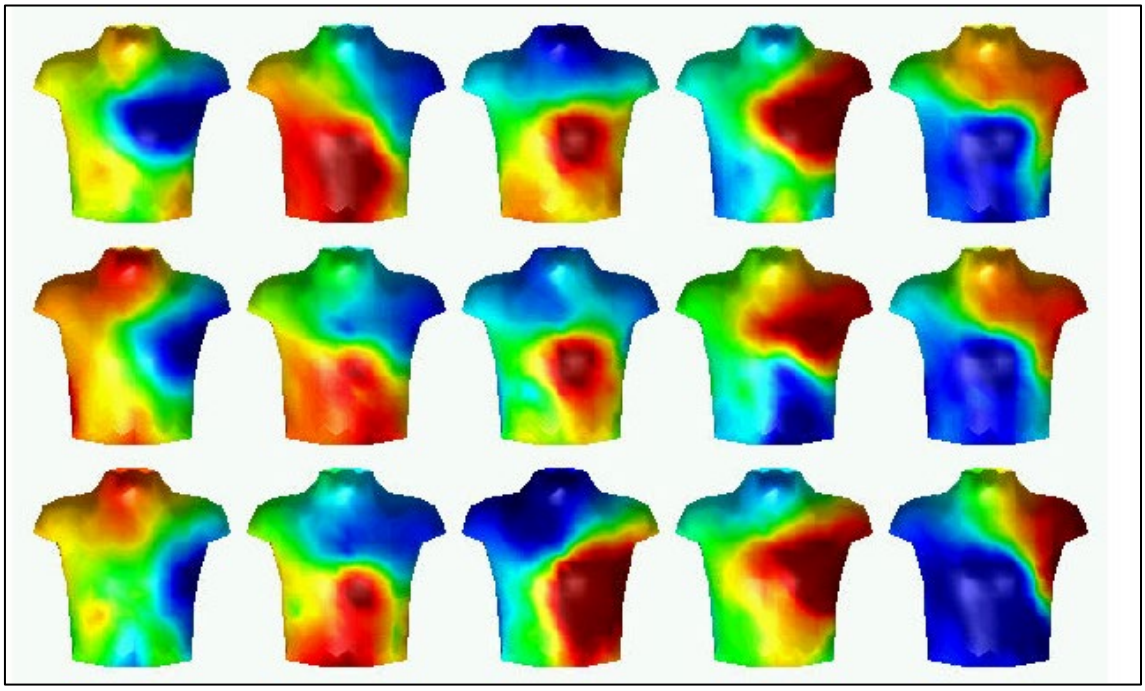

Figure 14. Example of body surface potential map. Blue areas indicate negative potential, while red areas indicate a positive potential.

2.2. Morphology

A typical ECG tracing is constituted by different waves (i.e. deflections) that represent the sequence of depolarization (contraction) and repolarization (relaxation) that atria and ventricles go through during a heartbeat. It usually has an order of magnitude of 1 mV, i.e. the potential difference of the extracellular currents at body surface.

The waves composing the ECG are:

- *P wave*, an upward deflection that represents the depolarization wavefront spreading from the SA node through the atria. As atrial systole is not extremely strong, the P wave has contained amplitude. It usually has a duration between 60 and 100 ms;
- *QRS complex*, that corresponds to ventricular depolarization. The idealized shape of the QRS complex is composed by three smaller waves, the R (upward), Q and S waves (downward). These waves are indeed detected in a different way depending on the location of the electrodes. QRS complex duration is normally 60 to 110 ms, that is a relatively short time, meaning that ventricular depolarization happens quite rapidly in time. Prolonged QRS complex duration indicates ventricular impairment, e.g. due to abnormal pacemaker sites that fire APs conducted over slow pathways.
- *T wave*, in the majority of cases an upward deflection caused by ventricular repolarization. As reported in chapter 2.1., we would expect a downward deflection, but it is not entirely true for the T wave. This is because the last cells to depolarize in the ventricles, i.e. epicardial cells, have shorter AP and therefore repolarize earlier than endocardial cells. As a consequence, repolarization wavefronts travel in opposite direction compared to depolarization wavefronts, causing the deflection to have, most of the time, positive voltage: a negative voltage, or discordant ECG, would indicate abnormalities. However, it has to be considered also the fact that, depending on the disposition of the electrodes, it is possible to obtain physiological T waves with negative voltage. In that case, it will be a positive polarity to indicate abnormalities in conduction. For what concerns duration, T wave is longer than QRS complex, between 160 and 200 ms,

as repolarization is not transmitted by high-velocity bundle branch and Purkinje fibers with respect to depolarization.

Sometimes, it also possible to observe a small positive wave, called U wave, after the T wave. Its origin is still unclear though: hypotheses consider it a remnant of ventricular repolarization (Figure 15).

In-between the ECG waves just described, there are flat periods, also known as isolines. The first one is the *PR segment*, going from the end of the P wave to the beginning of the QRS complex and representing the time taken by an impulse to travel from the AV node to the bundle of His. The second one is the *ST segment*, the isoline between the offset of the QRS complex and the onset of the T wave, representing the time at which both left and right ventricles are entirely depolarized (Figure 16). This segment, if depressed or elevated, becomes fundamental to diagnose ischemia or hypoxia. A third segment is represented by the *TP segment*, connecting the end of the T wave with the beginning of the P wave and representing the ECG baseline.

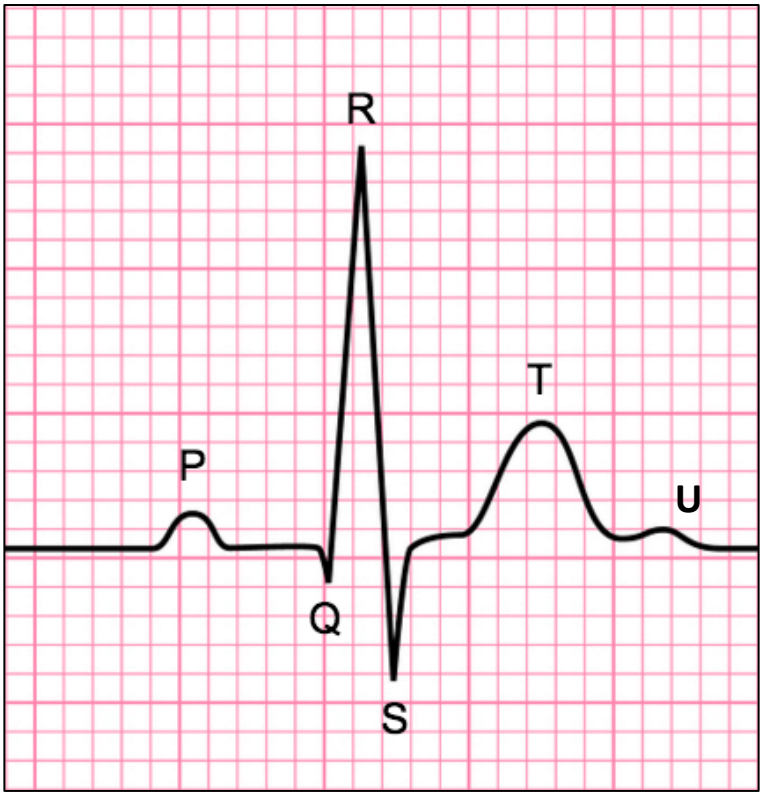

Figure 15. Example of ECG, with P wave, QRS complex and T wave. U wave is also visible soon after the end of the T wave.

Often, the morphology of the ECG is studied in terms of intervals (Figure 16):

- *PR interval* (or *PQ interval*), ECG tract going from the onset of the P wave to the beginning of the QRS complex. It represents the time interval between the start of atrial depolarization and the beginning of ventricular depolarization. In normal ECG, this interval should be less than 200 ms. If longer, we are probably in the presence of an AV conduction block;
- *QRS interval* (or *QRS duration*), going from the onset of the QRS complex to its offset, called J point. The offset is sometimes difficult to find, even in normal ECGs, as the J point may not be visible or may be substituted by a J wave, slurred or notched;
- *ST interval*, part of the ECG going from the end of the QRS complex to the end of the T wave;
- *RR interval*, time distance between two consecutive QRS, or R peaks. For heart rate (HR) close to 60 bpm, it can be around 1 s. If HR is higher, the RR interval will be lower than 1 s;

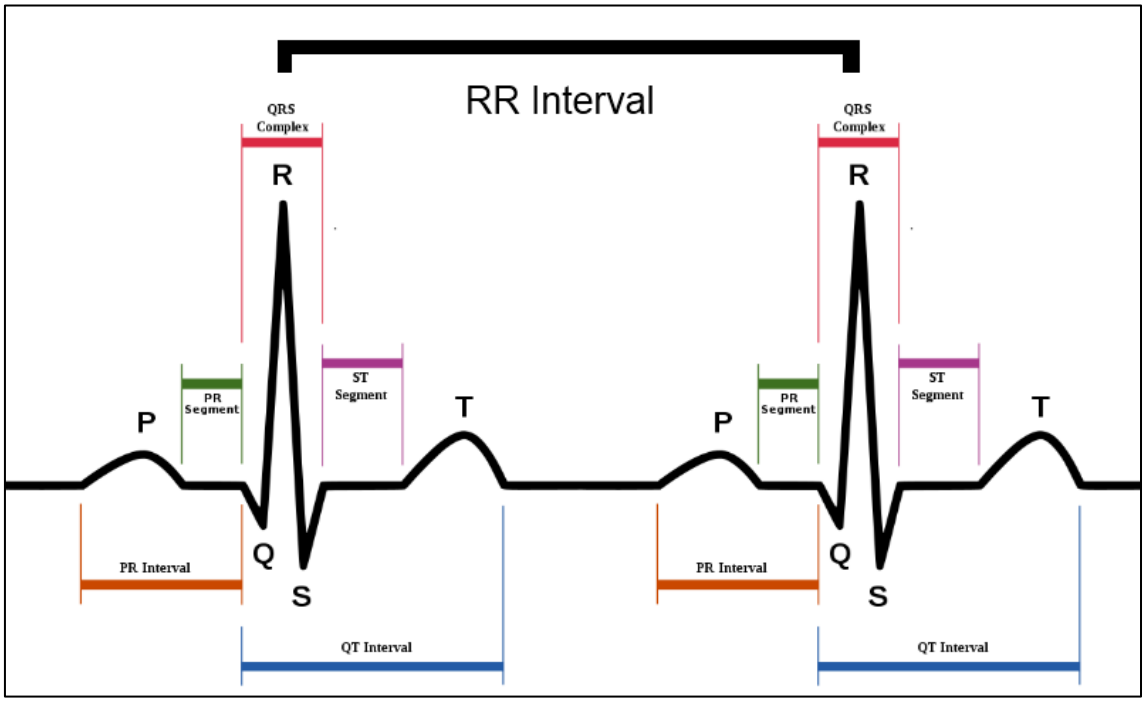

Figure 16. Example of ECG tracing with, underlined, the different intervals and segments.

- *QT interval*, interval going from the QRS complex onset to the T wave offset. It represents the time needed for both ventricular depolarization and repolarization to occur and it typically ranges between 280 and 430 ms. Longer intervals usually indicate susceptibility to possible tachyarrhythmias. As the QT interval also depends on HR, it is often expressed in terms of *corrected QT* (QTc). QTc can be computed by means of the Bazett's equation (1)

  $$QTc = QT/\sqrt{RR} \quad (1)$$

  where RR represents the RR interval. This computation allows to obtain a QT interval that is independent from HR [7].

2.3. Lead system configuration and electrodes arrangement

The description provided so far of the ECG constitutes a general view of its morphology, although hints about different wave shapes have been given. In fact, as several electrodes with distinct placements are used to record an ECG, also the potential differences, and therefore the ECG shape observed, will be diverse. To better understand this, it is necessary to introduce the *lead* concept. With the word lead we indicate the electrical potential differences measured between two points in space, by means of electrodes. The simplest ECG leads are usually composed by two electrodes [6].

Waller, during his experiment in 1887, selected five electrodes locations, one being the mouth and the others being the four limbs extremities. With this disposition, low contact impedance was achieved, and ten leads were obtained (Figure 17). Among these, five leads were selected as cardinal leads [8].

When Einthoven used the capillary electrometer to record his first ECG, he applied Waller's leads to construct a new lead system. In this new lead system, electrodes (at the time, jars with salt, water and copper plates benefitting of good signal-to-noise ratio) were placed on right and left arm (RA, LA) and on the left leg (foot, LL), and corresponding *bipolar limb leads* I, II and III were defined in the following way (2), (3), (4):

$$V_I = \Phi_L - \Phi_R \quad (2)$$

$$V_{II} = \Phi_F - \Phi_R \quad (3)$$

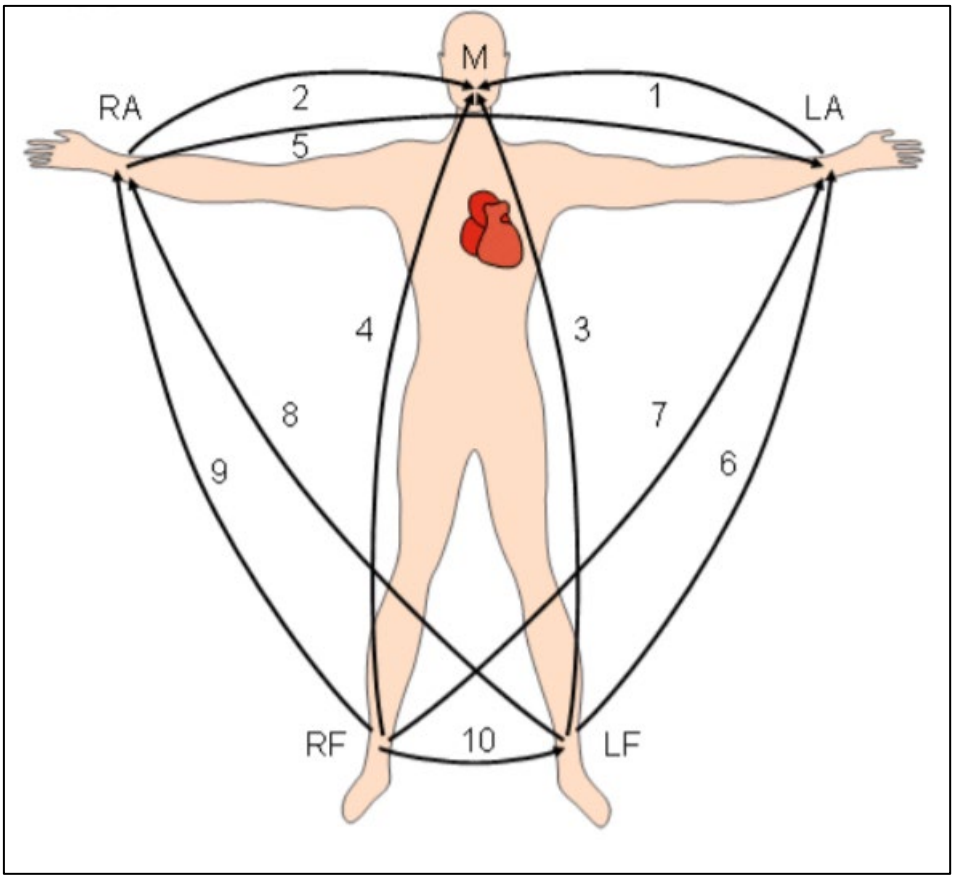

Figure 17. The ten ECG leads of Waller. RF: right foot; LF: left foot (equal to LL) [4].

$$V_{III} = \Phi_F - \Phi_L \tag{4}$$

where V_I, V_{II}, V_{III} are the voltage of Lead I (measured between LA and RA), II (between LA and LL) and III (between LL and RA) respectively, and Φ_L, Φ_R, Φ_F are the potential at LA, RA and LL respectively. The three leads, according to Kirchhoff's law, follow this relationship (5):

$$V_I + \mathrm{V}_{III} = \mathrm{V}_{II}. \tag{5}$$

Moreover, they were disposed, in the frontal plane, in an equilateral triangle (Einthoven triangle, Figure 18), upon which the heart vector, that lumps the electrical activity of the heart, is projected. This representation is very schematic, but all leads are equally sensitive: as the projections are dependent on the same heart vector, any change in direction of it would change the ECG amplitude in all the three leads [9].

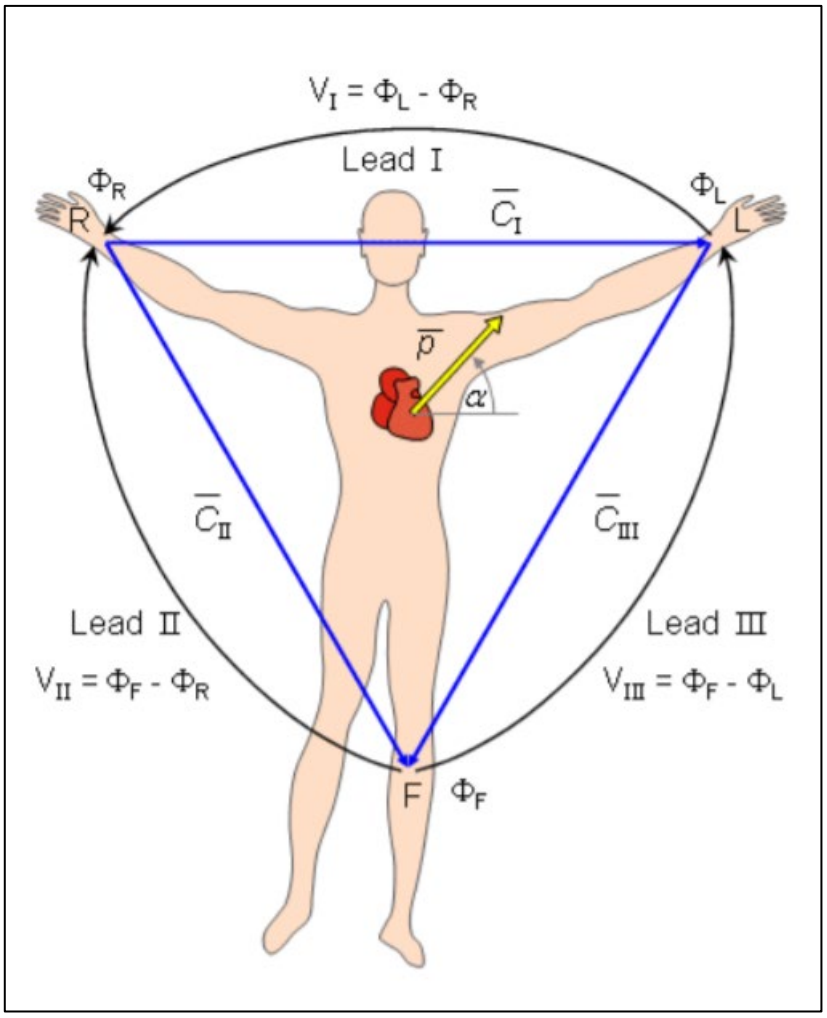

Figure 18. Einthoven's triangle. $\overline{C}_I$: Lead I; $\overline{C}_{II}$: Lead II; $\overline{C}_{III}$: Lead III [6].

Decades later, when the dipole concept had emerged, Ernest Frank developed a model of the torso, filled with conducting medium and covered by every possible electrode combination that could give ECG leads. This allowed to see what happened on the surface of the torso when the dipole varied in size and direction. Dutch physicist Herman Burger, then, perfected this model by introducing inhomogeneities in conduction due to the lungs: indeed, these deformations have consequences on what is measured at body surface. Burger also developed the idea that each ECG lead is associated with a lead vector. These lead vectors represent the directionality and the sensitivity, i.e. the magnitude, of the ECG leads. If we indicate the fixed lead vector with c, the ECG amplitude $V(t)$ could be written as follows (6):

$$V(t) = c \cdot p(t), \tag{6}$$

where $p(t)$ is the heart vector changing with time. Combining the lead vector concept with the new model of the torso, Burger elaborated a new triangle, where projections, compared to the Einthoven triangle, are skewed: lead vectors for Lead II and Lead III are longer than that of Lead I, meaning that the amplitude in the former leads has to be amplified (Figure 19). Burger triangle is not perfectly on the frontal plane, and its lead vectors are person-specific due to differences in the anatomy of the thorax in each individual. Standard ECG, however, implicitly uses simplified lead vectors.

In the meantime, during the 1930s, Frank Norman Wilson (1890-1952) elaborated a way to define *unipolar limb leads*, ideally obtained with respect to a remote reference located at infinite distance. He used a *central terminal* (CT), i.e. a 5 kΩ resistor located at the center of the Einthoven triangle and connected to each electrode of the limb leads (Figure 20). The central terminal potential was computed as the average of the limb potentials

$$\Phi_{CT} = \frac{\Phi_R+\Phi_L+\Phi_F}{3}. \quad (7)$$

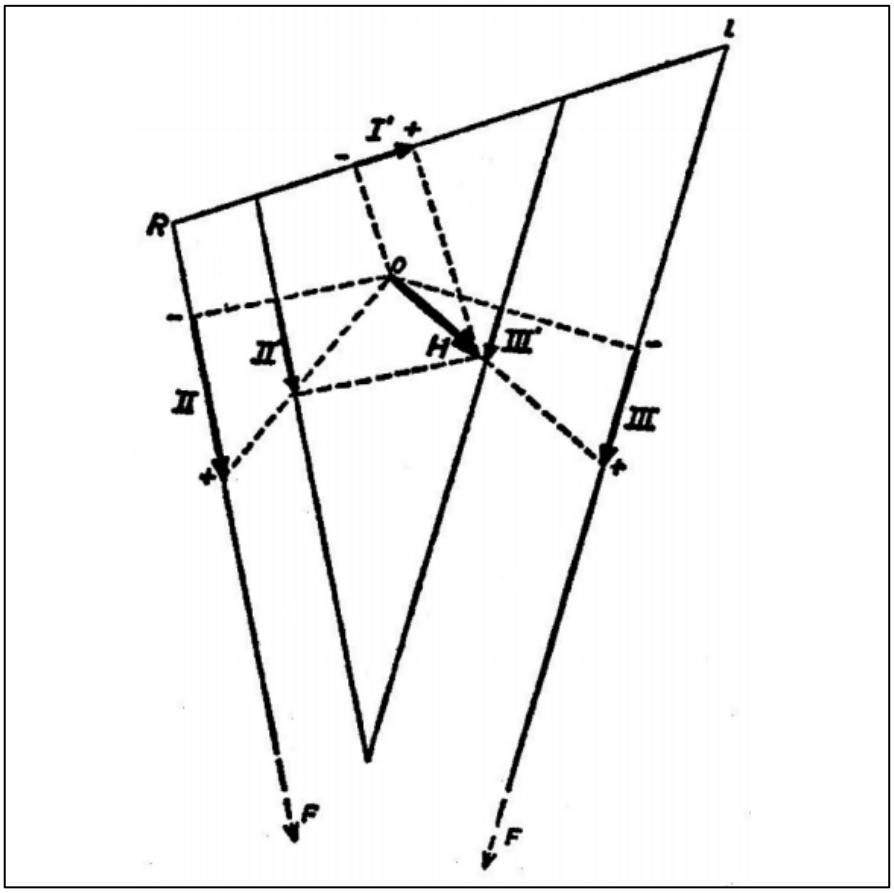

Figure 19. Burger's triangle. H: heart vector.

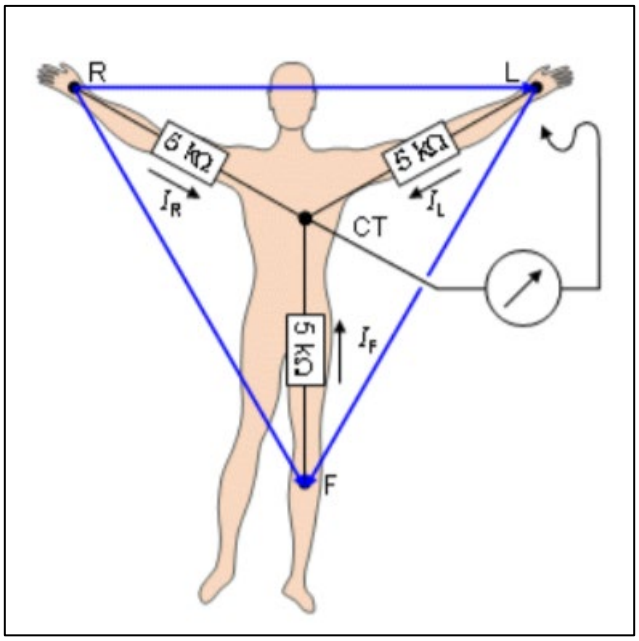

Figure 20. Wilson's central terminal. I_R: RA current; I_L: LA current; I_F: LL current [6].

Measuring the potential difference between each limb electrode and the central terminal, the three additional limb leads, V_R, V_L and V_F were obtained [10]. Then, in 1942, Emanuel Goldberger realized that the signals obtained could be augmented by neglecting the resistance from the central terminal. The new set of *augmented limb leads*, which name derives from the augmentation of the signal, were written in the following way (8), (9), (10) [11]:

- $aV_R = \Phi_R - \frac{\Phi_L + \Phi_F}{2}$ (8)
- $aV_L = \Phi_L - \frac{\Phi_R + \Phi_F}{2}$ (9)
- $aV_F = \Phi_F - \frac{\Phi_L + \Phi_R}{2}$ (10)

where aV_R represents the augmented lead referred to the right arm, aV_L represents the augmented lead referred to the left arm and aV_F represents the augmented lead referred to the left foot (Figure 21).

Finally, in 1944, Wilson proposed the use of *unipolar chest leads*, or *precordial leads*, to observe changes in potential close to the heart muscle. These leads are located as described below [12]:

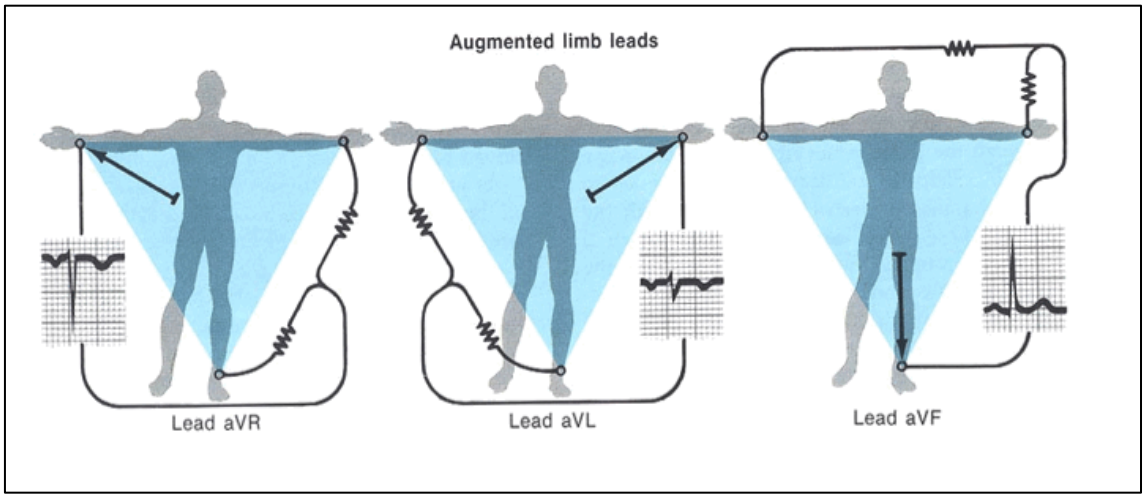

Figure 21. Augmented limb leads.

- V_1, in the fourth intercostal space and on the right side of the sternum;
- V_2, in the fourth intercostal space and on the left side of the sternum;
- V_3, between V_2 and V_4;
- V_4, in the fifth intercostal space at the midclavicular line;
- V_5, on the anterior axillary line and at the same horizontal level as V_4 and V_6;
- V_6, at the midline, aligned with V_4 and V_5 (Figure 22).

All the leads described so far, i.e. *bipolar limb leads*, *unipolar limb leads,* and *unipolar chest leads*, form the lead system for the *standard 12-lead ECG*. This system is vastly used in clinical environments and in resting conditions. Standard electrocardiography that can be carried out in clinical environments usually records all ECG leads simultaneously for a short time (10 s), and only parts of the ECG leads are displayed, except for a continuous, 10 s, rhythm strip following one lead only (Figure 23).

In exercise ECG, or also in ECG requiring longer recordings (24 to 48 hours), a configuration with modified electrodes' positions is preferred, in order to avoid distortions due to respiration, muscle activity and movements. One of these systems is the *Mason-Likar* extremity electrode positioning, very common in digital Holter recordings. Here, the extremity electrodes, normally placed on the wrists of right and left arm and left leg ankle, are moved under the right and left claviculae and at the left iliac crest, respectively, as, with standard placement, fingers motion would provide disturbances that cannot be interpreted. The precordial electrodes, instead, maintain the

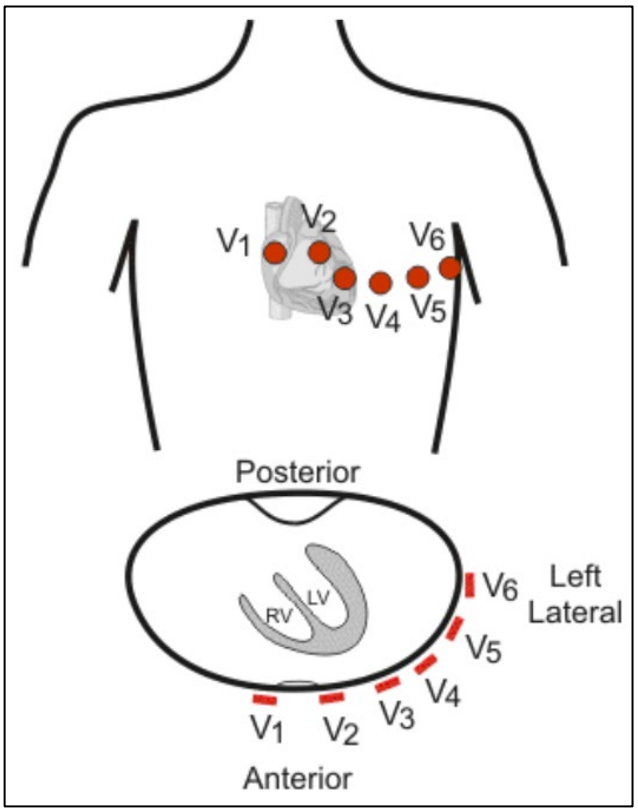

Figure 22. Unipolar precordial leads disposition. RV: right ventricle; LV: left ventricle [7].

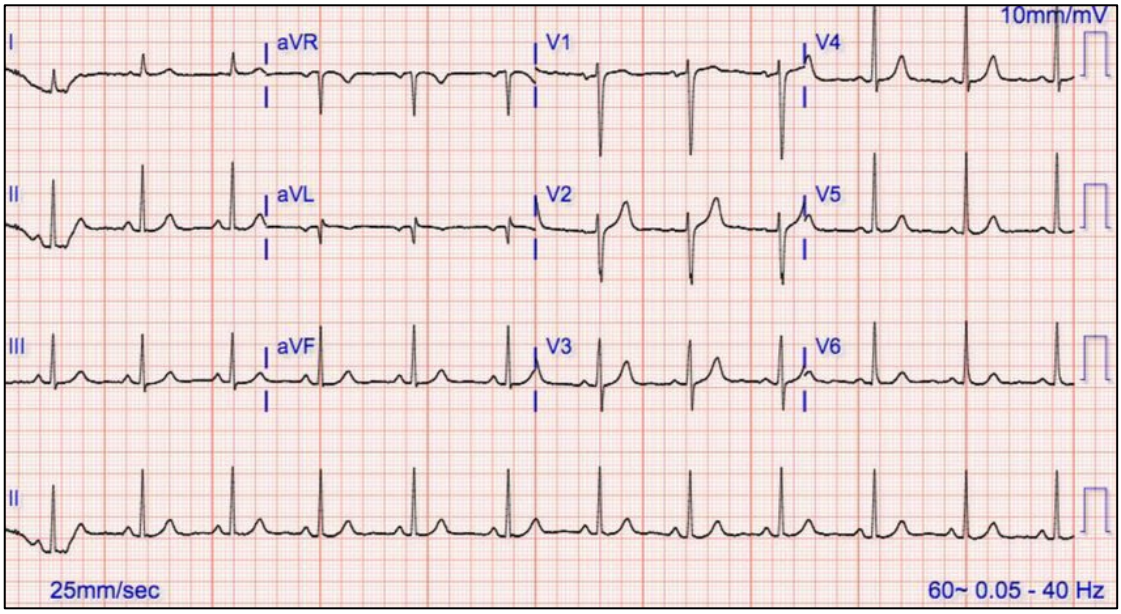

Figure 23. Example of normal sinus rhythm 12-lead ECG strip. The continuous rhythm strip is here given by lead II.

same position as in the standard 12-lead ECG (Figure 24). Despite the fact that part of the electrodes changes in position, ECG leads do not present much difference in form and amplitude from one system to the other, as electrodes are equipotential. However, it can be possible to observe higher QRS peaks in Mason-Likar "limb" leads compared to those in standard ECG [13].

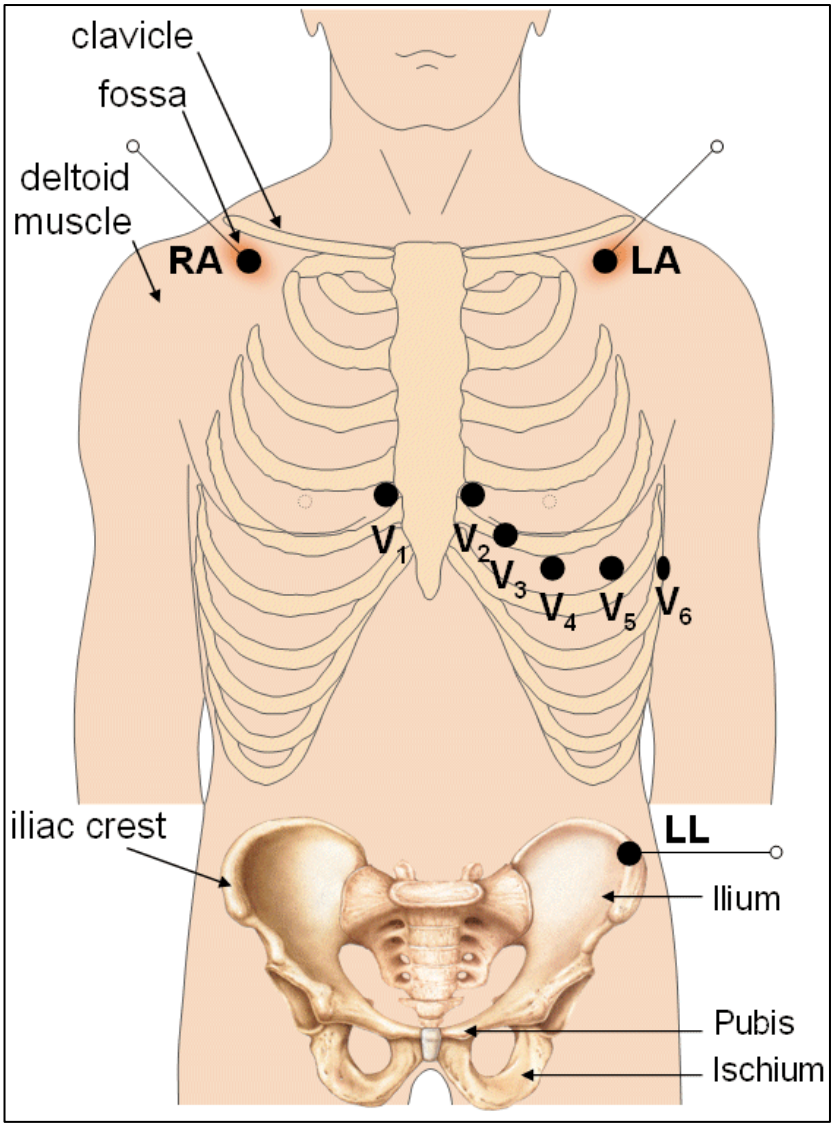

Figure 24. Mason-Likar electrodes placement.

3. CHAPTER 3: ELECTROCARDIOGRAPHIC ALTERNANS

In the previous chapter, the electrocardiographic signal has been described in all its components, i.e. P wave, QRS complex and T wave. As these waves depend on how depolarization and repolarization wavefronts propagate in the different chambers of the heart, their analysis may be able to identify the presence of pathologies affecting the cardiac muscle.

Pathological conditions, in fact, cause the cardiac APs to differ from those described in Chapter 1. As a consequence, since the ECG represents the lumped electrical activity of cardiac cells, variations in the APs will be reflected by morphological modifications of the ECG waveform. These modifications, or fluctuations, can be identified as electrocardiographic alternans, and their investigation, which is noninvasive, may lead to an early identification of heart diseases and prevention of possible death.

In this new chapter, we will delve into such electrocardiographic fluctuations, describing also alternans pertaining each wave composing the ECG.

3.1. T-wave alternans: definition, role and automatic methods for identification

The first kind of alternans here reported is the *T-wave alternans (TWA)*, described by Heinrich Ewald Hering in 1908 [14], [15]. It is defined as an electrophysiological phenomenon occurring at stable HR, characterized by beat-to-beat fluctuations, with an ABABAB pattern, of the morphology, amplitude, duration and polarity of the T-wave segment in the ECG (Figure 25). Such fluctuations are rarely directly visible and measurable from the ECG: in that case we would refer to macroscopic TWA. Microscopic or microvolt TWA (often simply identified as TWA), instead, seems to be more common. In both cases, anyway, TWA reflects spatiotemporal changes in cardiac AP repolarization that are linked to arrhythmias and intracellular ionic concentrations perturbations. In fact, it is possible to observe elevated TWA in cases of ventricular premature beats, coronary artery occlusion and reperfusion, long QT syndrome, mental stress, as well as increased HR. Increased HR largely affects TWA by altering intracellular Ca^{2+} handling between cytosol and sarcoplasmic reticulum. Moreover, reduced intracellular Ca^{2+} handling

Figure 25. Visual representation of TWA, with ABABAB pattern.

capability is often related to heart failure [16]. For this reasons, TWA is widely considered as a noninvasive and clinically useful index for cardiac pathologies that may lead to sudden cardiac death (SCD), and has been analyzed in several pathologies and conditions: elevated TWA was observed in partial epileptic patients [17], acute myocardial infarction patients [18], implanted cardiac defibrillator patients [19], as well as in fetal electrocardiography [20].

To investigate microvolt TWA, and also, at times, repolarization alternans (RA), i.e. a beat-to-beat alternation of the ST segment and T wave amplitude or morphology, different automatic methods have been developed. These methods are fundamental for the understanding and stratification of SCD risk, especially when alternans is identified for HR lower than 100 bpm (rest conditions): as TWA is HR dependent, it is easier to identify abnormalities and increased TWA at higher HR, without particular pathologies; TWA being present at lower HR, instead, indicates high SCD risk for the patient manifesting it [21], [22].

- *Fast Fourier transform spectral method*

  The Fast Fourier transform spectral method (FFTSM) was first introduced in 1988 by Smith et al [23] and subsequently modified by Rosenbaum et al [24] in 1994. According to this method, it is possible to identify beat-to-beat variations in the ECG repolarization segment by means of a spectral approach. First, all ECG repolarization segments are aligned and the power spectrum, i.e. the squared magnitude of the fast Fourier transform, is computed for each JT segment belonging to the tracings. The obtained power spectra are then summed into a cumulative spectrum, that will reach maximum amplitude, also called alternans

peak, at half of the cardiac cycle per beat (cpb). At this point, alternans ratio (AR) can be defined as (11)

$$\mathrm{AR} = \frac{\text{alternans peak} - \mu_{\mathrm{noise}}}{\sigma_{\mathrm{noise}}} \tag{11}$$

with μ_{noise} and σ_{noise} representing the mean and standard deviation of the spectral noise, estimated in noise windows belonging to the signals, respectively. If AR is greater than three, the alternans amplitude $\tilde{A}$ can be computed according to the following equation (12):

$$\tilde{A} = \sqrt{\frac{\text{alternans peak} - \mu_{\mathrm{noise}}}{N_s}} \tag{12}$$

where N_s is the number of samples of the JT segment. Determination of RA temporal distribution over the JT segments is provided by spectral decomposition. The area under the time-domain RA-magnitude curve obtained will have center of mass corresponding to the median RA magnitude [25].

- *Complex Demodulation method*

  The Complex Demodulation method (CDM), proposed by Nearing et al in 1991 [26], considers RA as a sinusoidal signal, with frequency f_{RA}=0.5 cpb, varying in amplitude and phase. Considering the ECG signals to study, their JT segments are divided into N_b groups of length equal to 10 ms. RR intervals belonging to these groups are used to define time series areas $X_b(n)$, with n=1, 2, …, N and b=1, 2, …, N_b. These time series areas are then filtered with a 16th order high-pass filter and subsequently modeled as a sinusoidal signal with amplitude $a_b(n)$ and phase $\varphi_b(n)$ that slowly vary and that can be represented in the following way (13):

  $$X_b(n) = a_b(n)\cos(2 \cdot \pi \cdot f_{RA} \cdot n \cdot \varphi_b(n)). \tag{13}$$

  $X_b(n)$ is multiplied by two times a complex exponential at alternans frequency and the result is filtered again, this time with a 16th order Butterworth low-pass filter with cut-off frequency corresponding to one fortieth of HR. In this way, only low-frequency components are preserved, and it is possible to write (14) and (15):

  $$Y_{b1}(n) = a_b(n) \cdot e^{j\varphi(n)} + a_b(n) \cdot e^{j(2\cdot\pi\cdot 2\cdot f_{RA}\cdot n\cdot\varphi(n))} \tag{14}$$

  $$Y_{b2}(n) = a_b(n) \cdot e^{j\varphi(n)}. \tag{15}$$

From the $Y_{b2}(n)$ equation, it is possible to obtain amplitude (16) and phase (17) of the alternans:

$$a_b(n) = |Y_{b2}(n)| \quad (16)$$

$$\varphi_b(n) = \tan^{-1}\left\{\frac{Im[Y_{b2}(n)]}{Re[Y_{b2}(n)]}\right\}, \quad (17)$$

with Im and Re representing imaginary and real parts of $Y_{b2}(n)$. These can finally be smoothed and the $a_b(n)$ are averaged over the N_b groups, in order to obtain the alternans associated to each JT segment (18) [25]:

$$A(n) = \frac{1}{N_b}\sum_{b=1}^{N_b} a_b\,(n) n = 1, 2, \ldots, N. \quad (18)$$

- *Modified moving-average method*

The Modified moving-average method (MMAM), developed by Nearing in collaboration with Verrier [27], is a vastly used method for TWA analysis, together with FFTSM, as both have been implemented for commercial machines. It is based on the distinction of two groups of beats, even, or beats A, and odd, or beats B, described by the following formulas (19) and (20):

$$\text{computed beat } A_m(p) = \text{computed beat } A_{m-1}(p) + \Delta_A \quad (19)$$

$$\text{computed beat } B_m(p) = \text{computed beat } B_{m-1}(p) + \Delta_B, \quad (20)$$

where m=1, 2, …, N/2, N is the number of type A or B beats analyzed and p is the sample point in a beat. Δ_A and Δ_B constitute instead noise correction factors, that take into account the morphology of the considered beats. Based on these equations, an estimate of the alternans can be obtained, computing first the difference between two consecutive beats, even and odd, and then evaluating the maximum of such difference (21):

$$A(m) = \max_{p=\text{JT onset}}^{p=\text{JT offset}} |\text{computed beat } A_m(p) - \text{computed beat } B_m(p)|. \quad (21)$$

Averaging the A(m) values (22), we have [25]:

$$\tilde{A} = \frac{1}{N/2}\sum_{m=1}^{N/2} A(m). \quad (22)$$

- *Laplacian likelihood ratio method*

The Laplacian likelihood ratio method (LLRM) was proposed by Martínez et al [28] and aligns the N ECGs that have to be analyzed, computing the difference between the nth JT segment, with n=1, 2, …, N, and the previous JT segment,

named $y_n(p)$. As each JT segment is constituted by N_s samples, $y_n(p)$ will be an $N_s \times 1$ row vector. Moreover, in order to consider every possible RA, the JT segments difference is computed on sliding windows of length L=32 beats. The matrix obtained from this process, with dimensions $N_s \times L$, will be (23):

$$Y_n = \left[y_{n-\frac{1}{2}}, \ldots, y_n, \ldots, y_{n+\frac{1}{2}-1}\right]. \quad (23)$$

Considering the Laplacian noise, Y_n is modeled according to the following equation (24):

$$Y_n = v_n e^T + W_n, \quad (24)$$

with $v_n = [v_n(0), \ldots, v_n(N_s - 1)]^T$ being the alternans-waveform matrix of dimension $N_s \times 1$, $e = [(-1)^0, \ldots, (-1)^{L-1}]^T$ alternans vector of dimension $L \times 1$ and $W_n = \left[w_{n-L/2}, \ldots, w_{n+L/2-1}\right]$ noise matrix of dimension $N_s \times L$ with samples modeled on the Laplacian distribution. At this point, the maximum estimate of v_n, identified with $\tilde{v}_n$, can be computed for each sample point p (p=0, 1, …, $N_s - 1$) as follows (25):

$$\tilde{v}_n(p) = \text{median}\left(\left\{y_{n+1}(p)(-1)^i\right\}_{i=-\frac{L}{2}}^{\frac{L}{2}-1}\right). \quad (25)$$

$\tilde{v}_n(p)$ will then be used to compute the alternans amplitude estimate for each n beat according to the equation (26):

$$A(n) = \sqrt{\frac{1}{N_s}\sum_{p=0}^{N_s-1}\tilde{v}_n^2(p)}. \quad (26)$$

This value is therefore computed as the mean of all A(n) over the beats [25].

- *Heart-rate adaptive match filter method*

  The Heart-rate Adaptive Match filter (HRAMF) is a popular and robust method, proposed by Burattini et al [29], for TWA analysis. This method takes into account the fact that TWA is characterized by a single frequency f_{TWA}, corresponding to half HR. However, also physiological variations of the HR, and therefore of the RR intervals, have to be considered: for this reason, the HRAMF assumes TWA to be characterized by a narrow frequency band centered around f_{TWA}.

Based on this consideration, the HRAMF is constituted by a 6th order bidirectional Butterworth band-pass filter, with passing band $2 \cdot df_{TWA}$= 0.12 Hz, centered in f_{TWA}. More specifically, it can be thought as a cascade of a low-pass filter with cut-off frequency equal to $f_{LPF} = f_{TWA} + df_{TWA}$, (with df_{TWA}= 0.06 Hz) and a high-pass filter with cut-off frequency $f_{LPF} = f_{TWA} - df_{TWA}$ (Figure 26). The squared module of the HRAMF transfer function will be defined as (27):

$$|H_{AMF}(f)|^2 = |H_{LPF}(f)|^2 \cdot |H_{HPF}(f)|^2 = \frac{1}{1+\left(\frac{f}{f_{LPF}}\right)^6} \cdot \frac{\left(\frac{f}{f_{HPF}}\right)^6}{1+\left(\frac{f}{f_{HPF}}\right)^6}. \quad (27)$$

Practical computerized applications involve the use of digital ECG recordings, so the HRAMF has also been designed to work in the digital domain. Analog filters have to be converted into digital filters in order to compute the digital HRAMF coefficients b_i and a_i, with i=0, 2, …, 6. Moreover, frequency adjustments have to be made, so that the digital filters will have the same frequency response at cut-off frequencies compared to the analog ones. Once all the adjustments are performed, the HRAMF transfer function will be (28):

$$H(z) = \frac{b_0+b_2z^{-2}+b_4z^{-4}+b_6z^{-6}}{1+a_1z^{-1}+a_2z^{-2}+a_3z^{-3}+a_4z^{-4}+a_5z^{-5}+a_6z^{-6}} \quad (28)$$

with b_i and a_i coefficients depending on HR and sampling frequency (a_1= a_3= a_5=0). The filter, as already mentioned, is applied bidirectionally, in order to avoid distortions caused by non-linearity of the phase response. Its results will be a vector containing TWA amplitude values computed for each beat and a sinusoidal signal, corresponding to the TWA signal, that has the same length of the processed ECG, frequency equal to f_{TWA} and maxima and minima falling inside the ST segment and T wave, if TWA is present (Figure 27). If the maxima and minima points fall outside the repolarization segment, i.e. we are in the presence of alternans of another ECG wave, TWA amplitude values are set to zero. Finally, if the ECG is not affected by alternans, the TWA signal output will correspond to a zero-constant signal [25], [30], [31].

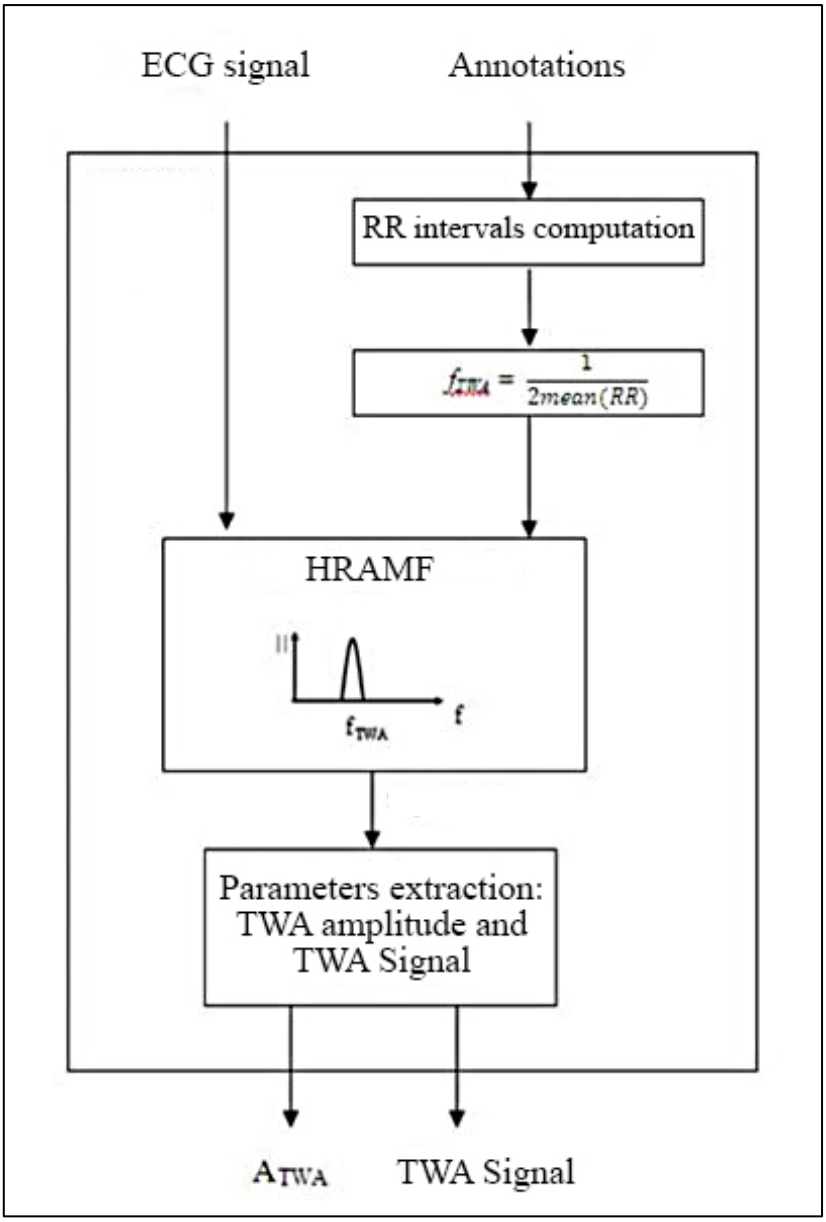

Figure 26. Block scheme of the HRAMF method. A_{TWA}: TWA amplitude.

3.2. P-wave alternans: definition, role and automatic methods for identification

Similarly to TWA, *P-wave alternans (PWA)* can be defined as beat-to-beat alternations of the morphology, amplitude, duration and polarity of the P wave, i.e. the ECG wave related to atrial depolarization [32]. Therefore, it reflects changes that may occur at the level of the depolarization wavefront travelling from the SA node towards the AV node and can serve as an index for pathologies affecting the atrial chambers.

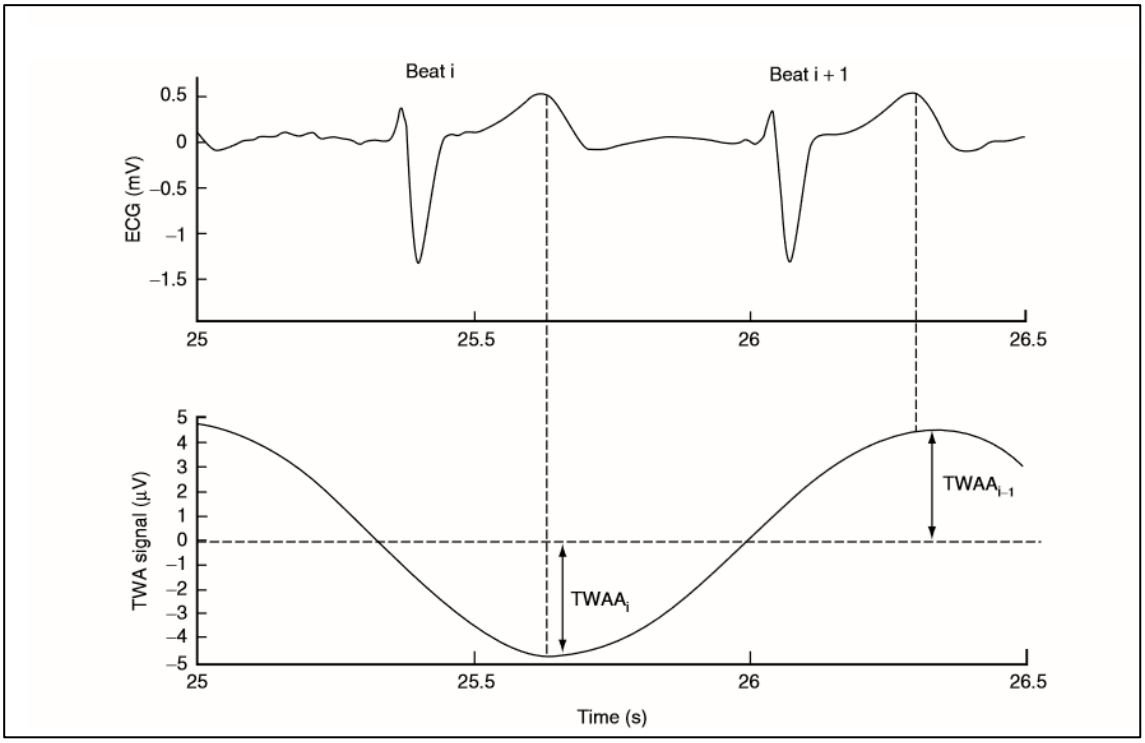

Figure 27. Comparison between the original ECG signal given as input to the HRAMF and the TWA Signal obtained. Maximum and minimum point of the sinusoidal signal correspond to the T wave in the original ECG. TWAA: TWA amplitude [19].

Despite its role, PWA has not been investigated in depth during the years, as greater focus was mostly given to ECG segments regarding ventricular activity. For this reason, and also to the best of our knowledge, PWA alone has never even been studied by means of automatic methods. Any automatic method applied for analysis of the P wave only examined P wave detection and delineation. One example is given by a special phase free wavelet transformation that was, in fact, applied on intracardiac electrograms and surface ECGs for P wave detection [33]. Other cases available in literature dealt with manual measurements, by means of calipers and magnifying glass, as PWA was already visible from the ECG ambulatorial recordings: examples are given by a patient affected by hyponatremia, i.e. Na^+ concentrations in blood being abnormally low [34] and a woman presenting atrial flutter (always preceded by PWA) [35]. Another case report analyzed PWA in a child with extreme pulsus alternans via doppler echogram [36].

3.3. QRS alternans: definition, role and automatic methods for identification

QRS alternans (QRSA) can also be described as alternations of the morphology, amplitude, duration and polarity of part of the ECG, in this case the QRS complex, i.e. the wave representing the electrical activity associated to ventricular depolarization. Given its definition and its relationship with ventricular activity, QRSA received major attention compared to PWA (although still less than TWA), and has therefore been used as an index for the detection of supraventricular and ventricular tachycardia [37].

The increased consideration can be also proved by the fact that, not only manual methods, but also automatic methods have been used for the evaluation of QRSA. Indeed, FFTSM was applied for QRSA analysis in [35]: the authors evaluated the presence of QRSA during episodes of ventricular tachycardia on recordings coming from an unselected collection of spontaneous tachycardia events. For each episode, series of 16 or 32 successive QRS complexes were retrieved. On these series, FFTSM was then performed. Following studies in 2010 [38] and 2012 [39] performed QRSA analysis, together with TWA analysis, during stress ECGs and in the presence of diabetes mellitus, by means of Principal Component Analysis (PCA), an adaptive technique usually employed to reduce the dimensionality of large datasets with variables not defined a priori, applied in these cases after QRS complex and T wave onset and offset detection [40]. A recent study published in 2020 also investigated QRSA and TWA, using a previously validated custom FFTSM, to understand how these may reflect cardiomyopathy and ventricular arrhythmia effects, as well as how QRSA and TWA interact with one another. The alternans classification proposed to study this interaction suggested that QRSA can be found and can predict late occurrence of ventricular arrhythmias independently from TWA, as TWA magnitude is rate dependent with respect to QRSA. The authors, however, later implied that QRS complex changes may be influenced by changes in the T wave (both QRS complex and T wave pertain ventricular activity), as QRSA magnitude was greater in the presence of TWA [41].

3.4. Electrocardiographic alternans identification methods

As previously mentioned, PWA and QRSA prompted limited interest compared to TWA, as TWA was soon recognized as a useful index to predict malignant arrhythmias and SCD, and several studies and automatic methods were devoted to its analysis. However, TWA reflects only the electrical activity of ventricular heart cells in condition of repolarization. As a consequence, the vision obtained on the summed APs activity with TWA analysis only may be partial. Both depolarization and repolarization changes in the different parts of the heart should be thoroughly investigated to properly detect anomalies and pathologies that may affect the well-being of individuals.

For this reason, the concept of *electrocardiographic alternans (ECGA)* was finally introduced at the beginning of 2020 by Marcantoni et al. It was first described as an electrophysiological phenomenon consisting in beat-to-beat variations of the morphology (amplitude, shape, polarity) of an electrocardiographic waveform, i.e. P wave, QRS complex or T wave, at stable HR. In particular, it could be seen as the prevalent nature of electrical alternans, i.e. PWA, QRSA or TWA [2].

In the study by Marcantoni et al, ECGA was studied on simulated ECG tracings, altered by the application of uniform rectangular waves to model alternans, by means of the HRAMF method. The HRAMF, originally designed for TWA, was, in this case, adapted to PWA and QRSA detection as well, preserving the same theoretical approach as before. In fact, the filter still assumed ECGA frequency to be a narrow band centered around half of mean HR (Figure 28) and returned as output a sinusoidal signal with maxima and minima located in correspondence of the ECG wave manifesting alternans: if located over the P wave, ECGA was defined as PWA; if over the QRS complex, ECGA corresponded to QRSA; if over the T wave, ECGA was defined as TWA (Figure 29) [2].

A much more recent study by Marcantoni et al, published in September 2020, applied such method for ECGA analysis on a 54 year-old patient affected by myocardial bridge, congenital heart condition in which the myocardium overlaps a coronary artery, therefore acting as a “bridge”, instead of being physiologically positioned underneath the artery. However, the prevalent alternans was, in this case, defined by means of PWA, QRSA and

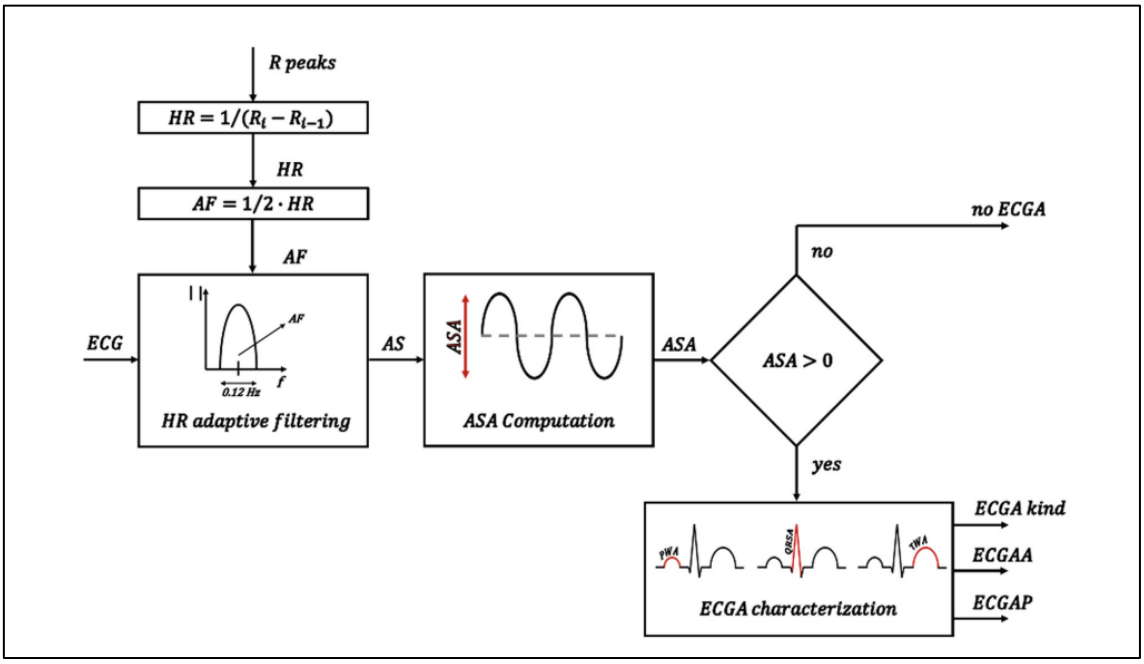

Figure 28. Block scheme of the HRAMF adapted for ECGA. As output, it will return the sinusoidal signal indicating the alternating waves, as well as the alternans amplitude and position. R_i: generic R peak; AF: ECGA frequency; AS: alternans signal; ASA: AS amplitude; ECGAA: ECGA amplitude; ECGAP: ECGA position [2].

TWA areas, computed as the product of the alternating wave and wave width: the prevalent alternans was characterized by the highest value in area [42].

Nowadays, the given interpretation of ECGA is changing. Rather than considering ECGA as only the prevalent alternans among PWA, QRSA and TWA, it is being regarded also as an expression of the three types of alternans. If we consider, in fact, cardiac alternans as an event happening at cellular level, ECGA can be considered as beat-to-beat fluctuations of the ECG signal, which comprehends the total activity of the heart. Obviously, this implies the necessity to have a reliable quantification of all alternans, devoid of reciprocal influence.

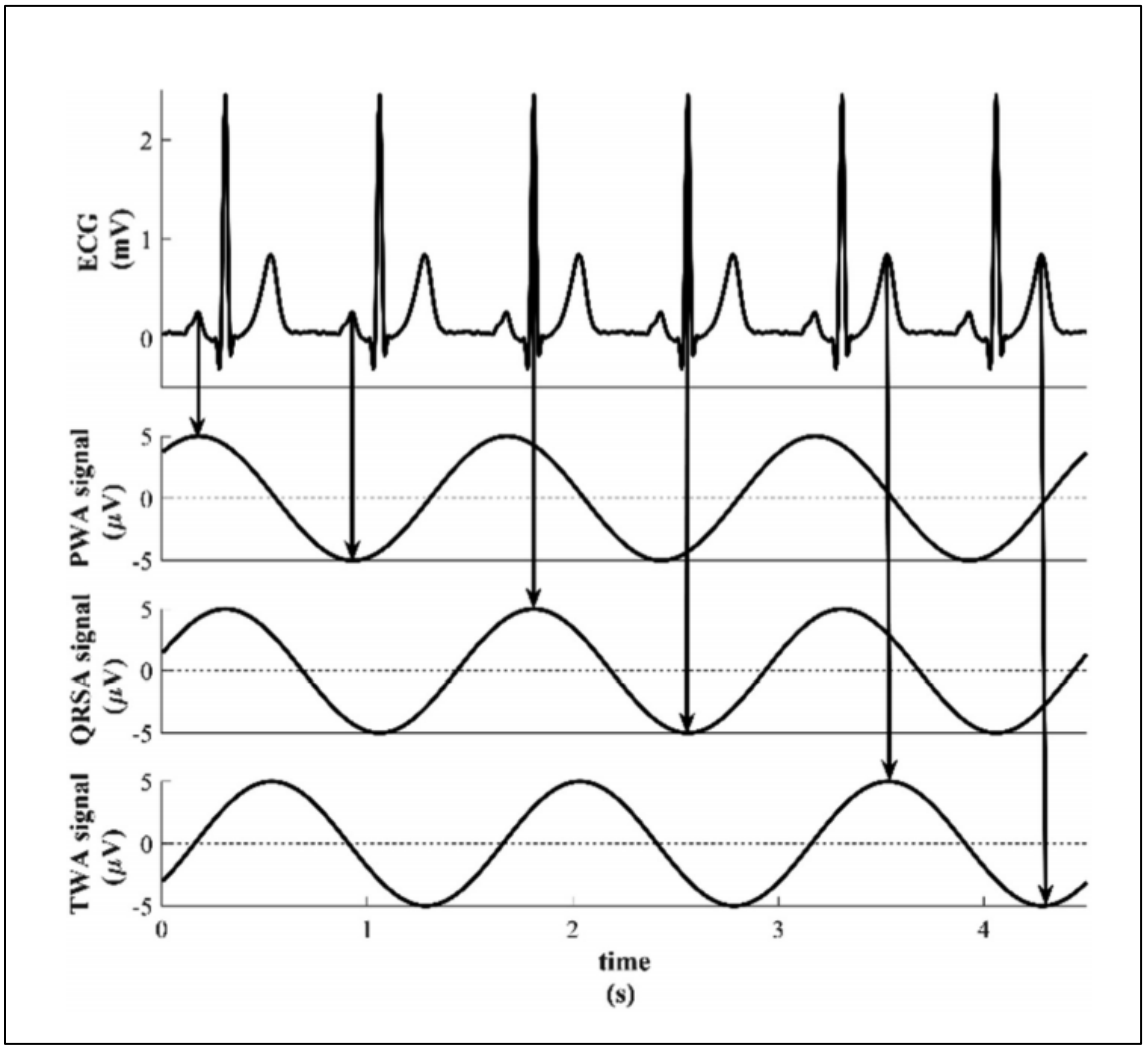

Figure 29. Sinusoidal signals for PWA, QRSA and TWA. Depending on the type of alternans, maxima and minima of the sinusoid will correspond to the alternating wave [2].

4. CHAPTER 4: URINARY SYSTEM

After describing in depth the cardiovascular system, the ECG and the possible changes that the ECG itself can encounter in terms of alternans, it is now time to delve into the urinary system. It is perhaps one of the most underappreciated apparatuses of our body, despite the several functions that it covers and that will be described in this chapter [4].

The urinary system is composed by:

- two *kidneys*;
- two *ureters*;
- the *urinary bladder*;
- the *urethra* (Figure 30).

Inside the kidneys, *urine* is produced, as a result of blood being filtered from toxins and wastes that have to be eliminated from the body. Urine then flows through the ureters, tubular structures that will bring urine to the bladder, where it will be stored until it is time for excretion. Finally, it is expelled from the body via the urethra [3], [4].

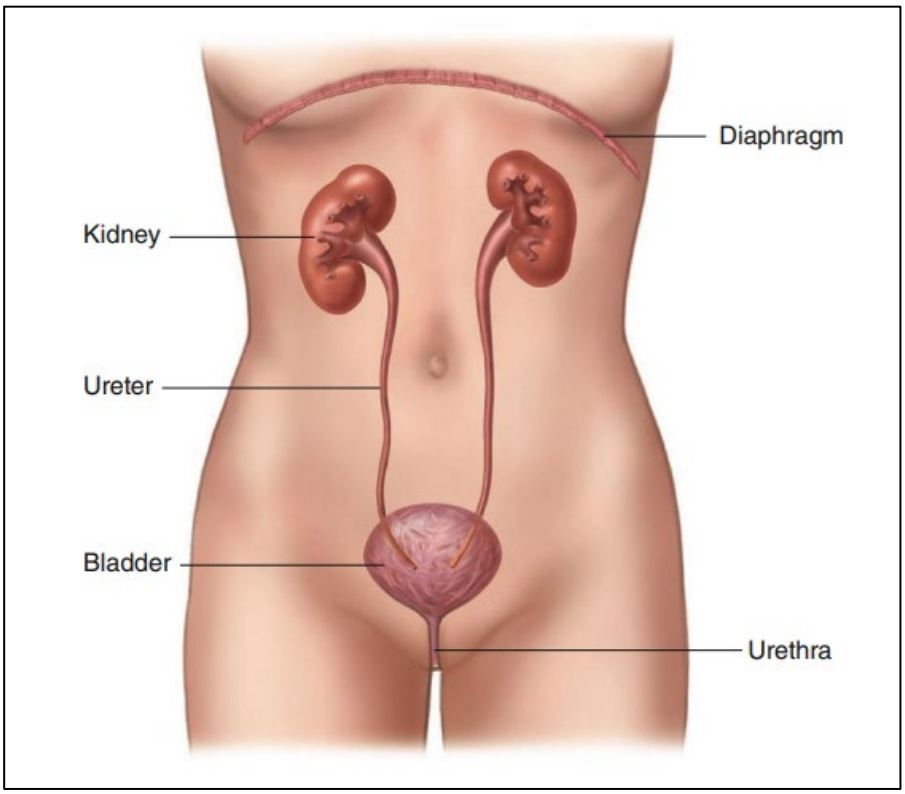

Figure 30. Urinary system [5].

For our purposes, we will concentrate in particular on the kidneys role, describing their anatomical structure first, and then venturing into the functions they absolve and how pathological conditions may affect them.

4.1. Anatomy of the kidneys

The kidneys are bean-shaped organs, about the size of a fist and weight of 115-170 g, lying in contact with the rear abdominal wall, at the level of the 12th rib and vertebrae T12-L3, thanks to collagen fibers. Precisely, they are located between the peritoneum and the abdominal cavity wall: for this reason, they are often described as retroperitoneal. The right kidney is usually in a lower position compared to the left one, to make space for the right lobe of the liver [3].

They receive blood coming from the renal arteries, that constitute branches of the aorta inside the systemic circulation. Renal arteries, and therefore arterial blood, enter the kidneys at the level of the renal hilum (a fissure which also receives nerves). Blood rich in oxygen, flowing at a high rate, is fundamental for the filtering action of the kidneys. Then, always from the hilum, blood that is cleared from wastes is returned into systemic circulation via renal veins, that will merge into the inferior vena cava [4].

From a macroscopic point of view, the kidneys are first protected by three layers of connective tissue:

- the *fibrous renal fascia*, layer that combines frontally with the peritoneum and posteriorly with the lumbar fascia. This layer allows to keep the kidneys, as well as other organs connected to it, in the right position, i.e. adherent with the abdominal wall;
- the *perirenal fat capsule*, adipose tissue that serves as a cushion and contributes to keep the kidneys in position, at the same time;
- the *fibrous capsule*, third layer that encapsulates the kidneys, keeping them anchored to the hilum and protecting them from trauma and infections (Figure 31).

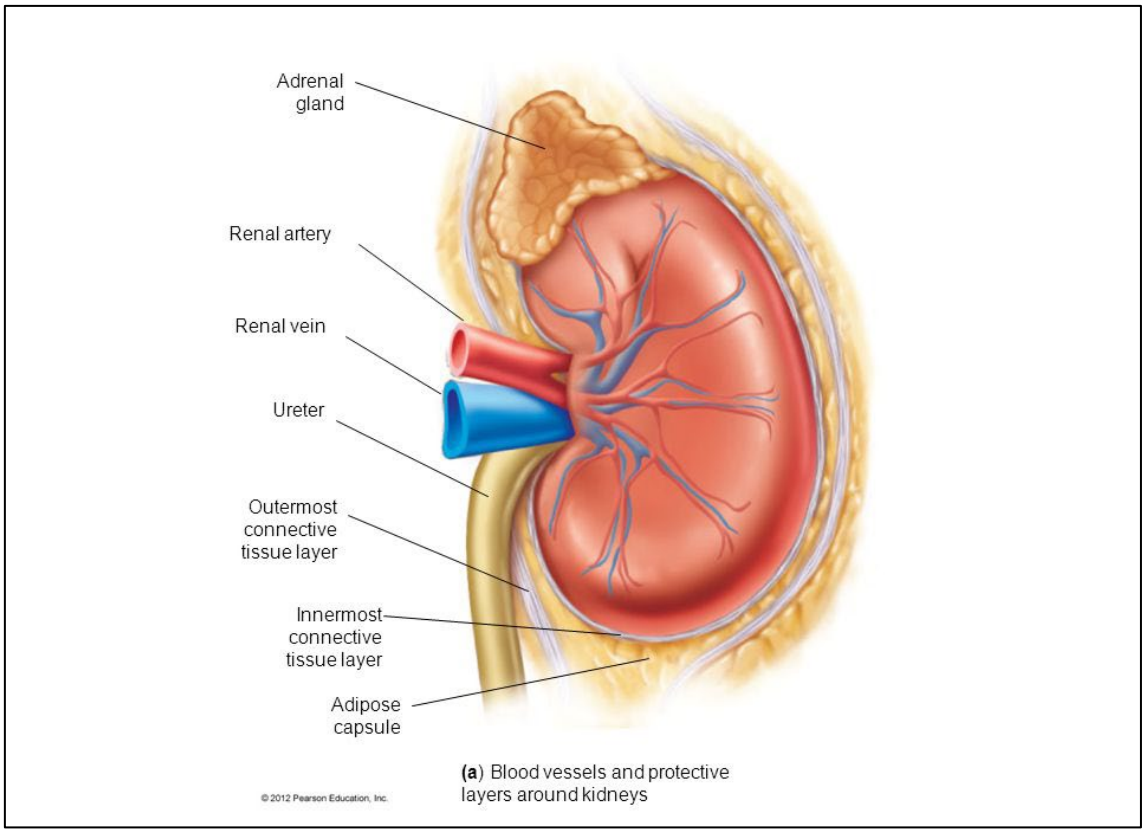

Figure 31. Kidney encapsulated by the three protective layers. The outermost layer corresponds to the fibrous renal fascia; the perirenal adipose capsule follows; finally the innermost layer represents the fibrous capsule.

We then encounter the *renal parenchyma*, glandular tissue that surrounds the renal sinus, a cavity filled with lymphatic, blood and nerve vessels as well as a urine collection system. The renal parenchyma can be divided into two main regions: a brown outer layer called *cortex* and a darker and striped inner region called *medulla*. Extensions of the cortex, called *renal columns*, reach into the medulla and divide it into 6-10 sections named *renal pyramids*. Renal pyramids have a conical shape, with a base directed towards the cortex and a tip, known as *papilla*, pointing towards the renal sinus. Each papilla then opens into tubules, that act as collecting ducts for urine, known as *minor calyces*. Two to three minor calyces usually converge into larger passageways called *major calyces*, that in turn converge into the renal sinus to form the *renal pelvis*, i.e. the initial section of the ureters (Figure 32) [3], [4].

Microscopically, each kidney is composed by approximately 1 million functional subunits that are called *nephrons* (Figure 32), that allow blood filtering and urine formation. Each nephron consists of two parts: the *renal corpuscle*, that filters blood, and the *renal tubule*, that modifies the filtrate into urine [3], [4], [5].

Inside the nephrons, at the level of both renal corpuscle and tubule, a series of three processes is actuated in order to produce urine:

1. *Glomerular filtration*. This process involves the filtration of liquid coming from the systemic circulation, removing wastes as well as chemical substances that are still useful for the body. The filtered liquid takes the name of glomerular filtrate, that, differently from blood, contains very few proteins and no cells. Once the glomerular filtrate passes into the renal tubule, its composition is soon modified into that of the tubular liquid;

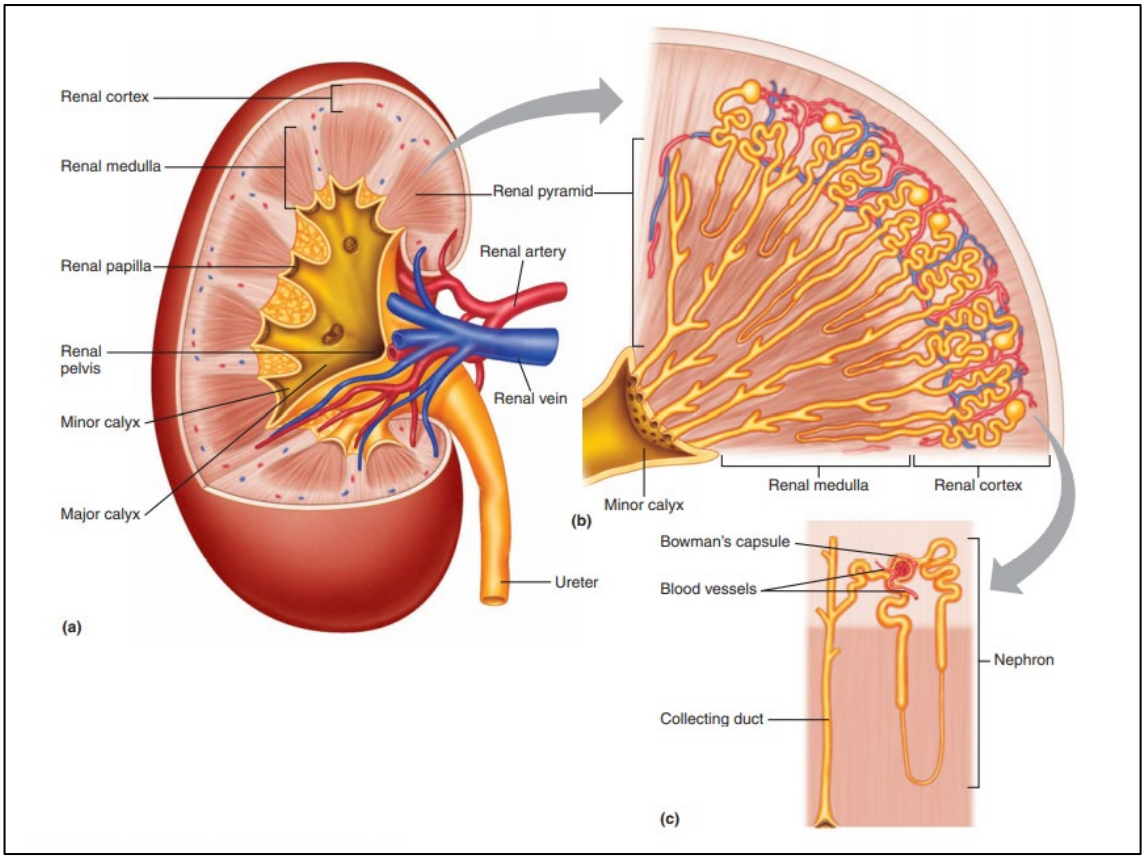

Figure 32. (a) Anatomy of the kidney. (b) Enlargement of a renal pyramid. (c) Magnified structure of a nephron belonging to the renal pyramid in (b) [4].

2. *Tubular reabsorption and tubular secretion*. These are two simultaneous processes that modify again the tubular liquid composition. Necessary substances, e.g. glucose, are reabsorbed and reintroduced into the blood stream. At the same time, hydrogen ions (H^+) and drugs, that need to be excreted via urine, are filtered from blood into the tubular liquid;
3. *Water conservation*. This process involves the reabsorption of variable quantities of water, that would otherwise be eliminated with metabolic wastes, from the tubular liquid, depending on needs. Without this process, mainly happening at the level of the renal tubule, the quantity of water lost in the form of urine would be excessive compared to the amount of blood (5 l) and water (about 40 l) actually contained in our body (Figure 33).

To be more precise about the location where these processes are actuated, it is possible to distinguish other structures that make up the renal corpuscle and tubule. The renal corpuscle is composed by a spherical structure at the end of the renal tubule that is called *Bowman's capsule* and a *glomerulus* of capillaries enclosed in it (Figures 33 and 34). Blood enters the glomerular capillaries via afferent arterioles and, there, it will undergo glomerular filtration. Specialized, octopus-like cells called podocytes, wrapped around the capillaries branching from the afferent arterioles and made of narrow filtration fissures, will contribute to the glomerular filtration process. Remaining blood will then leave the glomerulus via efferent arterioles [3], [4].

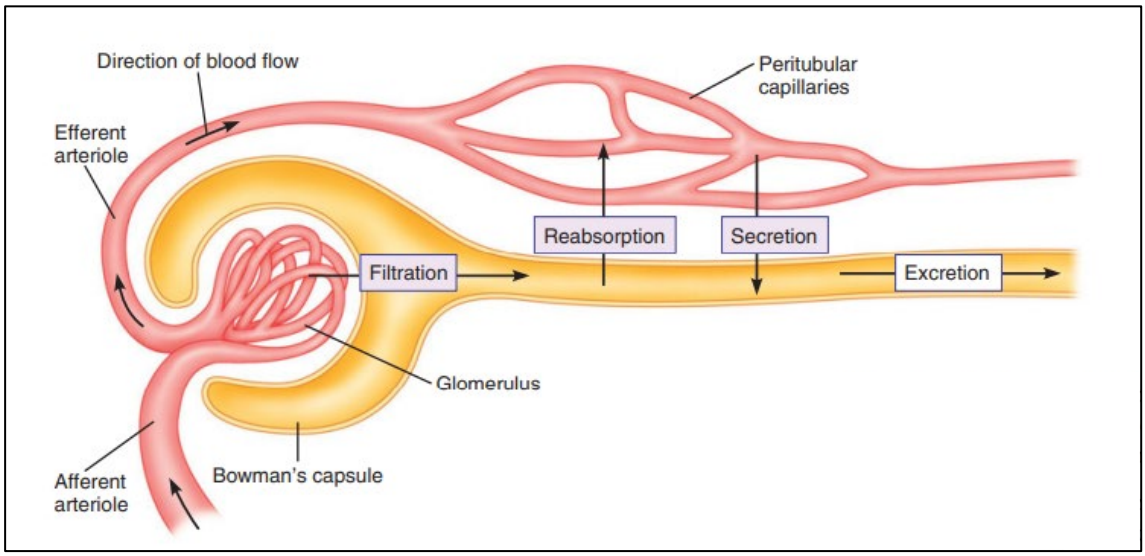

Figure 33. Depiction of the different functions carried out by a nephron [4].

The renal tubule finds its starting point at Bowman's capsule, and this initial portion takes the name of *proximal convoluted tubule*. The proximal convoluted tubule is responsible for the reabsorption and secretion process: in fact, about 65% of glomerular filtrate is here reabsorbed. A *proximal straight tubule* follows, forming, with the previous convoluted tubule, the *proximal tubule*. The proximal tubule then empties itself into the *loop of Henle*, a hairpin that is responsible, together with the proximal convoluted tubule, for reabsorption and water conservation. It is divided into descending limb, thin ascending limb and thick ascending limb. The ascending limb finally leads to the *distal convoluted tubule*, that represents the terminal portion of the nephron, connecting it with the collecting ducts of the minor calyces (Figure 34) [3], [4].

The loop of Henle can vary in length depending on the location of the nephrons: in fact, *cortical nephrons* and *juxtamedullary nephrons* can be distinguished. The majority of

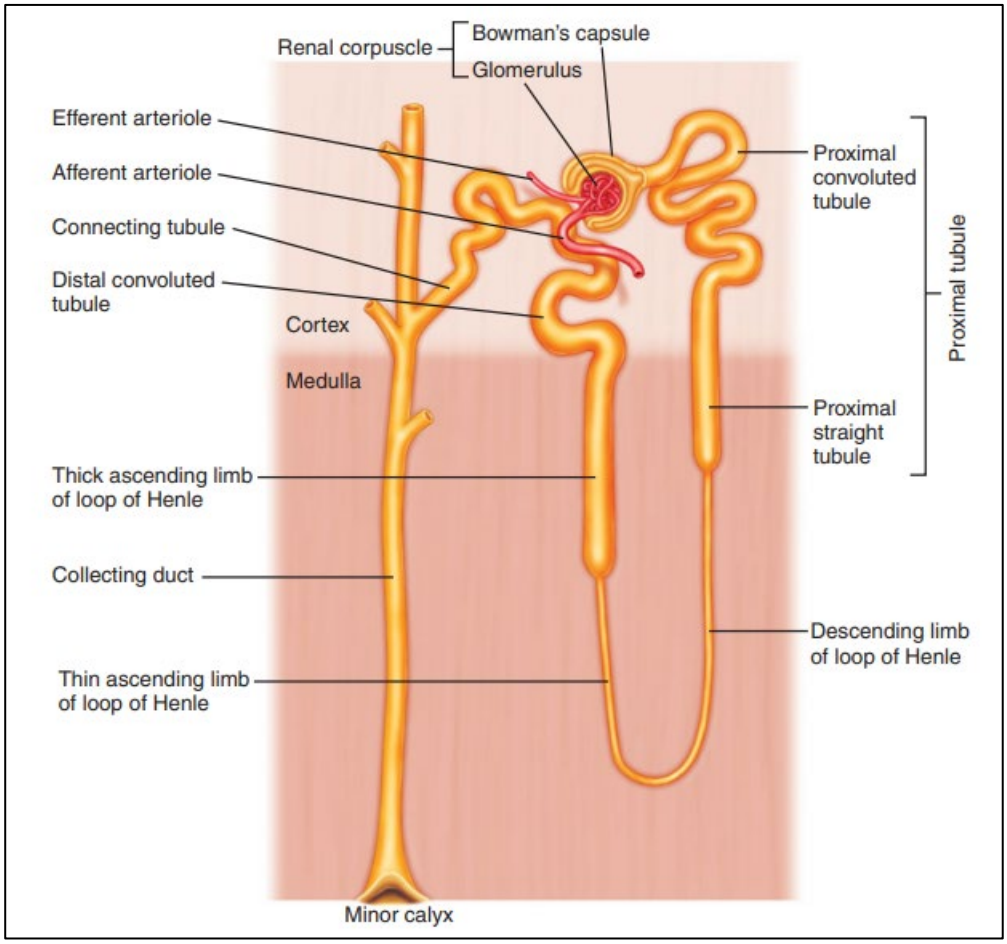

Figure 34. In depth representation of a nephron, where the whole structure going from the glomerulus to the loop of Henle is visible [4].

nephrons belongs to the former type, with the loop almost entirely contained in the renal cortex, except for the tip, that enters the medulla. The remaining nephrons (about 15-20%) belong instead to the latter group, with the loop of Henle going deep into the renal medulla: these ones are crucial for the production of highly concentrated urine and for water concentration [3], [4].

The distal tubule of the loop, at the site where it gets in touch with the afferent and efferent arterioles entering and leaving the nephron, gives rise to a structure called *juxtaglomerular apparatus*. This apparatus is composed by three types of specialized cells: epithelial cells, called *macula densa*, that work as sensors for the flux and composition of the tubular liquid; irregularly shaped macrophages called *mesangial cells*, that give structural support to the glomerular capillaries and regulate glomerular filtration; muscular cells called *juxtaglomerular cells*, that dilate and constrict arterioles and regulate arterial pressure via production of renin enzyme [3], [4].

4.2. Kidneys function

As mentioned at the beginning of this chapter, the kidneys are devoted to *excretion*, that is essentially the process involving the removal and elimination of wastes from body liquids, e.g. blood plasma, returning cleaned blood to systemic circulation. This is usually considered as the primary role absolved by the kidneys, but, in truth, kidneys are highly involved in several other functions, that have a significant impact on the regulation of body fluid volume and composition and that act in compliance with body needs. These additional functions they are involved into are:

- *Regulation of plasma volume and blood pressure*. Controlling the rate at which water is eliminated via urine, kidneys can regulate plasma volume, that has in turn an effect on total blood volume and finally on blood pressure;
- *Regulation of plasma osmolarity*. Kidneys also control the amount of water that is eliminated with respect to solutes, acting as regulators for the osmolarity, or solute concentration, in the plasma;

- *Regulation of plasma hydrogen ion concentration (pH)*. Kidneys, together with the lungs, contribute to the regulation of carbon dioxide and blood pH, modifying concentrations of bicarbonate, H^+, and acid-base balance in the plasma;
- *Secretion of renin enzyme*. Renin, also called angiotensinogenase, participates in the renin-angiotensin-aldosterone system, that regulates the volume of extracellular fluid, e.g. plasma, and arterial pressure;
- *Secretion of erythropoietin hormone*. Erythropoietin, mainly secreted in response to hypoxia, i.e. a lack of oxygen supply at tissue level, stimulates the production of red blood cells, increasing the capability of oxygen transportation via blood;
- *Contribution to the synthesis of calcitriol hormone*. Calcitriol, an active form of vitamin D, contributes to the homeostasis, or balance, of Ca^{2+};
- *Contribution to gluconeogenesis*. Gluconeogenesis represents the process in which glucose is produced from non-carbohydrate substrates, e.g. amino acids. In conditions of fasting, kidneys contribute to this process, helping with the maintenance of blood glucose concentrations inside normal ranges;
- *Regulation of plasma ionic composition*. Kidneys, increasing or decreasing the excretion of certain ions via urine, can regulate plasma concentrations of ions, e.g. Na^+, K^+, Ca^{2+}, as well as magnesium, chloride and phosphates.

Situations in which the functions here listed are compromised are dangerous for the affected individuals: it is important to remember how these processes, whether entirely performed by the kidneys or carried out in collaboration with other organs in our body, highly contribute to the global wellbeing of humans. It is therefore necessary to describe some of the most common pathologies that may affect the urinary system and in particular the kidneys [3], [4], [5].

4.3. Kidney diseases: chronic kidney failure

Kidney diseases represent certain types of “abnormalities” that can affect and decrease renal function. Unfortunately, many can be the causes for such abnormalities.

First of all, *congenital defects* can be possible: unsuccessful kidney development during the embryonic stage may compromise the classical, anatomical shape and position of the

kidneys. Incorrect development also at the level of bladder and ureters may cause urine reflux towards the kidneys, provoking infections and damages [4].

Other conditions can be inherited too. One example is represented by the polycystic kidney, characterized by the formation of cysts that enlarge over time, causing serious damage. Also kidney stones, that may cause severe pain, can sometimes be considered as inherited: this disorder, leading to excessive Ca^{2+} absorption from food, may cause urinary tract obstructions. Large stones will be surgically treated, either to be removed or to be broken down into small pieces that can be easily eliminated in natural ways. In this second case, lithotripsy, a particular ablation technique that uses shock ultrasound waves to destroy the stones, can be used. Moreover, diet and medications can help avoid their recurrent formation.

Diabetes, with its compromised production of insulin, is one of the leading causes of kidney disease, especially in western countries, e.g. United States. In fact, hyperglycemia, consequence of the inability to properly promote glucose intake by cells at the level of the liver, fat and skeletal muscles, can cause oxidative stress: it triggers vasodilation, necrosis factors and interferes with the junctions between tubule cells [4], [5].

Hypertension, i.e. high blood pressure, is also among the main causes of kidney failure. It increases glomerular hydrostatic pressure, producing shear stress on its vasculature. As a response, afferent and efferent arterioles dilate, contributing to increase even more the glomerular pressure and, as a consequence, glomerular filtration. With leaking capillaries, bigger solutes, e.g. proteins like albumin (present in blood plasma), will be eliminated via urine. The presence of albumin in urine is, therefore, one the first signs of pathology. Hypertension, as well as diabetes, can be kept under control with medications, but excessive quantities for a long time can be certainly harmful for the kidneys [4], [5].

Finally, traumas, hemorrhage and thrombosis can also contribute to the infection and disruption of the true glomerular structure of the nephrons, leading to *acute renal failure*, i.e. the sudden loss of renal function. Sometimes, depending on the pathology, e.g. transient events affecting the kidneys, function loss can be temporary: nephrons can either recover their function or, if irreversibly damaged, they can become hypertrophic, compensating renal function. When the function loss is not temporary, however, we are in the presence of *chronic kidney failure* [3].

Survival in chronic kidney failure is guaranteed until there is still more than one third of a single kidney working. When more than 75% of nephrons are compromised, homeostasis cannot be maintained, with possible development of acidosis, uremia and fluid stacking, and even anemia (since erythropoietin is produced by the kidneys, as seen in the previous paragraphs). This advanced stage of chronic kidney failure is usually identified as *End-Stage Renal Disease (ESRD)*. In this condition, intervention is of utmost importance, with one final solution being kidney transplant. If kidney transplant is not possible due to preexisting conditions or it is yet to be performed (the patient may be waiting for the right donor), a particular clinical procedure, called dialysis, can be used [3].

4.4. Consequences of kidney diseases

Untreated kidney disease can unfortunately lead ESRD patients to present several complications, most of which are often associated with increased risk of cardiovascular problems. This is legitimate, considering how both urinary and cardiovascular systems are strictly combined: blood, one of the main components of the latter, collects wastes coming from tissues at the periphery of the body and is purified inside the glomeruli, at the level of the nephrons, belonging to the former apparatus.

One of these possible complications is given by *anemia*: failing kidneys are not able to produce and secrete erythropoietin and, as a consequence, red blood cells production is greatly compromised.

Hypervolemia, i.e. the excessive buildup of fluids in the body, is also a common issue in individuals affected by kidney disease. Increased concentrations of Na^+, caused by considerable consumption of salty food, cannot be removed by the compromised kidneys. This causes discomfort and swelling at first, but can also lead, in advanced stages, to congestive heart failure, where the heart, due to fluid retention around it, is not able to efficiently pump blood into the arteries. Altered concentrations of Ca^{2+} are also linked to heart failure and can manifest themselves with increased TWA in the ECG.

Indeed, electrolyte disorders, that cannot be adjusted by failing kidneys, bring about changes in the shape of the cardiac APs, as Na^+, Ca^{2+} and K^+ intervene in different ways

into shaping the APs. *Hyperkalemia*, i.e. a common ESRD disorder in which extracellular K^+ concentrations are higher than physiological ranges ($[K^+]>5$ mmol/l), gives rise to APs with less negative resting potential. It also inactivates Na^+ channels, therefore reducing the upstroke of phase 0, i.e. depolarization phase, of the APs. This inactivation is generally compensated by Ca^{2+}, that allows to reach the threshold for the AP to be fired, although high Ca^{2+} (typical of hypercalcemia) shortens the plateau phase. Consequently, the rate of repolarization increases, and the resulting AP has shorter duration compared to a normal AP (Figure 35) [43]. The changes in AP are reflected by the ECG, that will present longer PR and QTc intervals: the P wave tends to flatten, and the QRS complex shifts towards the T wave and widens, indicating conduction delays; T waves will instead be narrow and tall-peaked (Figure 36) [44], [45]. In case of severe hyperkalemia, widened QRS complex and peaked T wave will merge into the so-called "sine wave" (Figure 37) [46].

Hypocalcemia, i.e. extracellular Ca^{2+} concentrations lower than physiological ranges ($[Ca^{2+}]<2.2$ mmol/l) is also frequently seen in settings of kidney disorders and in association with other electrolyte disturbances. Low extracellular Ca^{2+} decreases slow inward currents, as well as outward currents, during plateau phase, causing a prolongation of the AP duration and, consequently, a decrease in cardiac cells contractility. In the ECG, hypocalcemia is reflected by prolongation of the ST segment and QTc interval (Figure 38), as well as T wave alterations, consisting in upright or also low and flat T wave, or even inverted T wave in leads with upright QRS complex [46].

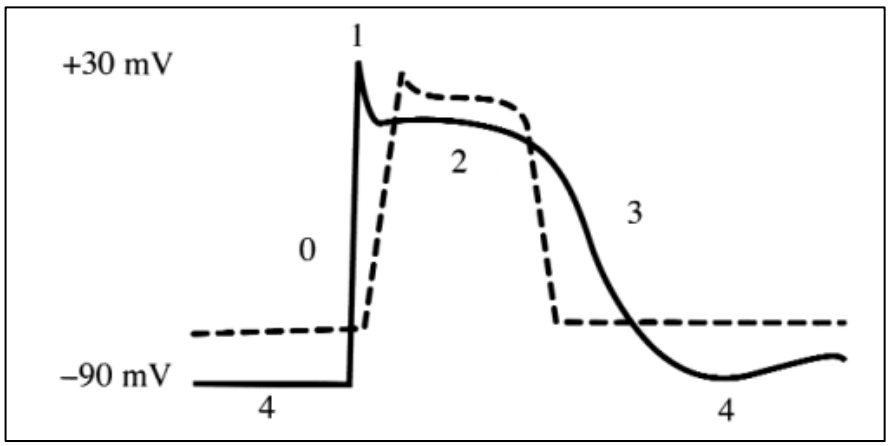

Figure 35. AP of a cardiac cell in case of hyperkalemia. Numbers represent AP phases.

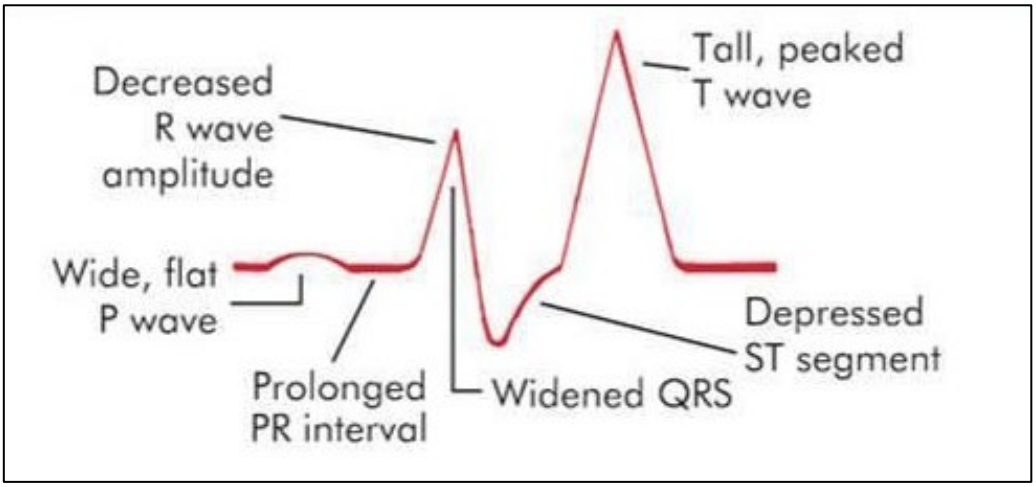

Figure 36. Example of ECG modifications in case of hyperkalemia.

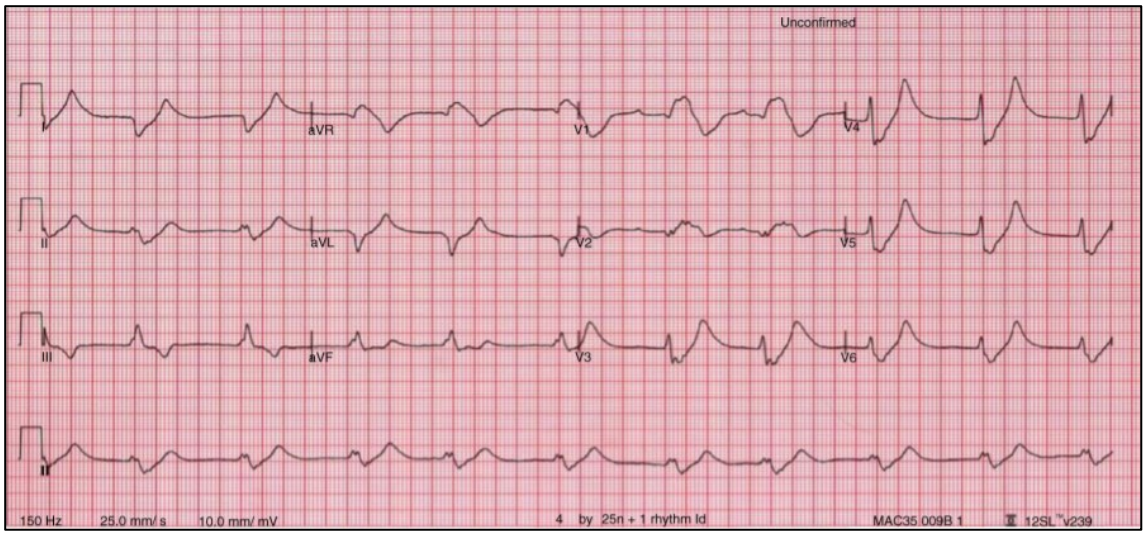

Figure 37. ECG showing QRS complex and T wave merging into the "sine wave", in the presence of severe hyperkalemia [46].

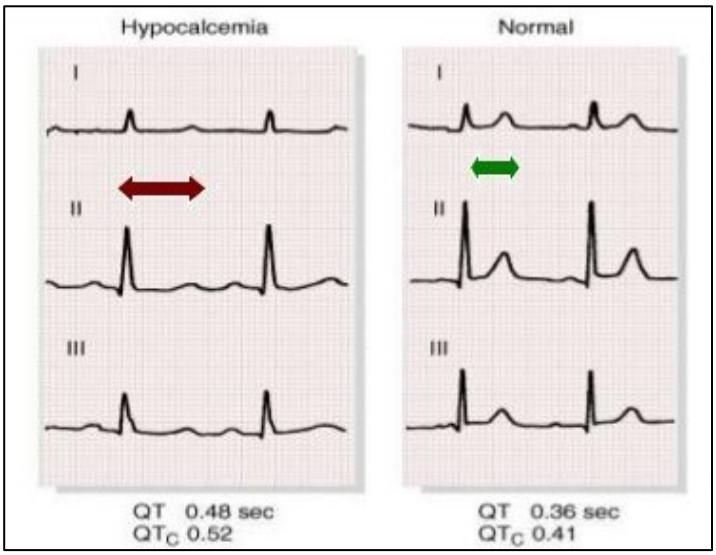

Figure 38. Example of ECG showing hypocalcemia consequences, i.e. longer QTc interval and ST segment, with respect to normal ECG.

5. CHAPTER 5: DIALYSIS

Dialysis, term deriving from Greek διάλυσις (dialysis, "dissolution": διά, dia, "through", and λύσις, lysis, "loosening or splitting"), represents a particular clinical treatment that was created in order to substitute kidney function and therefore avoid complications deriving from kidney failure (mentioned in the previous chapter), e.g. toxins and fluid accumulation, anemia and excessive loss of proteins.

Modern dialysis was first introduced during World War II by Dutch physician Willem Johan Kolff. In 1943, he built the first prototype of working “artificial kidney” (Figure 39), that was then used to successfully treat a 67-year old woman in uremic coma. The patient, after 11 hours of treatment, regained consciousness, proving how Kolff’s idea was indeed effective [47]. After World War II, the artificial kidney was redesigned in collaboration with Harvard’s Peter Bent Brigham Hospital in Boston, giving life to the stainless steel Kolff-Brigham dialysis machine, directly connected to the patient by means of surgical cannulas [48].

Kolff’s kidney, however, despite its effectiveness, was not able to eliminate excess of water in chronic kidney failure patients. For this reason, in 1946, Swedish professor Nils

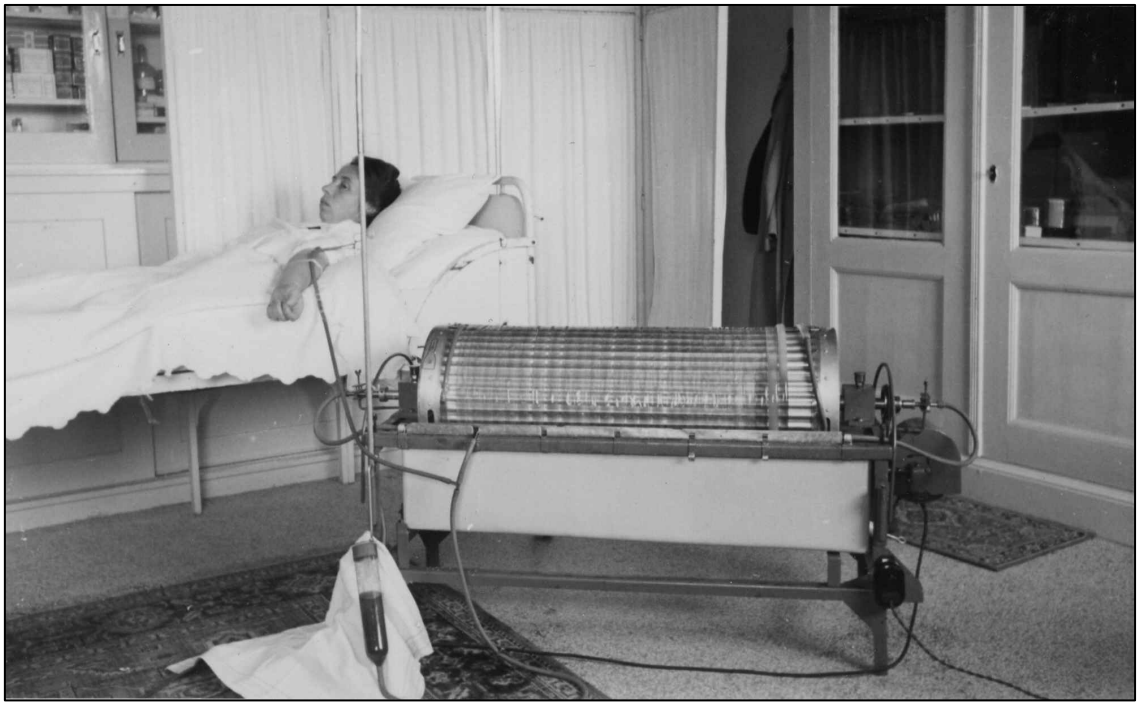

Figure 39. Kolff's artificial kidney.

Alwall enclosed a modified version of the artificial kidney inside a canister. To this canister, a negative pressure was applied, allowing *ultrafiltration*, i.e. the removal of excessive fluids, from treated patients. After that, Alwall also worked on the creation of an arteriovenous (AV) access, made of glass, that could be better paired with his machine [49].

Biomechanical engineers Wayne Quinton and Belding Scribner, in 1960, modified Alwall's glass AV access, employing new materials [50], [51]. Finally, in 1962, Scribner founded the world's first dialysis facility, the Seattle Artificial Kidney Center, now called Northwest Kidney Center.

From that moment on, dialysis has been constantly improving: if, at first, it was a treatment perceived as "exclusive" for those who could afford it and not entirely efficient, dialysis has become a safe therapy, easily accessible and available in different environments. Patients that undergo this treatment nowadays manage to live a relatively long life. This is also proved by the fact that the number of individuals who undergo dialysis treatment due to kidney failure is constantly increasing: if in 2010 2.62 million people received dialysis worldwide, this number is expected to double up by 2030 [52].

There are two main types of dialysis that can be performed, depending on the patient needs and conditions:

- *Hemodialysis*;
- *Peritoneal dialysis.*

We will describe both types in the next pages. However, considering our purpose, more focus will be given to the former type.

5.1. Hemodialysis

Hemodialysis (or haemodialysis, HD) consists in the extracorporeal removal of toxic wastes that are present in the blood, as well as ultrafiltration of excess fluids (Figure 40). Substituting in this way renal function loss, HD helps to keep blood pressure inside normal ranges and balance ionic concentrations, e.g. those regarding K^+, Na^+ and Ca^{2+}.

Figure 40. Person undergoing HD treatment.

ESRD patients undergoing this treatment are subjected to considerable physical stress, as they may present nausea, swelling, fatigue, buildup of wastes and high incidence of arrhythmias, that may be potentially life threatening. In fact, it has been observed that HD patients are at increased risk of SCD [53]. To limit the occurrence of complications, patients will need to take proper medications regularly, to control blood pressure and blood coagulation, and make considerable diet changes to limit fluid and mineral intake. It is however important to mention that HD does not constitute a definitive cure for kidney failure: it is either a temporary solution, in case of non-chronic pathology, or a lifelong treatment, in case of chronic pathology, unless kidney transplant is performed at a certain moment [3].

HD can be performed with different periodicity. Depending on that, HD can be classified in the following way:

- *Conventional or Standard HD*. It is commonly performed 3 times per week and has a duration of about 4 hours per treatment session. Blood is drawn from the

patient's body with a rate of 200-400 ml/min and the patients is exposed to increased quantities of water compared to healthy subjects;

- *Daily HD*. It is performed 6 times per week, for a duration of 2 hours. Despite the higher number of treatments during a week, it is usually regarded as a less stressful type of HD for the patient, because of its reduced duration. Nevertheless, it requires frequent AV access;
- *Nocturnal HD*. It is similar to Standard HD, although treatment session duration is increased, being close to 10 hours. As the name suggests, and also considering the treatment time stretch, each session is carried out during the night, while the patient is asleep.

Another classification can be made depending on where HD is carried out. In fact, it is possible to have:

- *HD at dialysis center*. Here, health care professionals and technicians set up the HD machine and connect it to the patient. Dialysis centers provide, for the most part, Standard HD treatment, although in recent years, Nocturnal HD has been made available as well, in order to meet patients' needs;
- *HD at home*. In this case, HD treatment can be self-managed or carried out with the help of trained personnel, e.g. a relative. This means that either the patient or the helper must be able to set up the home machine and prepare the vascular access site. The possibility to undergo treatment at home implies that patients may perform HD daily and for shorter hours.

5.1.1. Hemodialysis principle

The functioning of the HD machine is based on the principle of *diffusion*, i.e. a property pertaining substances dissolved in water.

In diffusion, solutes move from an area of high concentration to one of low concentration, therefore moving according to a concentration gradient. The compartments with different concentrations are usually separated by a semi-permeable membrane, that, given the size of its pores, only allows small solutes and fluid to pass in proportion to the gradient. After a certain amount of time, the two compartments, initially with different solutes

concentration, will have equal concentration, reaching a situation of equilibrium (Figure 41).

Applied to HD, the compartment with higher solutes concentration is represented by blood, that flows in contact with one side of the semi-permeable membrane. The compartment with lower solutes concentration is instead represented by the dialysis solution, also called *dialysate* (usually containing Na^+, Ca^{2+}, magnesium, chlorine and bicarbonate). Larger substances, e.g. red blood cells and large proteins, will remain in the blood, while smaller ions will pass through the membrane and reach the dialysate compartment. The filtering process here obtained will be equivalent to that operated at the level of the glomeruli in the kidneys [54].

Moreover, HD employs a counter-current flow between blood and dialysate. This helps maximizing the concentration gradient of the solutes and, consequently, removing extra minerals in an easier way. The dialysate composition also contributes to the diffusion of ions: it is in fact fundamental to tailor the dialysis solution according to the patient's needs. For example, the nephrologist may prescribe a dialysate with bicarbonate level higher than in normal blood, to favor the neutralization of acidosis, often present in ESRD patients. Other solutes concentrations may also be increased to prompt water movement away from blood, in case of edema [4].

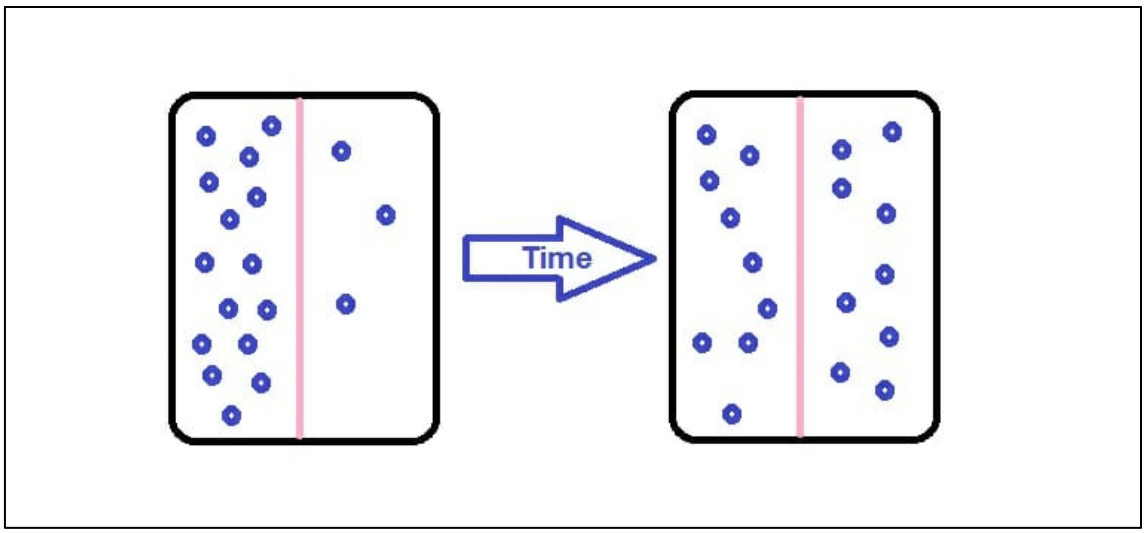

Figure 41. Visual representation of the diffusion process between two compartments with different solute concentrations, separated by a semi-permeable membrane.

5.1.2. Hemodialysis preparation and equipment

Prior to the beginning of the first HD, patients must be properly prepared for the treatment. The preparation consists in the surgical creation of a vascular access, or lifeline, that will allow the patient to be connected to the HD machine, usually by means of needles.

Vascular access can be of three types:

- *AV fistula*. It is a surgical connection between an artery and a vein, usually created at the level of the arm. Once the connection has been successfully performed and it has healed, the vein grows wider, allowing an easy placement of the HD needles. The bigger diameter, as well as the influence of arterial blood flowing with higher velocity and pressure, compared to venous blood, also allows blood to be drawn and reinserted into the body rather quickly. As the link is made between body tissues, and therefore it is less subjected to infections or blood clots, it is considered one of the safest and most stable vascular accesses;
- *AV graft*. This is also a surgical connection between artery and vein, but it is chosen when the two blood vessels are too small to form a fistula. As a consequence, the surgeon will link them by means of a flexible, synthetic tube, called graft. Compared to the fistula, the AV graft can be immediately used for HD soon after surgery, but it is also more inclined to infections and clots;
- *Central venous catheter*. It is a vascular access that is mainly used for emergency HD, consisting of a plastic tube that is temporarily inserted into a large vein, either in the neck or chest. From the central venous catheter, an external shunt will be made, inserting two cannulas that will connect to a large vein and a large artery, respectively. As mentioned for the AV graft, also the central venous catheter may become infected or obstructed by blood clots (Figure 42).

As soon as the vascular access site is healed, it is possible to proceed with the actual HD treatment. First of all, a set of needles and cellophane tubes will be connected to the patient: after the application of skin anesthetic, two needles, one carrying blood to the HD machine and one returning filtered blood to the body, will be inserted in the vascular access. Sometimes, also specialized needles designed with two openings can be used, although these are less efficient than the previous system.

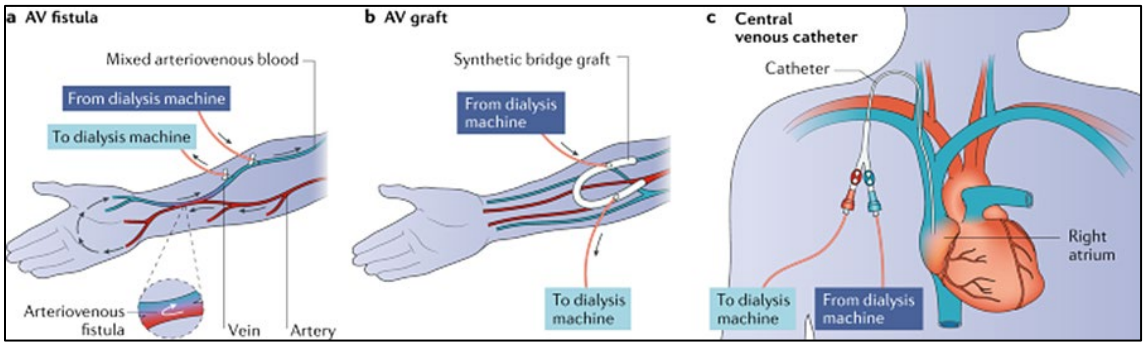

Figure 42. Depiction of the three different vascular accesses: (a) AV fistula, (b) AV graft, (c) central venous catheter.

Once the needles have been inserted, the first needle starts to collect blood from the patient, who may be sitting or lying on his back, and heparin is administered to prevent blood clots formation. Blood flowing towards the HD machine is pressure monitored, and when it reaches the HD machine core, it is finally filtered from toxic wastes, which will be collected by the dialysate. As soon as the filtering action is terminated, blood is relayed back to the body via the second needle. Eventual air bubbles will be trapped by an air detector (Figure 43).

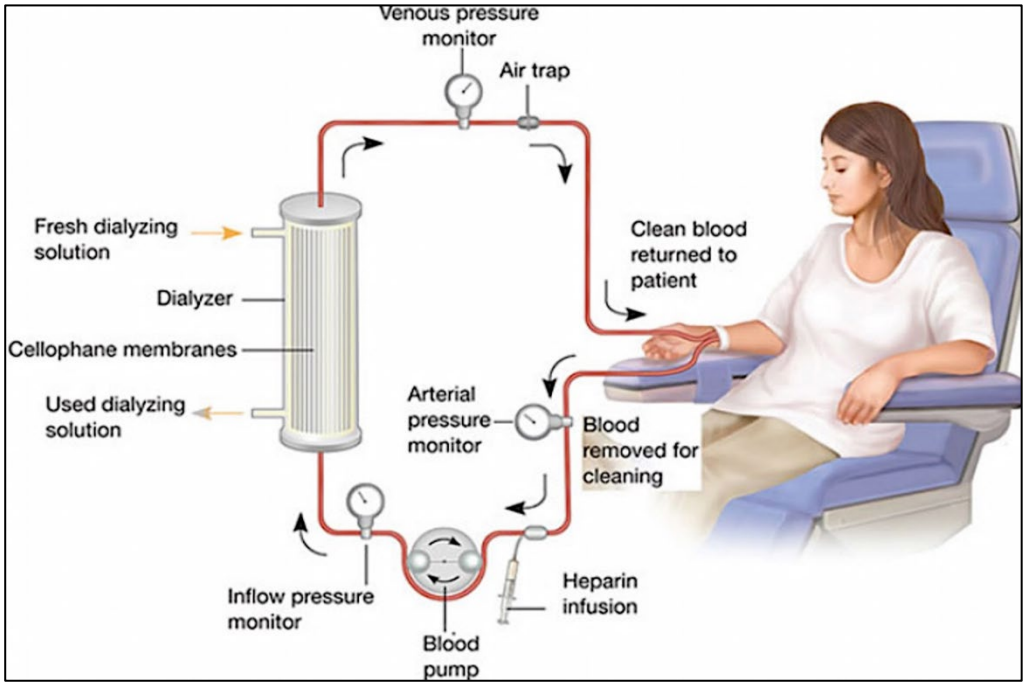

Figure 43. Path followed by blood during HD. Filtering process is done by the dialyzer.

The filtering process is carried out by a series of units, that altogether make up the HD machine (Figure 44). The core of the HD machine is represented by the dialysate pail and, in particular, by the dialyzer:

- *Dialysate pail*. It represents the storage block of the dialysate fluid, with the dialysate being regulated, as previously mentioned, by the nephrologist according to the patient's needs. Blood coming from the needles and flowing into this compartment will be monitored by a roller pump, that is devoted to the regulation of the blood flow rate by means of pressure gradients;
- *Dialyzer*. Located inside the dialysate pail, it constitutes the actual filtering section of the HD machine; hence it is often referred to as the "artificial kidney" of the machine. It is a large cylinder made of thousands of small hollow fibers, through which blood is allowed to flow in one direction. Around these fibers, dialysate is pumped in an opposite direction via two openings (Figure 45). This essentially creates two compartments, the "blood compartment" and the "dialysate compartment", that communicate with each other through the walls of the hollow

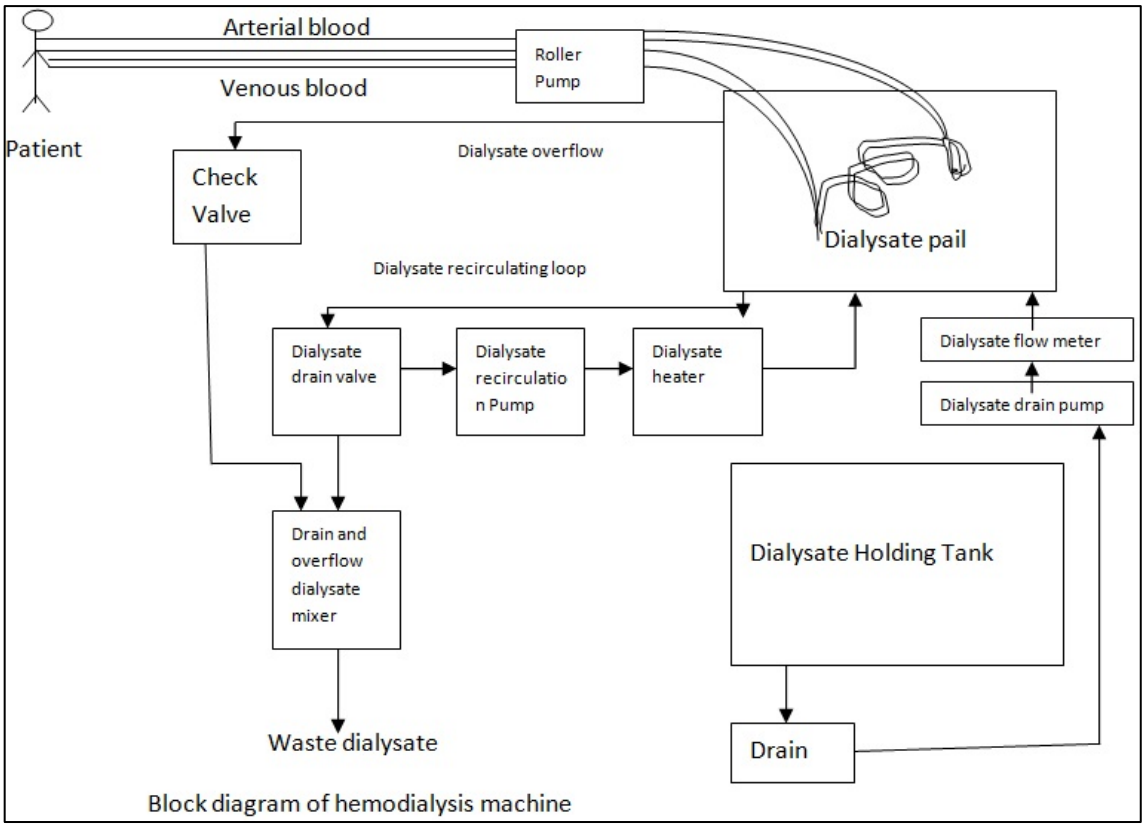

Figure 44. Block scheme of the HD machine.

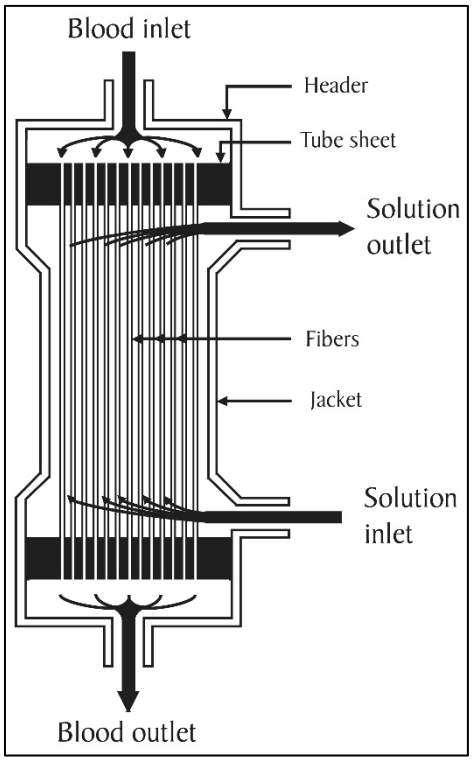

Figure 45. Scheme representing a dialyzer structure.

fibers. In fact, these are composed of a semi-permeable membrane (with surface areas of 0.8 to 2.2 square meters, and membrane permeability coefficient ranging from from 500 to 1500 mL/min), that permits the diffusion of wastes from blood into dialysate. Moreover, ultrafiltration can be accomplished by applying negative pressure to the dialysate compartment. The importance of the dialyzer is proved by the fact that, in recent years, great effort has been put into finding effective ways to reuse it. Attention has also been given to the materials and the dimension of the pores composing the semi-permeable membrane of the fibers [55], [56].

Other important components are represented by:

- *Dialysate heater*. This block will make sure that the dialysate coming into contact with blood will have the same body temperature of the patient. Any temperature variation will be immediately rectified;
- *Check valve*. This valve performs a control action on the dialysate flow in the dialysate pail. In case of an excess of dialysate, the overflowing quantity will be

diverted towards a drain mixer, where dialysate containing wastes is usually exhausted;

- *Dialysate recirculating loop*. This loop allows the reuse of dialysate solution for the same patient, during the same treatment. In fact, it converts part of the used dialysate into fresh and properly heated dialysis solution, that will be able to give the same outcome of a first-use dialysate;
- *Dialysate Holding tank*. This block holds the fresh dialysate that will be relayed to the dialysate pail when needed;
- *Flow meter*. This device contributes to the distribution of fresh dialysate to the dialysate pail. It also serves as an additional constraint to possible overflow;
- *Monitoring system*. The monitoring system is essential to keep track of all critical parameters, e.g. the patient's pressure, blood and dialysate flow rates, solution conductivity, temperature and pH. It triggers an alarm every time any of these parameters is out of normal ranges, allowing health care personnel to intervene;
- *Water system*. This system allows the purification of water that is to be mixed with the dialysate. Indeed, it is important to use ultra-pure water, so that no impurity will be accidentally introduced into the patient's bloodstream, causing dangerous solutes buildup. Moreover, water has to be mixed with the right proportions, as both an excessively concentrated and an excessively diluted dialysate could cause damage [55].

5.2. Peritoneal dialysis

Peritoneal dialysis (PD) consists in a renal replacement treatment that is usually performed at home, allowing the patients to be treated for longer periods of time during the day, with good results. In PD, the dialysate is stored inside bags and it is introduced in the abdominal cavity via a surgically implanted catheter, lingering outside the abdomen. The dialysate bag is generally put in an elevated position, to favor the flowing of the solution towards the target region (Figure 46). Once the bag has been emptied out, it is disconnected from the catheter, which is in turn sealed, so that the patient can execute normal tasks [57].

The dialysate solution in the abdomen, at the same time, exploits the peritoneum as a semi-permeable membrane: in this way, blood flowing through the vessels around the intestine is filtered from wastes, according to the diffusion principle.

After a certain number of hours from the beginning of the treatment, the dialysate has absorbed all the toxins and it is ready to be removed from the abdomen. The empty bag is again connected to the catheter, in a lowered position, and the unclean dialysate recollected in it is eliminated (Figure 46). The whole process is then repeater from 4 to 6 times a day [57].

PD can be executed either by hand or by a machine. Depending on that, two types of PD can be distinguished:

- *Continuous Ambulatory Peritoneal Dialysis (CAPD)*. CAPD is executed in clean places and all exchanges of dialysate bags are performed by hands. The person in charge, whether the patient or a health care professional, has to perform all tasks

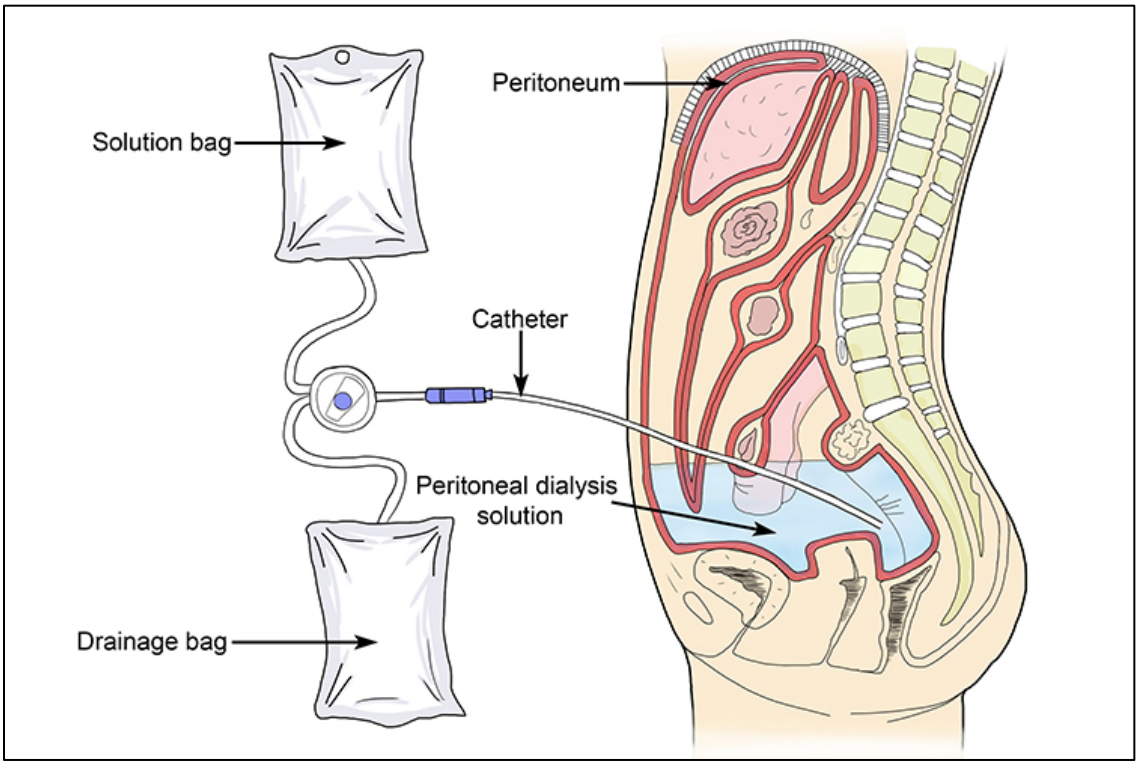

Figure 46. Example describing PD. To be noticed the solution bag, in upper position, that is emptied out, allowing dialysate to flow in the abdomen. The drainage bag, in lower position, will collect dialysate containing wastes.

with sanitized hands and surgical mask. They also need to bring the solution bags to body temperature;

- *Automated Peritoneal Dialysis (APD)*. APD is similar to CAPD, but the treatment is carried out by a machine, called cycler (Figure 47), to which up to five dialysate bags can be connected. The cycler, at a chosen time, will release a clamp on one of the bags, warming the solution and allowing it to flow inside the patient's abdomen. APD requires 8 to 10 hours for the treatment to be effective, so it is mainly performed during nighttime.

Both PD types require the patient or the caregiver to be properly trained. Moreover, adjustments in physical activity and, to a less extent compared to HD, in diet have to be made, in order to avoid buildup, in-between treatments, of minerals and fluids that could be potentially dangerous for the patient [57].

Figure 47. Cycler commonly used in APD. Three bags of dialysate solution are attached to it and will be used during treatment.

5.3. Consequences of dialysis

Both HD and PD, as seen in this chapter, aim to substitute compromised kidney function, allowing ESRD patients to live a long and relatively healthy life. While waiting for an eventual kidney transplant, dialysis indeed helps ESRD patients, by removing excess water and rebalancing electrolytic concentrations.

As for indirect effects on electrical cardiac function, rebalanced ionic concentrations usually give rise to close-to-normal APs, as ionic channels of cardiac cells membranes are not impaired anymore in their opening and closing action. At the level of the ECG, this reflects into P wave and QRS complexes increasing in amplitude, while T wave and QTc interval decrease in amplitude and duration, respectively, after the treatment [58]. This is exactly the opposite of what we would observe in dialysis patients showing hyperkalemia and hypocalcemia prior to treatment (as described in Chapter 4).

The elimination of fluid surplus via dialysis surely contrasts hypervolemia. However, dialysis is still associated with a high risk of developing congestive heart failure. This is especially true for HD: as HD patients are exposed to increased amounts of water in a relatively short time period during HD treatment, fluctuations of the patients' hemodynamic status are common. Such hemodynamic fluctuations may then lead to myocardial damage [59].

Moreover, as dialysate K^+ concentration is lower than serum K^+ one, it is possible that K^+ concentrations drop significantly after dialysis. This brings about a situation of *hypokalemia* ($[K^+]<3.5$ mmol/l), often associated with high mortality risk [60]. In hypokalemia, cardiac APs present an increased duration of phase 2, while phase 3 slope decreases. This produces a "tail" that increases the refractory period of the cell and decreases the resting potential at the end of the AP. These changes are mirrored by the ECG: T waves tend to decrease in amplitude and widen, and U waves may appear and merge with T waves. The ST segment might also depress in case of severe hypokalemia. In addition, P wave amplitude and duration and QRS duration are prone to increase (Figure 48) [43].

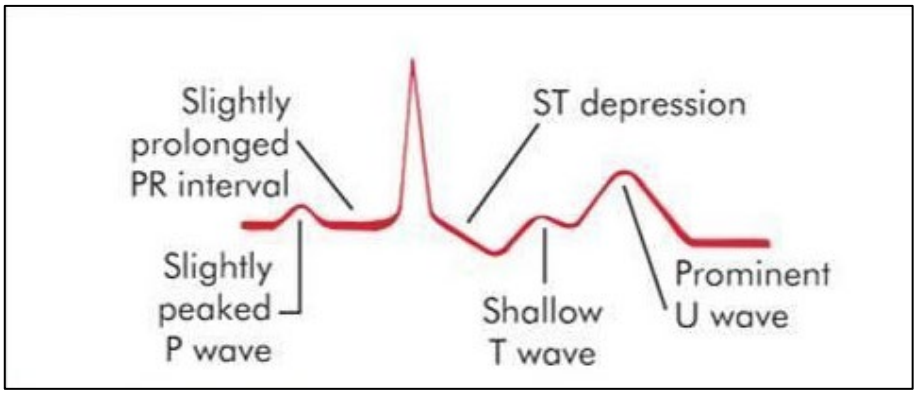

Figure 48. Example of ECG modifications in case of hypokalemia.

6. CHAPTER 6: ELECTROCARDIOGRAPHIC ALTERNANS IN DIALYSIS

In the previous chapters we reported the concept of ECGA, giving definitions of PWA, QRSA and TWA and providing a list of automatic methods that, during the years, have been used to detect them. Then, dialysis treatment was explained, with particular focus on HD, and its effects on cardiac electrical activity have also been taken into account. In this new chapter, we will now delve into some of the most significant results given by electrocardiographic analysis in HD patients. These results, produced over the course of the last two decades, will first describe the main electrocardiographic findings in dialysis. In several cases, in fact, the ECG has not been exclusively studied in terms of alternans. However, as ECGA represents an expression of the fluctuations involving all ECG waves, it is important to give the reader details about such findings. Then, studies involving the concept of alternans in HD will be reported: major focus will be initially given to TWA, due to its popularity; most recent results about ECGA in HD will be described as well.

6.1. Electrocardiographic findings in dialysis

One of the first study that, to our knowledge, started to investigate about electrocardiographic changes during HD was published in 1993. Fuenmayor et al investigated changes occurring in QRS amplitude on 8 patients submitted to HD. 12-lead ECGs were recorded, with the patients in recumbent position, before and after HD sessions, and QRS amplitude (as the algebraic sum of positive and negative waves of each QRS complex), HR and HR variability (HRV) were computed. K^+ and Na^+ concentrations, as well as ventricular volumes and mass, ejection fraction, arterial pressure and body weight were also monitored, in order to be compared with QRS amplitude changes. QRS amplitude significantly increased after HD ($P=0.0006$), while body weight ($P=0.0001$), end-diastolic volume ($P=0.043$), arterial pressure ($P=0.025$) and serum K^+ concentration ($P=0.023$) decreased. The causes of the elevation of QRS amplitude at the end of HD, however, were unclear, and a link with electrolyte rebalancing was yet to be considered [61].

In 1999, Ojanen et al used a dynamic vectorcardiographic monitoring system to study ST segment (as ST vector magnitude, ST-VM6) and QRS complex (as QRS vector difference, QRS-VD) of 15 HD patients, while bioimpedance analysis was used to detect changes in extracellular water. Blood volume, body weight and electrolyte concentrations were also taken into account. All measurements were obtained from recordings starting before a HD session and lasting until the end of the treatment. Mean QRS-VD increased during dialysis, going from 4.16±2.40 to 15.60±7.0 μV: this was due to a change in QRS amplitude, while QRS duration did not vary in a considerable way. ST segment did not undergo significant changes during HD as well. Statistically significant correlation was found between the changes in QRS-VD and body weight, as well as with extracellular water and electrolyte concentrations, leading to the conclusion that these indeed influence electrical cardiac activity. The authors, in fact, suggested that the loss of excessive fluids brings about an augmentation of electrical resistance of the tissues around the heart [62].

In 2002, Szabó et al investigated the effects of HD on ECG markers such as P wave duration and P wave dispersion. First 12-leads ECG recordings were performed, by means of Hewlett Packard Page Writer 200i (M1071A, China, paper speed=25 mm/s) on 28 non-diabetic patients, in supine position, at the beginning of HD. Then, new recordings were made at 15 and 30 min after the start of HD, at the end and 2 hours after the end of the HD session. Electrolyte concentrations were also monitored. P wave duration was measured by one observer (in order to exclude intra-observer variability) on the enlarged ECGs by means of calipers; P wave dispersion was then computed as the difference between the maximum and minimum value of P wave duration. Both duration and dispersion increased by the end of HD (P wave duration: 58±16 ms at the beginning of HD vs 98±8.9 ms at the end of HD; P wave dispersion: 23±10 ms at the beginning of HD vs 41±16 ms at the end of HD), as visible in Figure 49. These results had significant positive correlation with serum Ca^{2+} levels and negative correlation with serum K^{+} levels, leading to the conclusion that electrolyte changes due to HD indeed have an influence on the P wave [63].

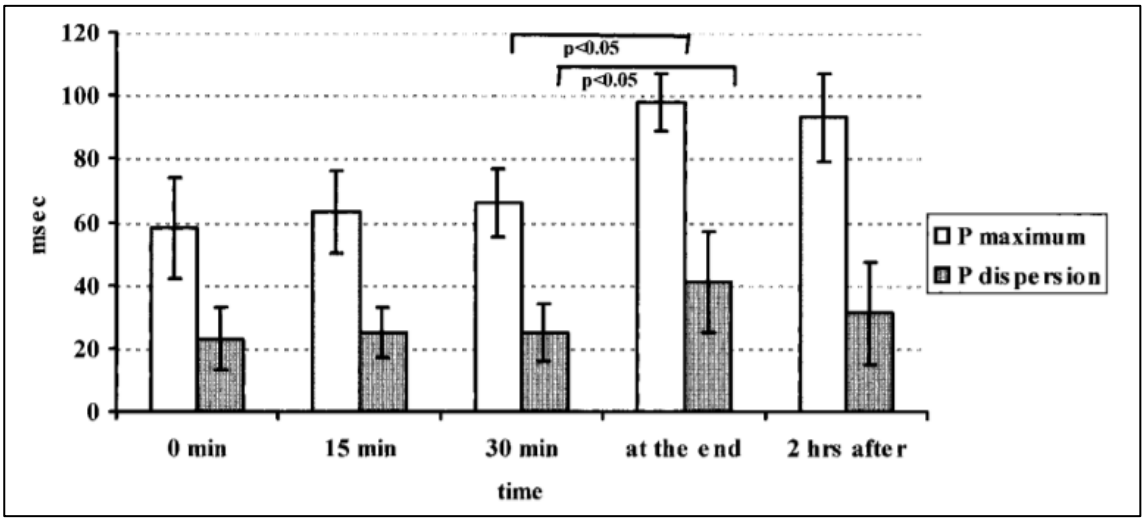

Figure 49. Maximum P wave duration and P wave dispersion during HD. It is possible to observe how P wave duration and dispersion increase towards the end of HD [63].

Similar results were obtained in 2004 by Tezcan et al. Also in this study, P wave duration and dispersion were considered. Here, 32 HD patients were selected and 12-lead ECG recordings in resting condition were performed, one before HD and one after HD. After that, P wave duration was manually measured, using magnifying glass and calipers; P wave dispersion was computed as described for Szabó et al [60]. Again, both P wave duration and P wave dispersion increased after HD (P wave duration: 98±13 ms before HD vs 125±12 ms after HD; P wave dispersion: 27±9 ms before HD vs 52±11 ms after HD), as reported in Figure 50. This increase in P wave duration was thought to be due to hypokalemia, common in HD patients, as seen in Chapter 5. It was also speculated that it could be the cause of the occurrence of atrial fibrillation, in some patients, between the third and fourth hour of treatment [64].

Following studies regarding P wave in HD analyzed its modifications with respect to those shown by the QRS complex in the same condition.

Madias, in 2005, investigated the relationship between P wave duration and dispersion changes and QRS amplitude and duration changes, in HD. Their association with electrolyte concentrations and fluids fluctuations during HD was also evaluated. The study was performed on a 36-year old woman under HD and rejected kidney transplant,

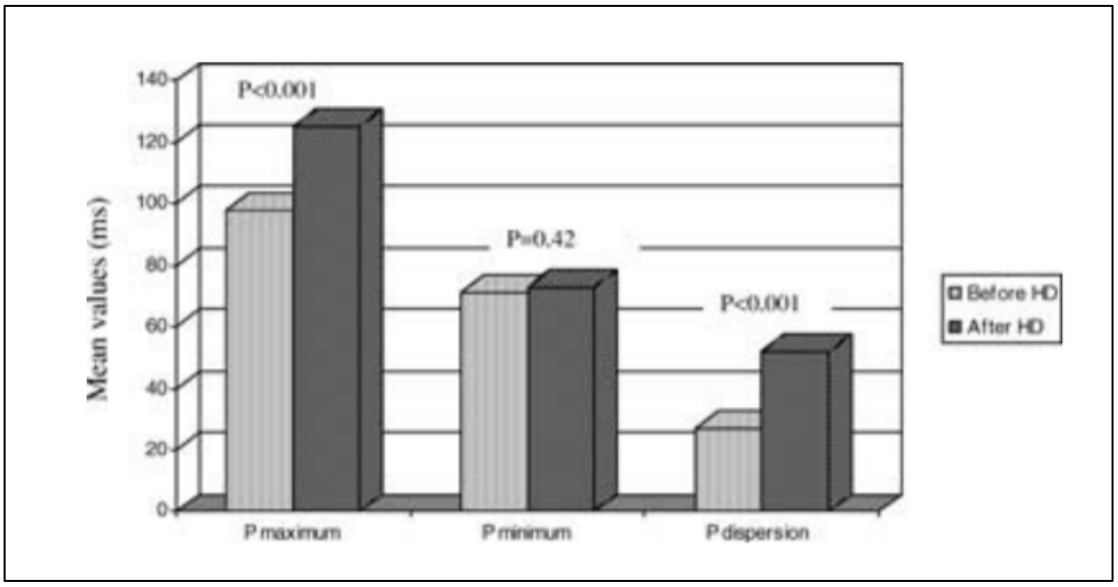

Figure 50. Mean values of maximum and minimum P wave dispersion and P wave duration before and after HD [64].

and standard ECGs were recorded before and after 26 HD sessions. Both P wave and QRS-related measurements were carried out via manual approach, and it was observed that both P wave and QRS duration and amplitude increased after HD. The author assumed that changes in QRS amplitude and duration, with amplitude and duration increasing or decreasing at the same time, are usually associated with electrolytic and fluid rebalancing given by the treatment. He also asserted that changes in the QRS complex bring about changes in the P wave, but the relationship between the latter and electrolytic rebalancing and fluid loss was still to be further investigated [65].

Drighil et al, in 2008, drew from the previous considerations, and analyzed 12-lead ECG recordings coming from 47 subjects undergoing a midweek HD session. The recordings were performed with an Agilent (HP, currently Philips, Andover, Mass) M1771A Page writer 200i electrocardiograph, before and after HD. Amplitude for both P wave and QRS complex was measured with magnifying glass and calipers; P wave dispersion was evaluated as in [60]. Both amplitude and dispersion were then summed across all leads, and mean QTc was computed starting from measured QT intervals. P wave and QRS duration and QTc increased after HD (66.1±13.4 ms, 77.9±11.5 ms and 406±30 ms before HD; 69±10.5 ms, 80.5±12.2 ms and 405±32 ms after HD, respectively), but no statistical differences were found between P wave duration and QTc before and after HD. Also P

wave and QRS amplitude increased after HD, as seen also in [62], although, in this study, the values obtained correlated poorly with electrolytes concentrations fluctuations and HR, due to low voltage of P wave. Regardless, the relationship between P wave and QRS complex modification was reiterated [66].

Later on, studies involving ECG parameters in HD started to include also measurements performed on T wave.

Astan el al, in 2015, selected 62 HD patients to investigate the effects of treatment on ECG parameters. 12-lead ECGs (Cardioline Delta 60 plus, Remco Italia S. p.A, Milan, Italy) were recorded before and after HD and, on lead II, P-wave and T-wave amplitude, QRS amplitude and duration, QT and QTc interval dispersion were calculated by two cardiologists, with digital calipers. On all leads, instead, the sum of T-wave amplitudes, QRS periods, QT and QTc dispersion were computed. All parameters, except for T-wave amplitude and QTc duration, appeared to be significantly greater after HD, compared to values prior to HD. The increase in P wave and QRS amplitude, according to the authors, was correlated with the withdrawal of fluids performed by HD: electrical stimuli coming from the heart propagate with a magnitude that is inversely proportional to body fluid distribution. T-wave amplitude decreasing trend was probably due to decreased serum K^+ levels caused by HD treatment [58].

Jebali et al, in 2020, studied standard 12-lead ECGs, recorded before and after HD, belonging to 66 patients. Serum K^+ and Ca^{2+} were also measured at the same time. Here, only prolonged QTc interval significantly correlated with K^+ concentrations, making the authors conclude that, in this case, hyperkalemia manifestations were less pronounced in HD patients. However, mean values of all other ECG parameters, e.g. HR, R wave amplitude, T wave amplitude, T/R wave ratio and QRS duration, significantly changed at the end of HD, compared to prior HD measurements, confirming the unstable electrical situation HD patients endure during treatment [67].

6.2. Electrocardiographic alternans in hemodialysis

For what concerns the concept of alternans in HD, to our knowledge, the first studies were mainly devoted to TWA analysis. The pilot study in that sense was performed in 2007 by

Friedman et al. Here, 9 HD patients were tested for TWA presence before and after an early week HD session, to verify if HD indeed produces modifications of the cardiac electrophysiology that can lead to ventricular arrhythmias. 7 out of 9 patients were non-negative to TWA in at least one of the two time periods considered, i.e. before and after HD. In particular, among 4 patients who did not show TWA prior HD treatment, 2 showed ECG tracings presenting TWA immediately after HD [68].

In 2008, two studies investigated about macroscopic TWA presence. Miyaji et al performed 12-lead ECG recordings on a 67-year-old male presenting cardiomyopathy and chronic kidney failure. At admission, the patient showed prolonged QT interval, ventricular fibrillation and macroscopic TWA. Unfortunately, even after HD treatment, long QT interval and macroscopic TWA persisted, probably due to the impaired ionic handling and preexisting structural abnormalities at cardiac level. Only resynchronization therapy was able to restore normal conditions, although reasons for that were still unclear [69]. Similarly, Andrade et al observed long QT interval and macroscopic TWA in a 64-year-old woman presenting ventricular fibrillation one hour into standard HD. Also in this case, macroscopic TWA was associated to unbalanced ionic concentrations, especially for Ca^{2+} [70].

In 2009, Kouidi et al selected a group of 63 patients on HD treatment for at least six months, to verify if physical exercise could bring benefits to the subjects' health. The patients were then randomly divided into two groups: group A, made of 32 patients, which participated in a 10-month exercise training program during HD, and group B, made of 31 patients, which continued receiving usual care and served as control group. On a non-HD day, ECG recordings were performed to test left ventricle conditions and ejection fraction. Moreover, a 3-channel Digital Ambulatory ECG Holter Recorder (model GBI-3S; Galix Biomedical Instrumentation Inc, Miami Beach, FL) was used to continuously record for 24 hours. New tests were then performed after 10 months, as follow up. From the Holter ECGs, HRV, signal averaged ECG and TWA were computed. In particular, TWA was analyzed by means of the FFTSM: positivity to TWA was obtained if the ratio between TWA magnitude and noise level was greater than 3 and alternans voltage was greater or equal to 1.9 μV during exercises with onset HR of 110 bpm or less. It was noticed that, among the 13 patients that were initially positive to TWA, those belonging to group A did not present TWA at follow-up. As many results were considered

undetermined, though, and there was no significant difference between groups A and B, it was concluded that exercise did not bring any particular benefit during HD [71].

In 2011, Patel et al performed a comparison between TWA presence in ESRD patients and in left ventricle hypertrophy (LVH) patients. The ESRD group was formed by 200 patients undergoing either HD or PD, while the LVH group was made of 30 hypertensive patients that had no evidence of renal pathologies. Standard 12-lead ECGs were continuously acquired 24 hours after the end of a dialysis session in ESRD group; they were then analyzed by means of the FFTSM. Patients were considered positive to TWA if alternans was present for at least 1 minute, with HR lower than 110 bpm in case of exercise or HR also greater than 110 bpm if in resting conditions. They were instead negative if tests did not meet positivity criteria at maximum HR equal to 105 bpm. All other results affected by noise or the impossibility to reach HR between 105 and 110 bpm were considered undetermined (with both undetermined and positive results being classified as abnormal). Abnormal TWA was majorly observed in ESRD patients with respect to LVH ones: in particular, 44 ESRD patients tested positive to TWA and 71 were undetermined; only 3 LVH patients were positive to TWA and 5 were undetermined (Figure 51) [72].

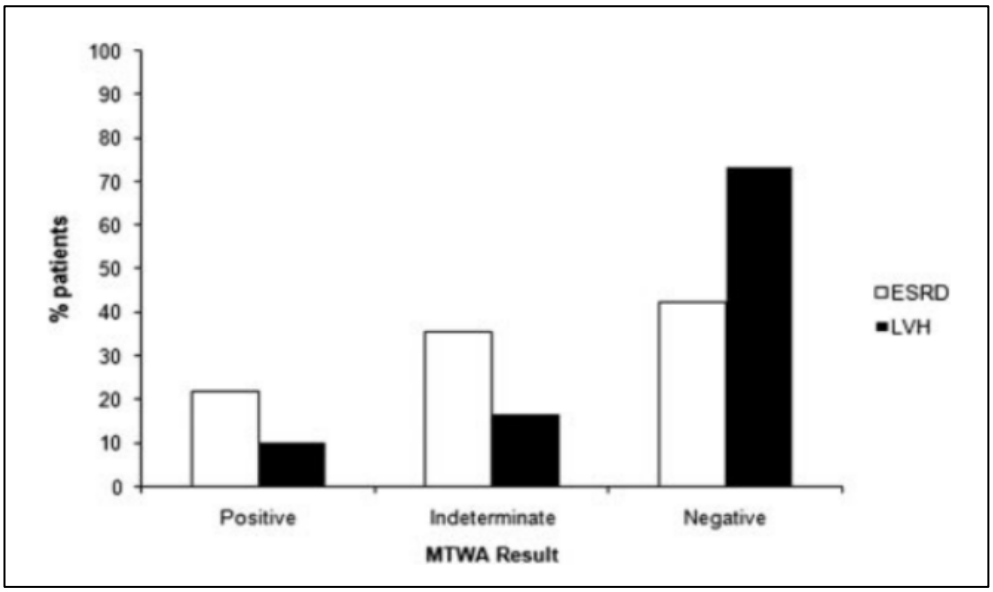

Figure 51. Microvolt TWA (MTWA) in ESRD and LVH patients. It is visible how a higher percentage of ESRD patients presents abnormal TWA, compared to LVH patients [72].

Until this moment, none of the studies listed in this section took into account alternans during the whole dialysis time period. Starting from a study by Secemsky et al, however, longer recordings covering also the entire dialysis session were made.

Secemsky et al, in 2011, in order to verify if there is a major incidence of SCD in the 24 hours that precede the first HD session of the week, selected 41 HD patients that were under HD treatment for at least 3 consecutive months (and also presented known SCD risk factors, e.g. diabetes, vascular problems, reduced ejection fraction). Ambulatory 3-lead (V2, V5 and aV_F) SEER Light Digital Holter monitor with sampling rate of 125 samples/s (GE Medical Systems, Milwaukee, Wisconsin) was used to continuously record ECGs for 72 hours. For statistical analysis, the recording was then divided in the following way:

1. -1HD, corresponding to the day before HD and representing the high SCD risk period before the first HD session of the week;
2. 0HD, corresponding to the HD day and representing an intermediate SCD risk period;
3. +1HD, corresponding to the day after HD and representing a low SCD risk period.

On these three time periods, TWA was analyzed by means of the MMAM and considered significant if its maximum magnitude was equal or greater than 53 μV in V_5; HRV, in terms of RR intervals standard deviation (SDNN), and HR turbulence (HRT) were also computed. Once analysis was completed, only 28 patients had sufficient data. It was observed that both SDNN and HRT scores were abnormal in at least one of the 24-hours periods considered, with no statistical difference among high, intermediate and low-risk intervals. Also for TWA, there was no significant difference among the three time periods: 27 out of 28 subjects presented maximum TWA higher than 53 μV in at least one of the 24-hours periods of recording, and 26 of them even had abnormal TWA in two or more periods. In fact, TWA peaks were equally distributed inside the three different SCD risk intervals (Figure 52) [73].

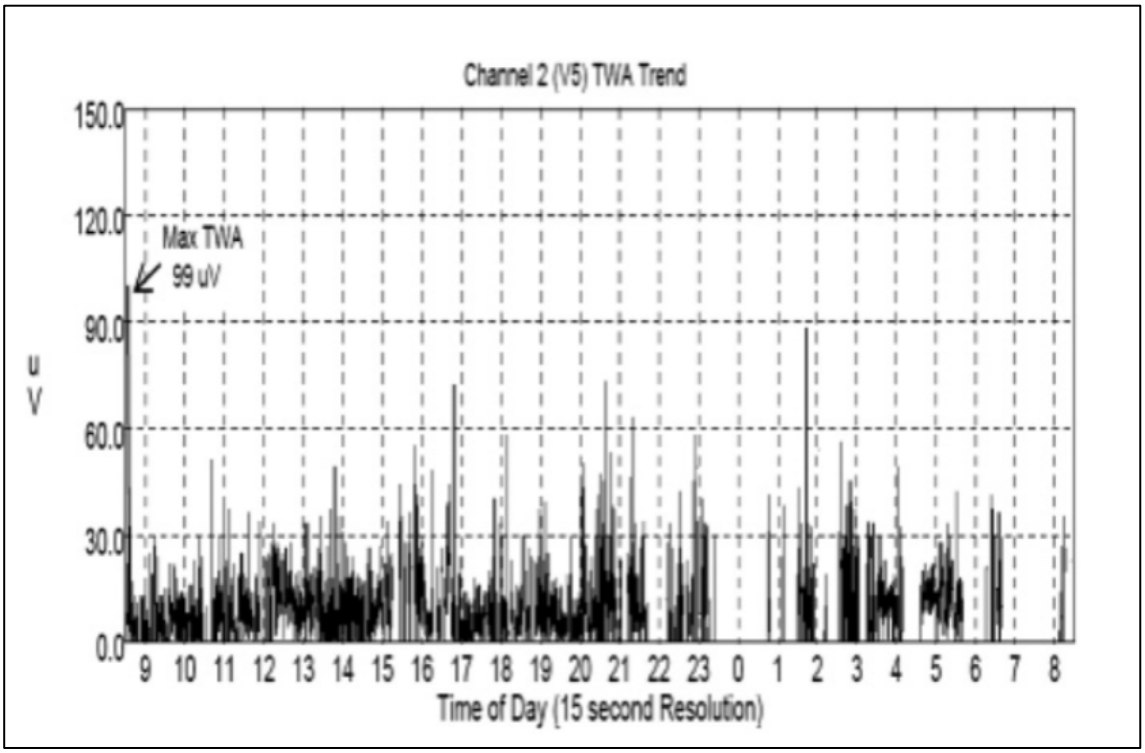

Figure 52. Distribution of TWA peaks over a 24-hour period. It is possible to observe how peaks greater than 53 μV are equally distributed during the same day [73].

Green et al, in a study published in 2012, selected a group of 19 patients and continuously recorded 48 hours ECGs by means of 12-lead digital Holter (CardioDayR, GE Healthcare, Little Chalfont, UK, 1,024 samples/s, 12 bit A/D resolution), starting from the arrival of the patients at the dialysis facility. Electrodes were positioned according to the Mason-Likar system, in order to avoid lead placements that could be affected by artifacts. At first, the acquisitions were analyzed in order to identify arrhythmias, HR trends and ST segment changes. Afterwards, MMAM was applied for TWA identification on four leads, selected because of their lowest level of noise. Mean TWA values were computed, and number and timing of TWA peaks was assessed (with peak corresponding to TWA greater or equal to 65 μV). From a statistical point of view, comparisons were made between mean group TWA computed before and during HD, as well as between mean group TWA during HD and after exactly 24 hours. The same kind of comparisons were also made for maximum TWA, peaks and HR. Mean group TWA (globally equal to 11.5 μV, with range for each patient going from 43 to 168 μV, and median value equal to 91 μV) slightly increased during HD, from 9.90±4.42 μV during the first hour to 11.98±3.3 μV during

the last hour. Specifically, 11 patients showed TWA increase greater than 1 μV during HD, while the other 8 patients did not present particular variations or decreasing trends in the values. Then, two hours after the end of the treatment, TWA values returned to baseline. The diminishing trend after treatment was also observed in terms of peaks: a peak that was present in correspondence of the last hour of HD was not perceived the next day, as TWA values generally decreased (Figure 53). It was noted, however, that there was no difference in peaks timing between the HD day and the following day. HR increased during HD, going from 84.3±8.9 bpm to 90.9±12.8 bpm, but, compared to TWA, it was also elevated during the following day of recording. There was, in fact, only a weak positive correlation between TWA and HR measurements. Moreover, the findings of the study could not be associated to electrolytic changes, probably due to the small sample size in the study [74].

A following study, made by Simova et al in 2015, went back to observing TWA behavior before and after HD, but investigated in addition also QRSA. 58 HD patients, undergoing treatment at the same dialysis center, were selected and standard 12-leads ECGs of 1-minute duration (500 Hz sampling rate) were recorded before and after HD. QRSA and TWA were then analyzed using the MMAM and PCA. Episodes of TWA were present in

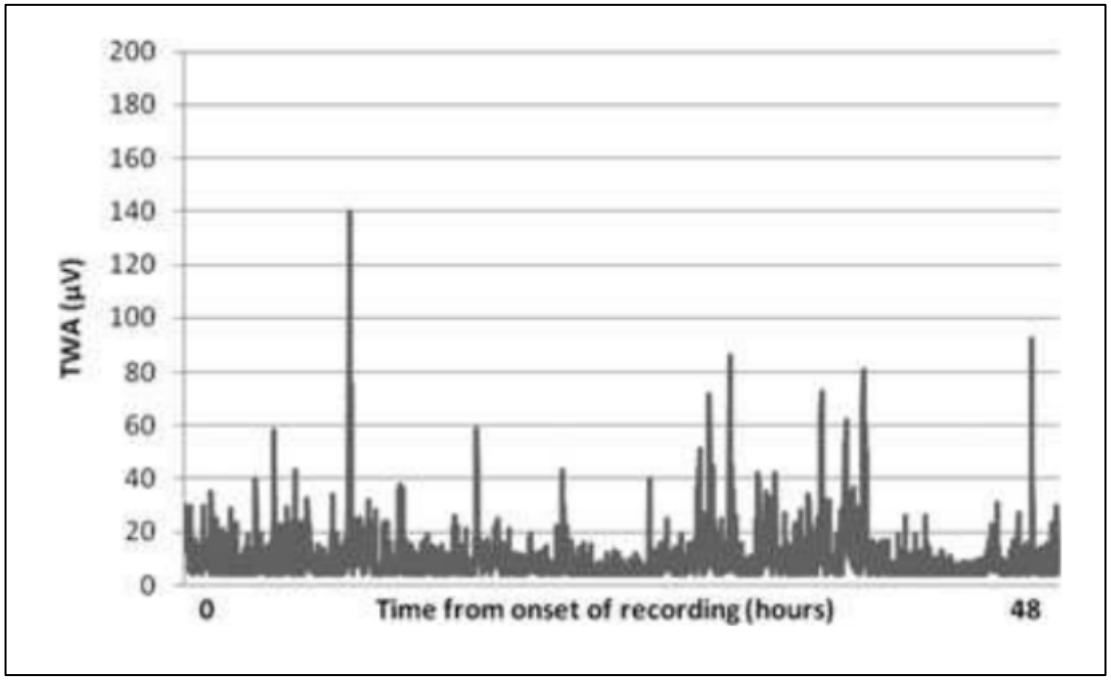

Figure 53. TWA trend observed over 48 hours on a patient undergoing HD treatment [74].

12 out of 58 patients before HD, and in 11 out of 58 patients after HD, meaning that there was no significant difference between one period and the other. QRSA was also present in 7 patients before HD, while almost disappeared after HD: QRSA persisted only in one patient. Moreover, both QRSA and TWA negatively correlated with the Body-Mass Index (BMI) of the patients, in line with the so-called "obesity paradox": despite obesity coinciding with increased incidence of diabetes and cardiovascular problems, higher presence of fat tissues in ESRD and HD patients seems to result in better survival. Finally, TWA positively correlated with HR [75].

Another study, by Kaplan et al, published in 2016, reconsidered longer recording times, in order to investigate if different treatment frequency could have influence on SCD risk in HD patients. In fact, by means of the Frequent Hemodialysis Network Daily Trial, the authors aimed to compare the benefits that could be obtained from Daily HD with respect to Standard HD. 245 HD patients were selected by the program, and KCI X5 digital Holter recorders (KCI Technology and Services, Branchburg, NJ) were used to acquire continuous 24-hours ECGs starting from one hour prior to the first HD session of the week. New ECGs were then recorded one year later (follow-up). Only 68 patients, equally divided into Standard and Daily HD groups, gave fully interpretable ECGs. Their acquisitions were then analyzed for HRT and TWA via MMAM and TWA values were considered abnormal if greater than 50 μV. It was observed that, in Standard HD group, maximum TWA was initially 52.4±1.5 μV and then slightly decreased, at follow-up, to 51.2±1.7 μV; in Daily HD group, maximum TWA was initially equal to 54.0±1.5 μV, while at follow-up it was equal to 49.9±1.7 μV. Also abnormal HRT decreased in both groups at follow-up, compared to initial scores. Consequently, the authors concluded that there was no particular difference in terms of HRT and TWA values between the Standard and Daily HD, however the latter resulted in benefits in terms of physical conditions. They also noticed that important decreasing trends are more visible in patients presenting quite elevated TWA [76].

In 2019, a case report by Leoni (the same author of this thesis) et al analyzed TWA, in an 82-year old male patient undergoing HD, using the HRAMF method. A 24-hour continuous 12-lead digital Holter recording was acquired and was divided, for comparisons, into four time periods: PRE-HD, before HD; IN-HD, during HD treatment; POST-HD, immediately after the end of HD; NT-HD, night period. Mean TWA values

obtained were particularly high in PRE-HD and IN-HD, with a peak at the second hour of treatment, indicating how these periods correspond to high SCD risk. Then, TWA started to decrease almost two hours after the end of HD, stabilizing at values around 50 μV and indicating that SCD risk decreases after treatment, with a trend (Figure 54) that seemed to be in accordance with that described by Green et al [74]. Moreover, statistical differences were found between PRE-HD and post HD periods; the same differences were found also between IN-HD and the following time periods (Table 1) [77].

Finally, in 2020, a new case report by Marcantoni et al, involving the same subject and time periods of [77], studied ECGA meant as the prevalent nature of electrical alternans in HD. The HRAMF was here applied and adapted to identify PWA, QRSA and TWA. TWA resulted as the prevalent alternans among the three, i.e. ECGA amplitude values corresponded to TWA amplitude ones. The distributions obtained resembled those reported in [74] and [77], as observed in Figure 55. However, TWA amplitudes were lower with respect to [77], as median values were computed instead of mean values (Table 2). In addition, it was noticed that, despite TWA being prevalent, also PWA and QRSA occurred (Table 3): the authors suggested that fluctuations of the wave considered as prevalent might be affected by fluctuations happening at the level of the other ECG waves, implying reciprocal influence [78].

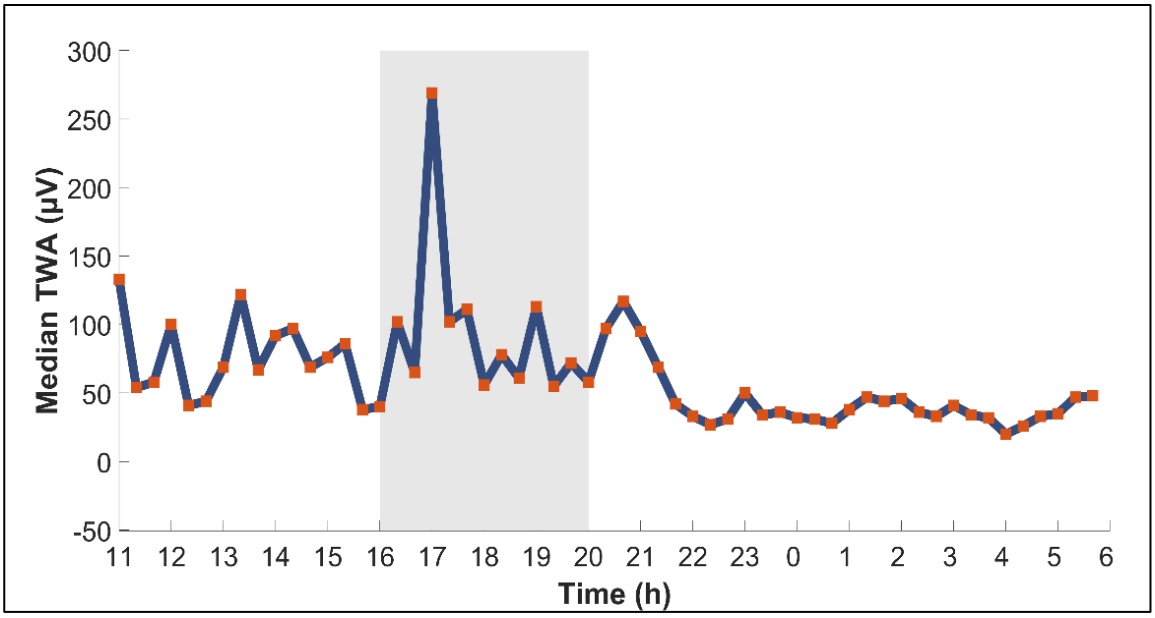

Figure 54. TWA trend obtained performing the median between all ECG leads. Values are computed every 20 minutes and grey area represents HD [77].

Table 1. TWA and HR distributions over the four time periods previously described. Global values are here reported in terms of 50th [25th;75th] percentile. NW: accepted windows [77].

		Distributions				Maximum values				NW (%)
		PRE-HD	IN-HD	POST-HD	NT-HD	PRE-HD	IN-HD	POST-HD	NT-HD	
HR (bpm)		59 [57;62]	62 [61;65]	66 [65;68]	59 [58;63]	82	83	82	79	100
TWA (μV)	I	48 [35;63]	46 [34;63]	23 [18;40]	21 [12;33]	1505	116	132	193	30
	II	80 [51;108]	76 [62;98]	44 [32;69]	61 [41;95]	383	216	268	353	61
	III	99 [58;152]	83 [57;147]	63 [36;97]	63 [40;103]	596	514	536	378	46
	V1	47 [33;62]	59 [46;90]	31 [21;45]	41 [26;65]	753	115	252	259	44
	V2	60 [44;82]	60 [48;69]	34 [22;56]	37 [24;54]	713	101	275	216	27
	V3	80 [56;119]	73 [52;96]	53 [35;85]	60 [39;99]	808	423	331	359	58
	V4	82 [51;129]	80 [58;112]	35 [20;81]	30 [20;50]	1171	239	360	229	66
	V5	102[60;150]	94 [59;119]	41 [26;91]	29 [20;50]	1187	313	373	175	70
	V6	68 [46;102]	110 [64;152]	51 [36;74]	36 [21;52]	1198	273	257	197	29
	aVR	82 [57;112]	67 [52;95]	49 [35;79]	34 [23;55]	1207	534	248	183	61
	aVL	69 [52;101]	79 [57;109]	35 [22;57]	34 [23;53]	1232	292	231	208	59
	aVF	54 [44;83]	103 [85;142]	26 [17;43]	32 [21;49]	1229	228	283	178	47
	TOT	**75 [57;82]**	**78 [64;89]**	**38 [33;50]***	**35 [31;51]***	**1179**	**256§**	**272§**	**212§**	**53**

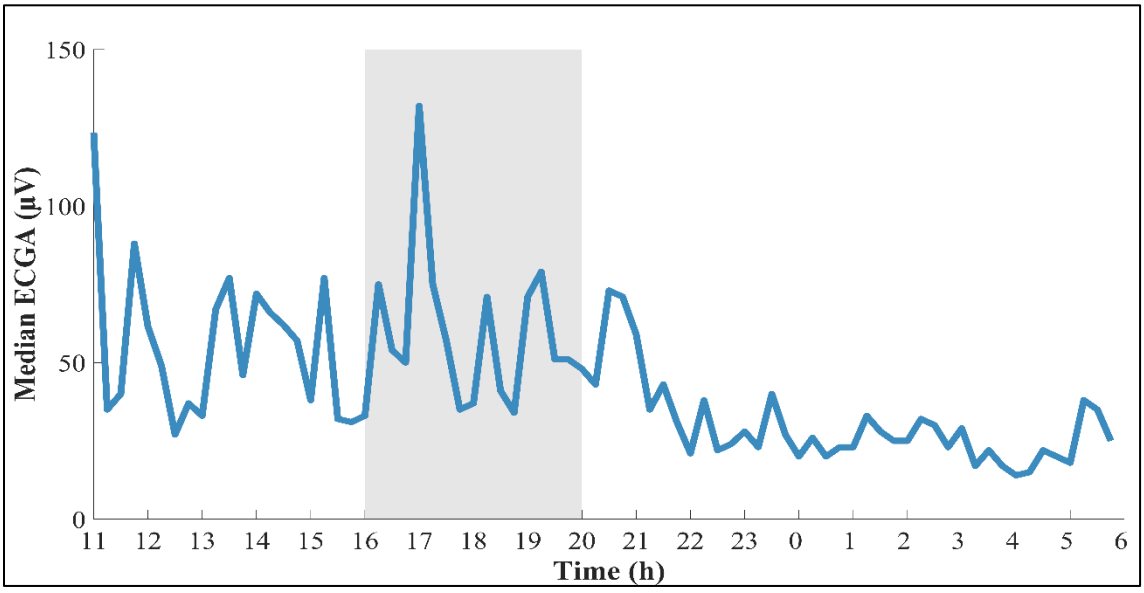

Figure 55. Median ECGA trend across all leads, with values computed in intervals of 15 minutes. Grey area corresponds to HD [78].

Table 2. HR and ECGA distributions expressed as 50th[25th;75th] percentile. NW: accepted windows [78].

	ECGA				NW
	PRE-HD	**IN-HD**	**POST-HD**	**NT-HD**	**Tot**
I	33 [27;41]	31 [27;46]	19 [15;29]	13 [10;17]	31
II	54 [35;75]	57 [46;76]	34 [25;47]	38 [27;57]	61
III	51 [32;84]	54 [41;80]	43 [29;76]	38 [28;56]	47
V_1	32 [24;45]	37 [32;41]	24 [17;34]	24 [17;37]	44
V_2	43 [30;57]	40 [35;44]	28 [18;45]	22 [17;31]	30
V_3	57 [36;82]	52 [42;72]	40 [27;59]	37 [27;52]	59
V_4	55 [31;74]	55 [41;73]	21 [16;37]	17 [13;25]	66
V_5	62 [38;92]	59 [42;77]	28 [19;42]	18 [14;23]	70
V_6	42 [30;63]	66 [47;112]	37 [32;47]	24 [14;40]	29
aV_R	58 [40;82]	52 [33;79]	37 [28;53]	21 [15;33]	62
aV_L	50 [35;66]	46 [34;70]	25 [17;35]	19 [14;28]	59
aV_F	38 [29;53]	56 [45;68]	19 [14;29]	20 [14;31]	47
Tot	51 [32;70]	53 [41;73]	28 [19;44]*	22 [15;32]*	53
HR	59 [57;62]	62 [61;65]	66 [65;68]	59 [58;63]	100

**: $p<10^{-3}$*

Table 3. Percentages of ECGA for each time period and lead [78].

	PRE-HD			IN-HD			POST-HD			NT-HD			Tot PERIODS		
	PWA	**QRSA**	**TWA**	**PWA**	**QRSA**	**TWA**	**PWA**	**QRSA**	**TWA**	**PWA**	**QRSA**	**TWA**	**PWA**	**QRSA**	**TWA**
I	10	7	83	19	9	72	11	8	81	11	9	80	13	8	79
II	10	7	83	13	8	79	10	6	84	8	5	87	10	7	83
III	11	6	83	12	7	81	9	5	86	7	5	88	10	6	84
V_1	10	7	83	11	7	82	9	6	85	9	6	85	10	7	83
V_2	11	7	82	12	10	78	10	6	84	8	6	86	10	7	83
V_3	10	7	83	12	7	81	9	6	85	8	5	87	10	6	84
V_4	10	7	83	12	10	78	10	8	82	11	7	82	11	8	81
V_5	12	8	80	17	10	73	11	8	81	12	8	80	13	9	78
V_6	11	8	81	10	8	82	20	16	64	12	9	79	13	10	77
aV_R	11	7	82	13	8	79	12	8	80	10	6	84	12	7	81
aV_L	10	7	83	11	8	81	11	6	83	9	6	85	10	7	83
aV_F	10	6	84	9	6	85	12	7	81	9	7	84	10	7	83
Tot	10	7	83	13	8	79	11	8	81	10	7	83	11	8	81

7. CHAPTER 7: IDENTIFICATION OF ELECTROCARDIOGRAPHIC ALTERNANS IN AN END STAGE RENAL DISEASE PATIENT IN HEMODIALYSIS

In Chapter 6, results concerning electrocardiographic findings and ECGA in HD have been described. As it has been observed, different automatic methods have been used to analyze ECGA in HD during the years. More recently, the HRAMF method was also applied for alternans analysis in HD, first for TWA investigation only, and then for ECGA, interpreted as the prevalent nature of electrical alternans, i.e. PWA, QRSA or TWA. As anticipated in Chapter 3, however, the interpretation of the ECGA concept is changing, with ECGA being considered not only as the prevalent alternans among PWA, QRSA and TWA, but also as an expression of all three alternans. This obviously calls for a new method that is able to quantify all alternans in a reliable way, avoiding reciprocal influence among the three types of alternans during analysis. For this reason, an improved ECGA identification method, based on the HRAMF, will be here proposed. The identification method will be structured in order to avoid such reciprocal influences and will be applied for ECGA analysis on a ESRD patient undergoing HD treatment.

7.1. Materials

For our purpose, a standard 12-lead (I, II, III, V_1, V_2, V_3, V_4, V_5, V_6, aV_R, aV_L, aV_F) ECG recording was continuously acquired over a period of 24 hours on a chronic kidney failure patient, undergoing HD treatment for 11 years [77], [78]. The continuous ECG was acquired by means of a wearable 12-lead M12 Global Instrumentation® digital Holter ECG recorder (Manlius, NY, sampling rate: 1000 Hz).

The ECG acquisition started at 11:00 am (hour zero) of a HD treatment day and lasted until 11:00 am of the following day. HD session went from 4:00 pm to 8:00 pm, as its duration was of 4 hours (i.e. the usual duration of Standard, or Conventional, HD). During the recording, the patient performed normal daily activities, e.g. walking, eating, sleeping; during HD, instead, the patient rested lying on his back. Additional information on the acquisition and on the patient is provided in Table 4.

Table 4. Information about the HD patient and the acquired ECG signal.

Patient information
Name: xxxxxxxxxxxxxxxx
Age: 82 years
Gender: male
Pathology: chronic kidney failure treated with extracorporeal HD
Recording Information
Duration: 24 h, from 11:00 (hour zero) of a HD day to 11:00 am of the following day; HD, from 4:00 pm to 8:00 pm
Minimum HR: 46 bpm (during the night)
Maximum HR: 92 bpm
Mean HR: 61 bpm
Ventricular ectopic beats: 585 • **Isolated: 477** • **Coupled: 51** • **Runs: 1**
Supraventricular ectopic beats: 140 • **Isolated: 122** • **Coupled: 4** • **Runs: 2**

The study was conducted in compliance with the ethical principles of the Helsinki Declaration and approved by the institutional expert committee; the patient gave his informed consent prior to testing.

7.2. Electrocardiographic alternans identification

The acquired ECG was analyzed by means of the HRAMF on Matlab 2018b. Each ECG lead, before ECGA analysis, was processed according to a series of steps, that are reported in Figure 56 and that will be described in the following pages.

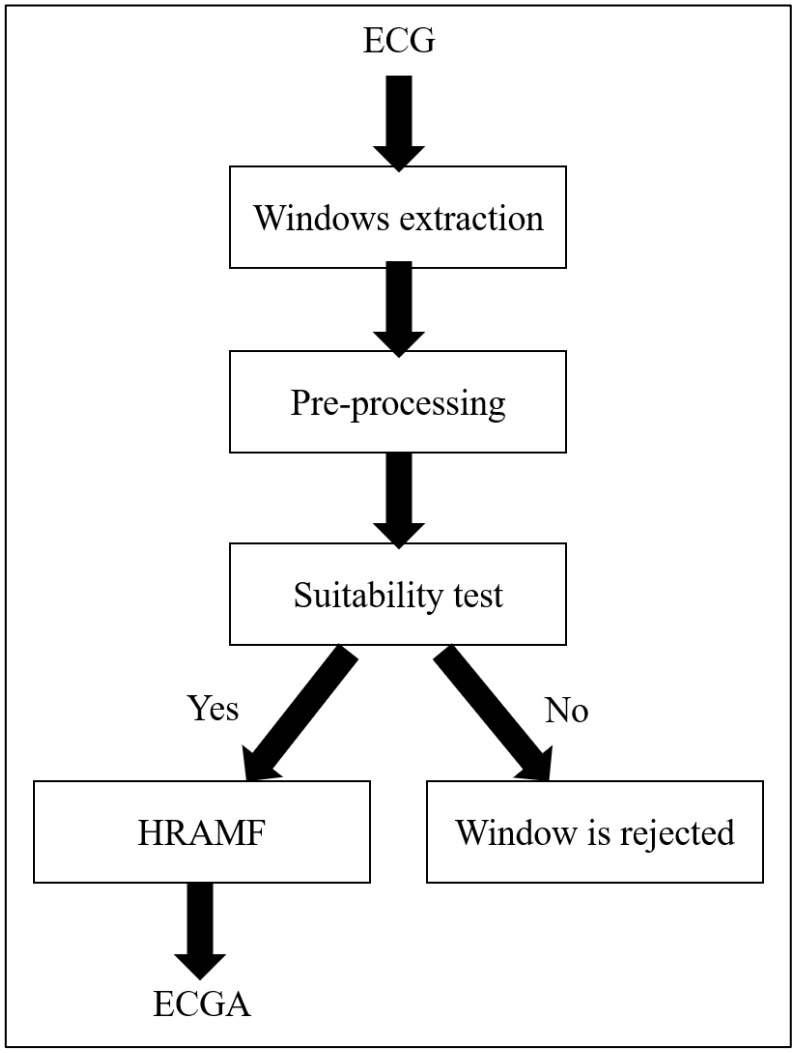

Figure 56. Block scheme representing the steps applied for ECGA analysis.

1. *Windows extraction*

   The ECG signal, for each lead, was first divided into recursively extracted windows, meaning that each window would find its start point 1 s after the previous window. All windows had a duration of 150 s, so that at least 128 beats would be contained in them.

2. *Pre-processing*

   All ECG windows were initially down sampled, from 1000 Hz to 200 Hz, and bidirectionally Butterworth filtered, with a low-pass filter with cut-off frequency of 45 Hz and a high-pass filter with cut-off frequency of 0.3 Hz, to remove respiration and power line artifacts. Pan-Tompkins' algorithm was then applied

to locate R-peaks positions, which were in turn used to identify ECG waves fiducial points, i.e. the onset, offset and peaks of the P wave, the QRS complex and the T wave. These fiducial points were obtained by defining temporal intervals that were either fixed or depending on HR [7].

When all ECG wave points had been found, the ECG windows were again filtered with a 6^{th} order bidirectional Butterworth band-pass filter, with low cut-off frequency equal to 35 Hz, in order to further remove high and low frequency components. Baseline was also removed, after being reconstructed by cubic spline interpolation: reference points for the baseline were found 80 ms before the R peaks. Afterwards, for each window and for each lead, QRS complexes and T waves were compared with the computed median QRS complex and T wave of the window. If correlation between one ECG wave and the corresponding median wave was less than 85%, the whole beat was discarded, since it may have been noisy or ectopic, and substituted with the computed median beat of the window. Then, to further prepare for ECGA analysis as an expression of PWA, QRSA and TWA, and study each alternans independently from the others, ECG waves that had to be excluded in the analysis were zeroed out (or brought to baseline values) in the following manner:

- for PWA analysis, P wave amplitudes were unvaried, while QRS complex and T wave were zeroed out;
- for QRSA analysis, QRS complex amplitudes were unvaried, while P wave and T wave were zeroed out;
- for TWA analysis, T wave amplitudes were unvaried, while P wave and QRS complex were zeroed out.

3. *Suitability test*

Once the pre-processing phase was completed, each window had to pass a suitability check, given by two conditions:

- the number of replaced beats per window had to be not greater than 10;
- the HR standard deviation had to be less or at maximum equal to 10% of the mean HR, i.e. we had to be in the presence of sinus rhythm.

If these two conditions were met, the window was considered suitable for ECGA analysis by means of the HRAMF method, otherwise the window was rejected and ECGA evaluation remained undetermined. Rejected windows were identified by a default value equal to -1.

4. *HRAMF method application*

   Suitable windows were analyzed for ECGA by means of a modified HRAMF. The new HRAMF, taking as input the processed ECG windows and their corresponding ECG waves fiducial points, was adapted to identify PWA, QRSA and TWA. As output, the HRAMF returned three separate pseudo sinusoidal signals, one for each type of alternans, where maxima and minima fell into the corresponding ECG wave. If alternans was not present, the sinusoid amplitude was equal to zero. If alternans was present, the sinusoid amplitude was greater than zero. PWA, QRSA and/or TWA amplitude values (μV), associated to each beat of the considered window, were directly computed from the related pseudo sinusoid amplitude in correspondence of the P wave, QRS complex and/or T wave, respectively. The amplitude values obtained for each beat for PWA, QRSA and TWA were gathered into three separate vectors.

Since distributions of alternans amplitudes could be normal or not, median values for each type of alternans were computed for each window. Moreover, PWA, QRSA and TWA areas (PWAA, QRSAA and TWAA respectively; μV·s) were calculated as the product between each alternans amplitude and the mean duration of the corresponding ECG wave [42].

7.3. Statistical analysis

To perform comparisons between the different types of alternans at different time periods during the HD day, the recording was divided into four macro-time periods:

- PRE-HD, preceding HD and going from 11:00 am to 4:00 pm;
- IN-HD, covering the whole HD session and going from 4:00 pm to 8:00 pm;

- POST-HD, following HD and going from 8:00 pm to 1:00 am;
- NT-HD, night period following POST-HD and going from 1:00 am to 6:00 am.

For each time period and for each lead, Lilliefors test, based on the Kolmogorov-Smirnov test, was applied to check if HR, PWA, QRSA and TWA, PWAA, QRSAA and TWAA distributions could be normal or not. In case of non-normality, distributions were described in terms of 50^{th} [25^{th};75^{th}] percentiles. Moreover, the percentage of windows accepted for ECGA analysis (NW) was obtained for all leads and time periods, and 50^{th} [25^{th};75^{th}] percentiles across all leads and for each time period were also computed.

Statistical comparisons among PWA, QRSA and TWA distributions in the different time periods and across all leads were performed by means of Wilcoxon rank-sum test, with statistical significance *p* set to 0.05. Statistical comparisons were also carried out, for each lead, between different types of alternans in the same time period. In the same manner, correlation coefficients between different types of alternans inside the same time period were computed.

Normal reference ECGA values were derived from previous studies, performed by means of the HRAMF, on normal male subjects. These reference values referred only to TWA [79], [80], while there were no reference values for PWA and QRSA analyzed with the same method. To have a basis for comparison between healthy and pathological subjects, reference values for TWA were also extended to PWA and QRSA, thus all types of alternans were considered pathological for values above 15 μV. Finally, the prevalent alternans was determined by the alternans with higher area with respect to the others.

7.4. Results

An overview of HR and NW results is reported in Table 5, with HR median values ranging from 59 bpm in PRE-HD and NT-HD to 66 bpm during POST-HD. NW was equal or lower than 70% (reached in lead V_5) among all leads, and windows were especially rejected during PRE-HD and IN-HD.

Table 5. ECGA (μV) and HR (bpm) distributions for all time periods, expressed as 50th [25th;75th] percentiles. NW expressed in percentage are also reported.

	PRE-HD			IN-HD			POST-HD			NT-HD			NW
	PWA	**QRSA**	**TWA**	**PWA**	**QRSA**	**TWA**	**PWA**	**QRSA**	**TWA**	**PWA**	**QRSA**	**TWA**	
I	9 [4;11]	10 [0;14]	**15 [13;20]**	12 [5;20]	**19 [0;26]**	14 [14;24]	0 [0;7]	**23 [17;26]**	10 [7;14]	0 [0;0]	0 [0;12]	**7 [5;9]**	31
II	13 [8;21]	19 [13;27]	**27 [18;37]**	16 [10;26]	**28 [21;34]**	26 [21;33]	9 [7;12]	12 [9;16]	**18 [13;26]**	7 [0;11]	12 [4;17]	**20 [14;31]**	61
III	13 [9;21]	16 [10;24]	**28 [18;44]**	13 [10;18]	24 [18;33]	**29 [21;39]**	10 [8;14]	**26 [19;33]**	23 [15;38]	7 [0;11]	15 [9;22]	**21 [15;32]**	47
V_1	8 [0;11]	0 [0;12]	**15 [11;22]**	8 [0;13]	11 [0;14]	**17 [13;21]**	6 [0;9]	**12 [9;15]**	**12 [8;18]**	0 [0;7]	0 [0;12]	**12 [9;19]**	44
V_2	11 [7;16]	16 [10;24]	**22 [15;30]**	13 [10;15]	**24 [17;29]**	23 [19;25]	6 [0;10]	**23 [19;28]**	16 [10;24]	0 [0;0]	9 [0;15]	**12 [9;16]**	30
V_3	13 [8;22]	20 [14;30]	**29 [19;41]**	15 [11;19]	25 [21;34]	**28 [22;33]**	10 [7;13]	18 [13;23]	**20 [14;32]**	6 [0;10]	13 [6;18]	**20 [14;29]**	59
V_4	13 [6;18]	16 [3;24]	**31 [18;42]**	17 [13;22]	23 [17;32]	**29 [21;41]**	6 [0;10]	**36 [22;49]**	20 [15;27]	0 [0;3]	0 [0;30]	**12 [8;18]**	66
V_5	14 [8;21]	23 [13;31]	**40 [23;59]**	19 [13;26]	26 [18;38]	**37 [24;49]**	0 [0;10]	12 [0;18]	**21 [14;29]**	0 [0;0]	0 [0;7]	**10 [8;16]**	70
V_6	9 [0;14]	16 [10;23]	**26 [16;40]**	19 [13;32]	37 [26;45]	**38 [24;66]**	6 [0;11]	**54 [25;85]**	21 [16;28]	0 [0;0]	10 [0;54]	**13 [9;22]**	29
aV_R	14 [8;22]	29 [19;37]	**31 [22;43]**	18 [10;26]	**41 [27;47]**	32 [17;39]	5 [0;10]	**39 [21;58]**	26 [18;33]	0 [0;5]	**15 [0;23]**	12 [9;20]	62
aV_L	13 [3;19]	23 [12;31]	**25 [17;34]**	14 [6;19]	**27 [19;36]**	23 [16;31]	0 [0;8]	**21 [14;31]**	15 [11;22]	0 [0;0]	**10 [0;16]**	**10 [7;16]**	59
aV_F	10 [0,14]	13 [0;22]	**20 [15;29]**	10 [8;13]	**27 [22;36]**	22 [18;28]	0 [0;6]	**18 [12;25]**	10 [7;16]	0 [0;0]	**10 [0;17]**	**10 [6;16]**	47
Tot	13 [7;19]	16 [10;24]	**27 [18;39]**	15¢ [10;20]	26* [19;34]	**27 [20;33]**	6§ [0;10]	**22 [16;27]**	19* [14;27]	0º [0;2]	10* [0;17]	**12§ [9;19]**	53
HR		59 [57;62]			62 [61;65]			66 [65;68]			59 [58;63]		100

*PRE-HD vs all other time periods ¢: $p < 0.05$; *: $p < 10^{-2}$; §: $p < 10^{-3}$; º: $p < 10^{-4}$*

Distributions concerning ECGA median amplitude values are reported, also in Table 5, in terms of 50th [25th;75th] percentiles, as all distributions were not normal. In several cases, TWA amplitude values were higher compared to PWA and QRSA ones across all time periods. In particular, TWA highest median amplitude value was observed in lead V_6 during IN-HD. However, during IN-HD and especially during POST-HD, also QRSA appeared to have the highest amplitude values with respect to the other kinds of alternans, reaching 41 μV in IN-HD for lead aV_R and 54 μV in POST-HD for lead V_6.

TWA median amplitude values and percentiles were especially high in PRE-HD and IN-HD, while decreased after the end of the treatment. QRSA values instead, seemed to increase already during treatment and even more so in POST-HD, only to decrease again to very low amplitudes in NT-HD. PWA was always the alternans presenting the lowest median amplitude values: values slightly increased during IN-HD and dramatically decreased soon after the end of the treatment. Moreover, PWA values were always smaller than 15 μV, considered as physiological threshold, except for leads II, V_4, V_5, V_6 and aV_R during IN-HD (Table 5).

The trend just described can be observed also in Figure 57, where PWA, QRSA and TWA evolution of median values, calculated in intervals of 15 minutes over the course of the recording and over all precordial leads, is represented. Values for all three kinds of alternans increased during IN-HD, with a peak in correspondence of the second hour of treatment (IN-HD). TWA and PWA then started to decrease about one hour after the end of HD, almost stabilizing themselves, while QRSA decreased between the end of POST-HD and the beginning of NT-HD (around 1:00 am). Obviously, this graph excluded rejected windows, but temporal information was kept.

The tendency of QRSA amplitude values to increase during and especially after treatment is even more visible in lead V_6. Lead V_6, together with leads V_5 and III, and V_4 and aV_R, was the most sensitive leads, since its amplitude values were the highest among all leads. This can be observed in Table 5, as well as in Figures 58, 59 and 60, representing PWA, QRSA and TWA amplitude trends for all 12 leads.

The differences in ECGA trends described so far seem to be reflected by statistical analysis concerning the distributions reported in Table 5. In fact, statistical differences across all leads between PRE-HD and POST-HD, and PRE-HD and NT-HD, were

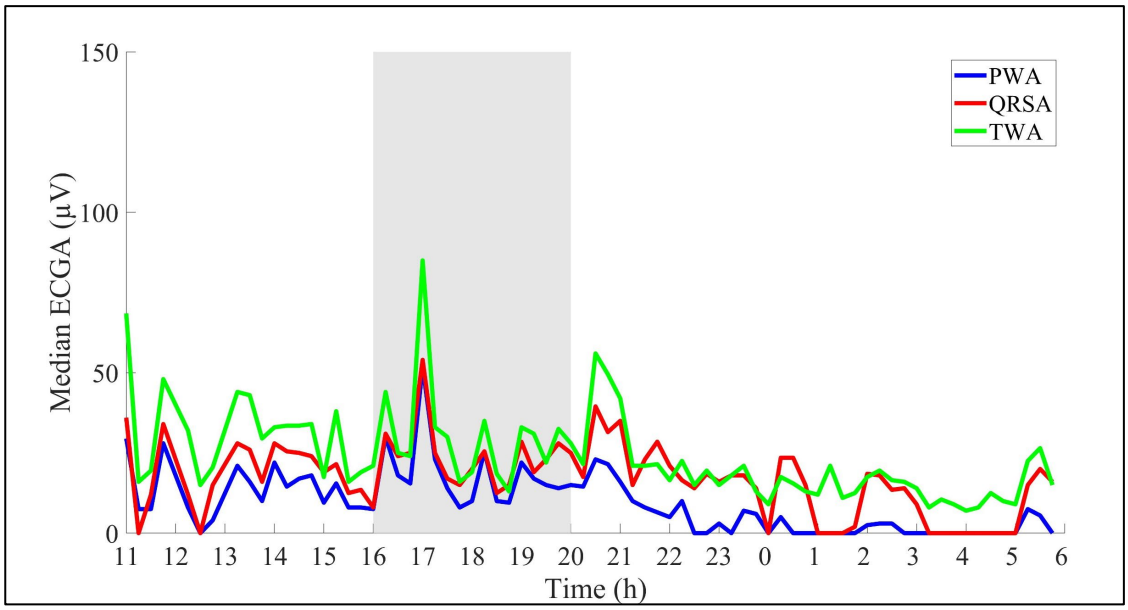

Figure 57. ECGA trend over the whole recording and across all precordial leads, described by median amplitude values computed in intervals of 15 minutes. Grey area corresponds to IN-HD.

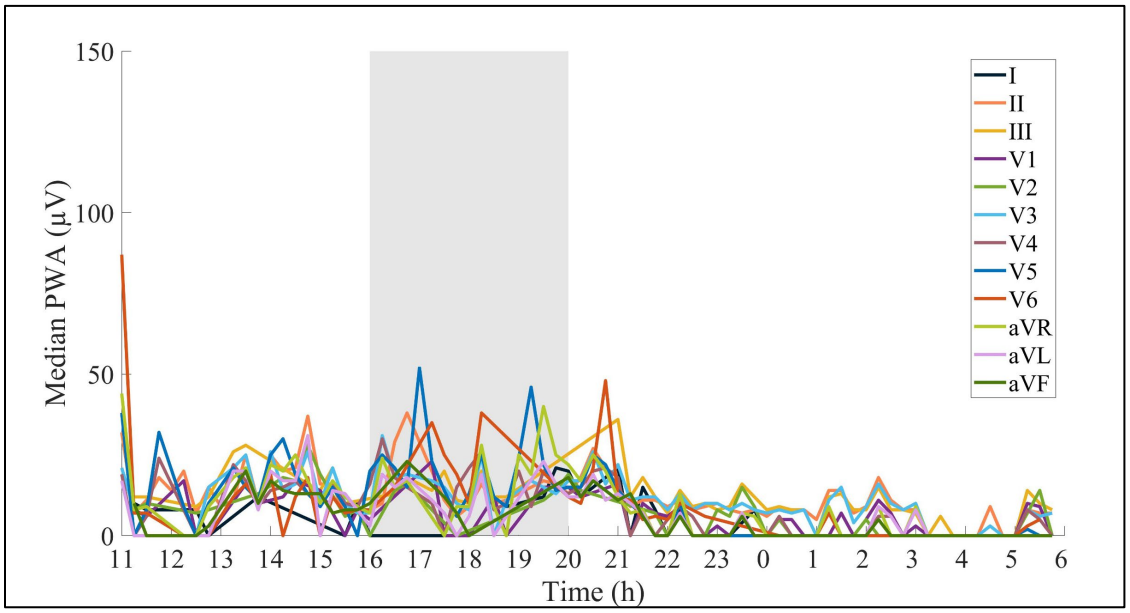

Figure 58. PWA trend over the whole recording and for all leads, described by median amplitude values computed in intervals of 15 minutes. Grey area corresponds to IN-HD.

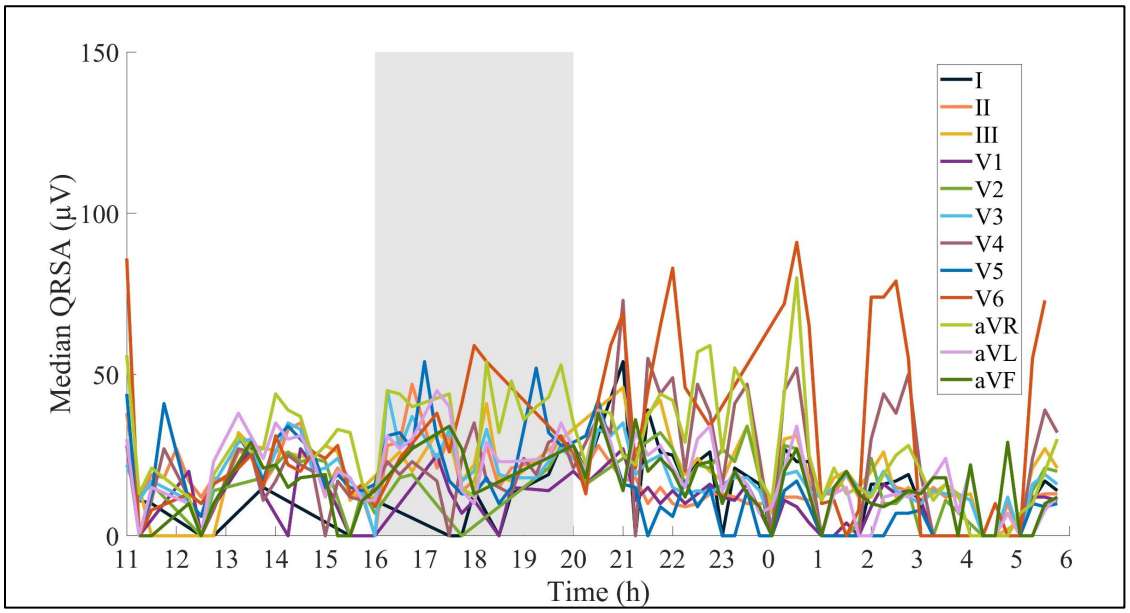

Figure 59. QRSA trend over the whole recording and for all leads, described by median amplitude values computed in intervals of 15 minutes. Grey area corresponds to IN-HD.

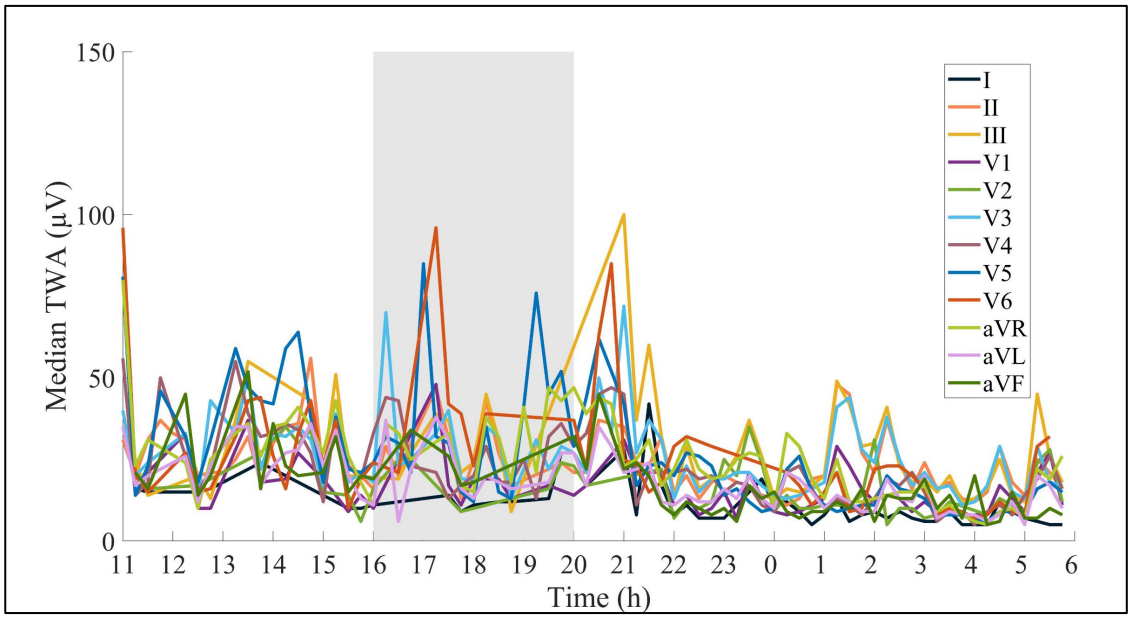

Figure 60. TWA trend over the whole recording and for all leads, described by median amplitude values computed in intervals of 15 minutes. Grey area corresponds to IN-HD.

observed for PWA (PRE-HD vs POST-HD: p=2.65x10^{-4}; PRE-HD vs NT-HD: p=2.02x10^{-5}) and TWA (PRE-HD vs POST-HD: p=0.00775; PRE-HD vs NT-HD: p=2.31x10^{-4}). Statistical differences were also found between IN-HD and POST-HD, and IN-HD and NT-HD for both PWA (IN-HD vs POST-HD: p=8.88x10^{-5}; IN-HD vs NT-HD: p=2.20x10^{-5}) and TWA (IN-HD vs POST-HD: p=0.00382; IN-HD vs NT-HD: p=1.47x10^{-4}). There was also statistical difference between PRE-HD and IN-HD for PWA (PRE-HD vs IN-HD: p=0.0434). No statistical differences were instead observed between PRE-HD and IN-HD, and POST-HD and NT-HD for TWA (PRE-HD vs IN-HD: p=0.817; POST-HD vs NT-HD: p=0.0573), and between POST-HD and NT-HD for PWA (POST-HD vs NT-HD: p=0.0713).

For QRSA, there were statistical differences between PRE-HD and IN-HD, and PRE-HD and NT-HD (PRE-HD vs IN-HD: p=5.41x10^{-3}; PRE-HD vs NT-HD: p=1.82x10^{-3}). Statistical differences were also observed between IN-HD and NT-HD, and POST-HD and NT-HD (IN-HD vs NT-HD: p=9.17x10^{-5}; POST-HD vs NT-HD: p=3.96x10^{-4}), while no differences were found between PRE-HD and POST-HD, and IN-HD and POST-HD (PRE-HD vs POST-HD: p=0.817; IN-HD vs POST-HD: p=0.247).

In Table 6, correlation coefficients computed between different kinds of alternans in the same time period and for each lead are reported. In most cases, moderate positive correlation was found for PWA vs QRSA, PWA vs TWA and QRSA vs TWA in PRE-HD and IN-HD. Correlation coefficients then slightly decreased in IN-HD and POST-HD, especially for PWA vs QRSA, and in NT-HD, where coefficients were not higher than 0.65 for the majority of leads and alternans comparisons. Leads from II to V_3, however, still showed high correlation for PWA vs TWA in NT-HD.

Still in Table 6, statistical differences between PWA and QRSA amplitudes, PWA and TWA amplitudes, and QRSA and TWA amplitudes were observed in almost all leads and time periods. The only exception was given by QRSA vs TWA comparison in NT-HD for lead aV_R, where no statistical difference was found (p=0.99).

In Table 7, correlation coefficients between different types of alternans, during the whole recording, are reported in terms of 50^{th} [25^{th};75^{th}] percentiles. For each lead and for each alternans comparison, weak to moderate positive correlation was observed. However, interquartile ranges (given by the difference between 75^{th} and 25^{th} percentiles) of correlation coefficients were considerable across the whole recording, in all cases.

Table 6. Correlation coefficients among the different types of alternans, for the same time periods. High correlation values are reported in bold.

	PRE-HD			IN-HD			POST-HD			NT-HD		
	PWA vs QRSA	**PWA vs TWA**	**QRSA vs TWA**	**PWA vs QRSA**	**PWA vs TWA**	**QRSA vs TWA**	**PWA vs QRSA**	**PWA vs TWA**	**QRSA vs TWA**	**PWA vs QRSA**	**PWA vs TWA**	**QRSA vs TWA**
I	0.55 §	0.30 *	0.36 *	**0.86** §	0.65 §	**0.76** *	0.42 *	**0.79** *	0.41 *	0.14 *	0.24 *	-0.01 *
II	0.66 *	0.66 *	0.65 *	**0.78** *	0.27 *	0.36 *	0.55 *	0.67 *	0.63 *	0.58 *	**0.81** *	0.60 *
III	0.69 §	**0.78** *	**0.80** *	0.51 *	**0.80** *	0.62 *	0.64 *	**0.88** *	**0.70** *	0.53 *	**0.84** *	0.55 *
V_1	0.57 §	0.53 *	0.68 *	0.30 §	0.62 *	0.55 *	0.37 *	0.59 *	0.36 *	0.62 *	**0.76** *	0.45 *
V_2	0.57 *	0.58 *	0.65 *	**0.76** *	0.29 *	0.27 §	0.26 *	**0.73** *	0.28 *	0.51 *	**0.78** *	0.56 *
V_3	0.61 *	**0.71** *	0.66 *	0.60 *	0.45 *	0.54 §	0.55 *	**0.77** *	0.70 *	0.54 *	**0.82** *	0.58 *
V_4	**0.71** *	**0.75** *	**0.79** *	0.39 *	0.51 *	0.50 *	0.23 *	**0.75** *	0.55 *	0.39 *	0.59 *	0.62 *
V_5	**0.77** *	**0.73** *	**0.76** *	0.66 *	0.67 *	0.71 *	**0.79** *	**0.78** *	**0.76** *	0.36 *	0.58 *	0.46 *
V_6	0.64 *	0.67 *	0.55 *	-0.03 *	**0.78** *	-0.01 §	-0.09 *	**0.74** *	0.21 *	0.24 *	0.58 *	0.67 *
aV_R	**0.71** *	0.67 *	0.59 *	0.52 *	0.68 *	0.56 *	-0.09 *	**0.71** *	0.26 *	0.40 *	0.66 *	0.53
aV_L	0.64 *	0.59 *	0.60 *	0.47 *	0.31 *	**0.75** §	0.28 *	0.66 *	0.40 *	0.05 *	0.64 *	0.21 *
aV_F	**0.71** *	0.67 *	0.67 *	0.29 *	0.61 *	0.29 §	0.20 *	**0.87** *	0.17 *	0.19 *	0.49 *	0.51 *
Tot	0.65 *	0.67 *	0.65 *	0.51 *	0.61 *	0.55 §	0.33 *	**0.74** *	0.41 *	0.40 *	0.65 *	0.54 *

*§: $p< 10^{-3}$; *: $p< 10^{-15}$*

Table 7. Correlation coefficients for comparisons among the different types of alternans, described in terms of 50th [25th;75th] percentiles.

	PWA vs QRSA	PWA vs TWA	QRSA vs TWA
I	0.14 [-0.04;0.59]	0.31 [-0.05;0.60]	0.04 [-0.11;0.44]
II	0.44 [0.13;0.63]	0.50 [0.17;0.64]	0.49 [0.26;0.68]
III	0.21 [-0.04;0.43]	0.61 [0.41;0.84]	0.53 [0.04;0.77]
V_1	0.25 [$-8.54x10^{-4}$;0.52]	0.38 [0.04;0.79]	0.29 [0.09;0.64]
V_2	0.17 [-0.12;0.47]	0.39 [0.07;0.71]	0.37 [-0.04;0.54]
V_3	0.33 [0.06;0.60]	0.56 [0.26;0.78]	0.53 [0.26;0.73]
V_4	0.25 [0.06;0.60]	0.47 [0.22;0.69]	0.45 [0.14;0.71]
V_5	0.47 [0.12;0.72]	0.51 [0.25;0.75]	0.44 [0.14;0.69]
V_6	0.26 [0.01;0.60]	0.34 [$9.48x10^{-4}$;0.57]	0.44 [0.04;0.75]
aV_R	0.21 [-0.09;0.57]	0.46 [0.17;0.70]	0.32 [0.08;0.64]
aV_L	0.13 [-0.09;0.60]	0.49 [0.16;0.64]	0.45 [0.05;0.63]
aV_F	0.15 [-0.04;0.40]	0.56 [0.14;0.74]	0.28 [-0.14;0.62]
Tot	0.23 [-0.02;0.59]	0.48 [0.17;0.71]	0.44 [0.07;0.66]

In Table 8, results for ECGA areas distributions are reported. TWA was the prevalent alternans, as median TWAA was greater than both PWAA (that was always the area with lowest values) and QRSAA in all leads and all time periods, except for lead V_6 in POST-HD, where QRSAA (4.3 μV·s) was slightly higher than TWAA (4.2 μV·s). Median area values for the three types of alternans, similarly to Table 5 and Figure 57, were higher in PRE-HD and IN-HD, only to decrease in POST-HD and NT-HD.

The trend observed in Table 8 is also noticeable in Figure 61, where ECGA areas progression over the whole recording and for all precordial leads are shown. PWAA, QRSAA and TWAA also presented a peak in correspondence of the second hour of HD, and areas decreased after treatment, particularly one hour after the end of HD. During the

Table 8. ECGA area (µV·s) distributions for all time periods, expressed as 50th [25th;75th] percentiles.

	PRE-HD			IN-HD			POST-HD			NT-HD		
	PWAA	**QRSAA**	**TWAA**	**PWAA**	**QRSAA**	**TWAA**	**PWAA**	**QRSAA**	**TWAA**	**PWAA**	**QRSAA**	**TWAA**
I	0.9 [0.4;1]	0.8 [0;1.1]	**3 [2.6;4]**	1.2 [0.5;2]	1.5 [0;2.1]	**2.8 [2.2;4.8]**	0 [0;0.7]	1.8 [1.4;2]	**2 [1.4;3]**	0 [0;0]	0 [0;1]	**1.4 [1;1.8]**
II	1.3 [0.8;2]	1.5 [1;2.2]	**5.4 [3.6;7.4]**	1.6 [1;2.6]	2.2 [1.7;3]	**5.2 [4.2;6.6]**	0.9 [0.7;1]	1 [0.7;1]	**3.6 [2.6;5]**	0.7 [0;1.1]	1 [0.3;1]	**4 [2.8;6]**
III	1.3 [0.9;2]	1.3 [0.8;2]	**5.6 [3.6;8.8]**	1.3 [1;1.8]	1.9 [1.4;3]	**5.8 [4.2;7.8]**	1 [0.8;1]	2 [1.5;3]	**4.6 [3;7.6]**	0.7 [0;1.1]	1.2 [0.7;2]	**4.2 [3;6.4]**
V_1	0.8 [0;1]	0 [0;1]	**3 [2.2;4.4]**	0.8 [0;1.3]	0.9 [0;1.1]	**3.4 [2.6;4.2]**	0.6 [0;0.9]	1 [0.7;1]	**2.4 [1.6;4]**	0 [0;0.7]	0 [0;1]	**2.4 [1.8;4]**
V_2	1.1 [0.7;2]	1.3 [0.8;2]	**4.4 [3;6]**	1.3 [1;1.5]	1.9 [1.4;3]	**4.6 [3.8;5]**	0.6 [0;1]	1.8 [1.5;2]	**3.2 [2;4.8]**	0 [0;0]	0.7 [0;1.2]	**2.4 [1.8;3]**
V_3	1.3 [0.8;2]	1.6 [1.1;2]	**5.8 [3.8;8.2]**	1.5 [1.1;2]	2 [1.7;3]	**5.6 [4.4;6.6]**	1 [0.7;1]	1.4 [1;1.8]	**4 [2.8;6]**	0.6 [0;1]	1 [0.5;1]	**4 [2.8;6]**
V_4	1.3 [0.6;2]	1.3 [0.2;2]	**6.2 [3.6;8.4]**	1.7 [1.3;2]	1.8 [1.4;3]	**5.8 [4.2;8.2]**	0.6 [0;1]	2.9 [1.8;4]	**4 [3;5.4]**	0 [0;0.3]	0 [0;2.4]	**2.4 [1.6;4]**
V_5	1.4 [0.8;2]	1.8 [1;2.5]	**8 [4.6;12]**	1.9 [1.3;3]	2.1 [1.4;3]	**7.4 [4.8;9.8]**	0 [0;1]	1 [0;1.4]	**4.2 [2.8;6]**	0 [0;0]	0 [0;5.6]	**2 [1.6;3]**
V_6	0.9 [0;1.4]	1.3 [0.8;2]	**5.2 [3.2;8]**	1.9 [1.3;3]	3 [2.1;4]	**7.6 [4.8;13]**	0.6 [0;1.1]	**4.3 [2;6.8]**	4.2 [3.2;6]	0 [0;0]	0.8 [0;4.3]	**2.6 [1.8;4]**
aV$_R$	1.4 [0.8;2]	2.3 [1.5;3]	**6.2 [4.4;8.6]**	1.8 [1;2.6]	3.3 [2.2;4]	**6.4 [3.4;7.8]**	0.5 [0;1]	3.1 [1.7;5]	**5.2 [3.6;7]**	0 [0;0.5]	1.2 [0;1.8]	**2.4 [1.8;4]**
aV$_L$	1.3 [0.3;2]	1.8 [1;2.5]	**5 [3.4;6.8]**	1.4 [0.6;2]	2.2 [1.5;3]	**4.6 [3.2;6.2]**	0 [0;0.8]	1.7 [1.1;3]	**3 [2.2;4]**	0 [0;0]	0.8 [0;1.3]	**2 [1.4;3]**
aV$_F$	1 [0,1.4]	1 [0;1.8]	**4 [3;5.8]**	1 [0.8;1]	2.2 [1.8;3]	**4.3 [3.6;5.6]**	0 [0;0.6]	1.4 [1;2]	**2 [1.4;3]**	0 [0;0]	0.8 [0;1.4]	**2 [1.2;3]**
Tot	1.3 [0.7;2]	1.3 [0.8;2]	**5.3 [3.5;7.7]**	1.5 [1;2]	2 [1.5;3]	**5.4 [4;6.6]**	0.6 [0;1]	1.8 [1.2;2]	**3.8 [2.7;5]**	0 [0;0.2]	0.8 [0;1.4]	**2.4 [1.8;4]**

night hours, TWAA values were always lower than 5 µV·s, while PWAA and QRSAA reached values close or even equal to 0 µV·s.

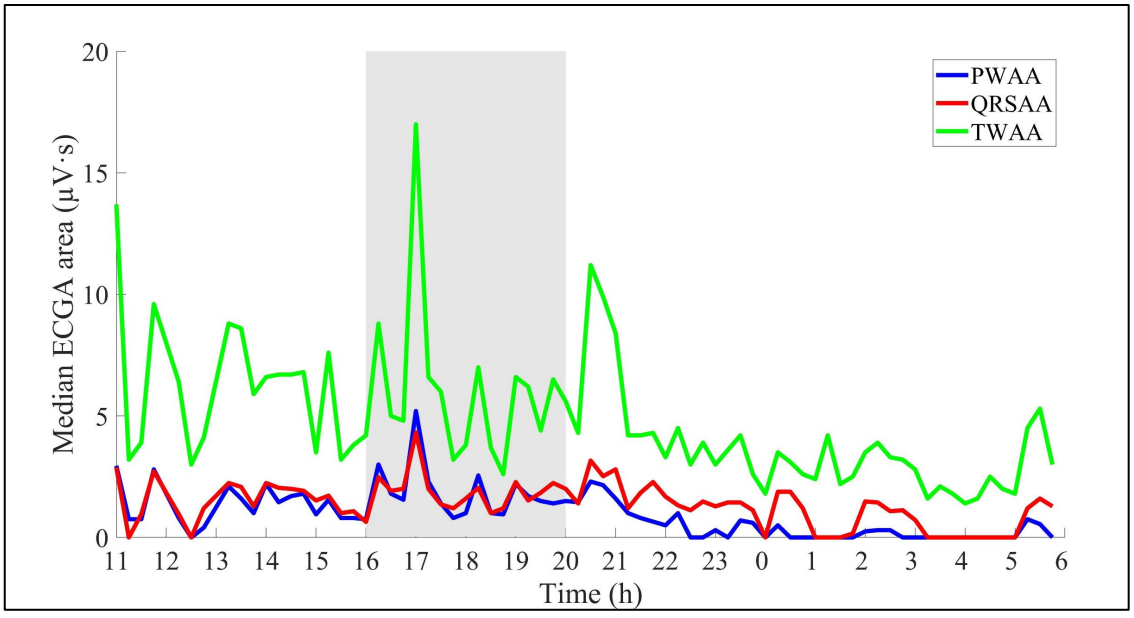

Figure 61. ECGA area trends over the whole recording and across all precordial leads, with median values computed in intervals of 15 minutes. Grey area corresponds to IN-HD.

7.5. Discussions

This thesis work marks the first time that an improved quantification method for ECGA has been applied for alternans analysis in a HD patient. The new method, based on the HRAMF, aimed to remove any possible reciprocal influence that PWA, QRSA and TWA may exert on each other during quantification, according to the changing interpretation of ECGA. Not only ECGA should be seen as the prevalent nature of alternans in the ECG, but also as an expression of the three types of alternans, that should be therefore robustly and reliably measured. For these reasons, while the previous ECGA quantification methods computed PWA, QRSA and TWA from a single pseudo sinusoidal signal obtained from the filtered ECG window [2], [42], [78], the new method here applied relied on the computation of alternans from three separate sinusoidal signals, each obtained by filtering ECG windows where certain ECG waves had been previously brought to baseline, depending on the considered kind of alternans (e.g. QRS complex and T wave were zeroed out when PWA was studied).

Statistical analysis performed on the HD case here presented allowed to see the effects of such improved method. Values of *p* for PWA and QRSA among different time periods (Table 5) showed statistical differences even between PRE-HD and IN-HD periods, compared to previous unpublished results (Table 9). In fact, results in Table 9, obtained for the same patient with an earlier ECGA identification method, showed no statistical difference between PRE-HD and IN-HD periods. Moreover, additional *p*-values reported in Table 6, obtained comparing different types of alternans inside the same macro-time period, showed statistical differences throughout the entire recording. As this suggests that alternans distributions are made of significantly different values, it could also be a first confirmation of the fact that the method was indeed able to quantify PWA, QRSA and TWA in an independent manner. Correlation coefficients from Tables 6 and 7 seem to corroborate this result. Weak-to-moderate correlation was in fact observed among the different types of alternans, in each time period and throughout the whole recording, whereas previous unpublished results, performed with the same method as of Table 9, showed very high positive correlation among PWA, QRSA and TWA.

The presence of weak correlation among PWA, QRSA and TWA, however, lets us assume that certain phenomena involving and influencing the three alternans cannot be

Table 9. HR (bpm), PWA, QRSA and TWA distributions (μV) for PRE-HD, IN-HD, POST-HD and NT-HD periods, expressed as 50th [25th;75th] percentiles, obtained with previous quantification methods. NW is reported in percentage.

	PRE-HD			IN-HD			POST-HD			NT-HD			NW
	PWA	QRSA	TWA	PWA	QRSA	TWA	PWA	QRSA	TWA	PWA	QRSA	TWA	
I	53 [43;69]	**62 [49;74]**	33 [27;41]	60 [35;76]	**81 [43;106]**	31 [27;46]	29 [23;40]	**37 [30;51]**	19 [15;29]	21 [18;26]	**26 [20;33]**	13 [10;17]	31
II	79 [56;111]	**94 [64;128]**	54 [35;75]	96 [77;119]	**100 [74;128]**	57 [46;76]	46 [36;62]	**55 [42;75]**	34 [25;47]	49 [37;68]	**58 [43;80]**	38 [27;57]	61
III	74 [54;136]	**84 [62;126]**	51 [32;84]	91 [62;134]	**95 [68;142]**	54 [41;80]	55 [41;91]	**67 [47;104]**	43 [29;76]	50 [36;70]	**59 [44;86]**	38 [28;56]	47
V_1	47 [36;64]	**54 [38;72]**	32 [24;45]	53 [31;66]	**55 [45;65]**	37 [32;41]	32 [25;48]	**39 [30;55]**	24 [17;34]	33 [26;46]	**38 [29;52]**	24 [17;37]	44
V_2	67 [47;95]	**76 [59;96]**	43 [30;57]	60 [55;73]	**71 [62;83]**	40 [35;44]	38 [28;58]	**48 [36;74]**	28 [18;45]	30 [23;40]	**38 [29;49]**	22 [17;31]	30
V_3	81 [56;123]	**95 [62;136]**	57 [36;82]	86 [73;120]	**95 [72;120]**	52 [42;72]	54 [37;76]	**60 [43;89]**	40 [27;59]	48 [36;65]	**58 [42;77]**	37 [27;52]	59
V_4	79 [45;107]	**85 [53;127]**	55 [31;74]	87 [65;108]	**104 [81;129]**	55 [41;73]	31 [24;51]	**33 [26;65]**	21 [16;37]	27 [22;35]	**30 [25;37]**	17 [13;25]	66
V_5	101 [57;143]	**116 [73;168]**	62 [38;92]	119 [84;152]	**134 [99;175]**	59 [42;77]	34 [25;61]	**51 [35;74]**	28 [19;42]	27 [22;35]	**34 [26;46]**	18 [14;23]	70
V_6	70 [49;105]	**83 [54;110]**	42 [30;63]	**126 [80;193]**	120 [82;182]	66 [47;112]	80 [61;91]	**96 [78;113]**	37 [32;47]	38 [23;70]	**42 [27;86]**	24 [14;40]	29
aV_R	94 [60;128]	**101 [68;139]**	58 [40;82]	91 [56;144]	**94 [70;136]**	52 [33;79]	**65 [49;81]**	64 [51;83]	37 [28;53]	32 [23;47]	**35 [26;50]**	21 [15;33]	62
aV_L	70 [48;104]	**81 [56;119]**	50 [35;66]	71 [46;106]	**87 [49;114]**	46 [34;70]	**38 [30;51]**	37 [28;57]	25 [17;35]	28 [21;37]	**30 [22;40]**	19 [14;28]	59
aV_F	58 [43,78]	**67 [47;92]**	38 [29;53]	59 [50;75]	**83 [61;113]**	56 [45;68]	29 [24;41]	**31 [25;42]**	19 [14;29]	29 [20;41]	**31 [22;47]**	20 [14;31]	47
Tot	72 [49;106]	**84 [58;123]**	51 [32;70]	78 [59;115]	**95 [69;124]**	53 [41;73]	38 * [29;60]	**50 * [36;74]**	28 § [19;44]	31 ° [23;44]	**37 ° [27;50]**	22 § [15;32]	53
HR		59 [57;62]			62 [61;65]			66 [65;68]			59 [58;63]		100

**: $p<10^{-2}$; §: $p<10^{-3}$; °: $p<10^{-4}$*

ruled out, as they may happen a priori on a physiological level. It has been in fact noted by [41] and [65] that changes in one ECG wave may bring in turn changes in the other ECG waves. It has been also observed that discordant alternans in AP duration, where duration alternates out of phase, can affect T wave and QRS complex width and amplitude, producing both QRSA and TWA. Such fluctuations could therefore coexist: changes in AP, usually caused by ionic accumulation or slow recovery of ion channels, e.g. L-type Ca^{2+} channels and K^+ channels [81], could be extended to the entire ventricles, affecting both ventricular depolarization and repolarization at the same time. Hyperkalemia and hypocalcemia, as seen in Chapter 4, are in fact often observed simultaneously in ESRD patients prior to HD treatment, with the former causing peaked T waves and widened QRS complexes and the latter decreasing cardiac contractility and leading to heart failure [16], [43], and electrolytes concentrations are thus known to well correlate with ECG findings in HD patients [58], [63], [65]. For these reasons, we could suppose that the correlation coefficients here found may depend on omitted variables such as electrolyte concentrations. Future researches taking also into account how ionic

concentrations may affect ECGA in HD could contribute to lower the already weak correlation that was here noticed.

Ionic concentrations rebalancing performed by HD treatment may also be at the basis of the trends observed in Figures 57 and 61, and Tables 5 and 8. TWA showed increased amplitude values before and during HD, highlighting PRE-HD and IN-HD as periods characterized by high SCD risk. In particular, an alternans peak, for TWA but also for QRSA and PWA, was observed during the second hour of HD, perhaps due to cardiac distress and ectopic beats happening during HD (cardiac distress also caused ECG windows to be especially rejected before and during HD, as seen also in [77] and [78] for the same patient). Median amplitude values then decreased one hour after the end of HD, probably as a consequence of treatment itself. This evolution in time appears to be in agreement with those reported by [74], [77] and [78], where TWA and, therefore, SCD risk were elevated before and during HD and decreased only after treatment, most likely thanks to HD effects again. Amplitude values here reported, for all kinds of alternans (see also Table 9), are much lower than [78], as expected thanks to the new and improved quantification method, that avoids alternans overestimation due to reciprocal influence, as well as to the computation of median values, that allow to exclude extremely noisy measurements.

PWA, always lower than 15 μV [79], [80], showed a similar trend compared to TWA and almost disappeared in NT-HD. The only exceptions in this time period are given by limb leads II and III, where PWA assumed values around 7 μV. QRSA instead started to increase already during IN-HD, showing highest amplitude values in POST-HD. Such an increase has been here observed for the first time in terms of alternans: previously published studies mentioning QRSA only investigated about QRSA episodes [75]. One could assume that the increment in QRSA amplitude after HD may be related to a general increase of QRS complex duration and amplitude following ionic rebalancing treatment [58]. These changes in QRS complex have been in fact described in [61], [65] and [66], where HD patients were studied. Following the same reasoning, PWA trends here observed would appear to be in contrast with previous ECG findings. However, according to [64], increases in P wave duration and amplitude could be related to possible hypokalemia that may have manifested itself after HD treatment in [64] and that may have been absent in our case study.

QRSA increase after HD, as previously mentioned in the chapter dedicated to the results, was especially evident in certain leads, one of them being precordial lead V_6. QRSA trend for lead V_6 is reported in Figure 62, where it is possible to easily observe how, immediately after HD, QRSA dramatically increases in amplitude, compared to TWA and PWA which instead decrease towards very low amplitudes. A possible explanation for certain leads being the most sensitive to alternans (Figures 58, 59 and 60) could be given by the lead dependency of alternans: the concept, formalized for TWA [82], could be extended to other types of alternans as well [78]. Still in terms of ECGA amplitude, TWA being the highest in PRE-HD, IN-HD and NT-HD, and then QRSA increasing in POST-HD, given the corresponding ECG waves, indicate cardiac problems at the level of the ventricles that could be due to chronic kidney failure and HD treatment distress. As PWA instead appears to be much lower in amplitude compared to the others and in almost all cases under physiological threshold [79], [80], pathologies affecting the atrial chambers of the heart could be excluded. Physiological threshold, however, should be revised once reliable reference values for PWA and QRSA are obtained.

For what concerns ECGA area, with areas considered for the first time by [42] in order to take into account the different lengths of each ECG wave, distress affecting the

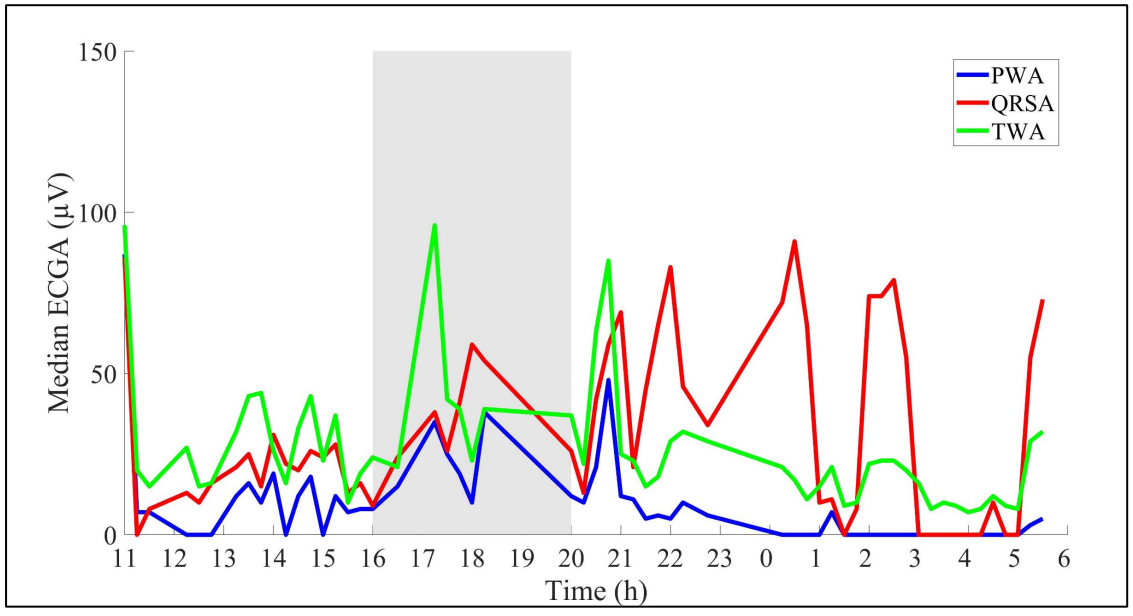

Figure 62. Median ECGA trend over the whole recording and for lead V_6. Median amplitude values were computed in intervals of 15 minutes. Grey are represents HD.

ventricles is still confirmed. In fact, ECGA can be identified with TWA, with the prevalence of TWA being perceivable throughout the entire recording. Exceptions are found only in POST-HD for lead V_6, where QRSA is prevalent. As PWAA, QRSAA and TWAA are computed multiplying PWA amplitude with P-wave mean duration, QRSA amplitude with QRS mean duration and TWA amplitude with T-wave mean duration, respectively, the increased sensitivity shown by certain leads, e.g. V_5 and V_6, is maintained. In Figure 63, it is possible to observe, again for lead V_6, how QRSAA increases after HD treatment, while TWAA and PWAA decline.

Despite this study being limited to a single HD patient, the results here obtained proved that the improved method for ECGA quantification, based on the HRAMF, could reliably measure PWA, QRSA and TWA in an independent way, as trends observed, in particular for TWA, were mostly concordant with those reported by previous studies. The new method also allowed us to delve into the relationship among the different types of alternans, as well as their clinical meaning, as it was noted that HD treatment mainly affects electrical activity at the level of the ventricles. Future studies involving ECGA quantification with this method are however encouraged, based on availability of data: an increased HD population would help further investigate and eventually confirm our findings.

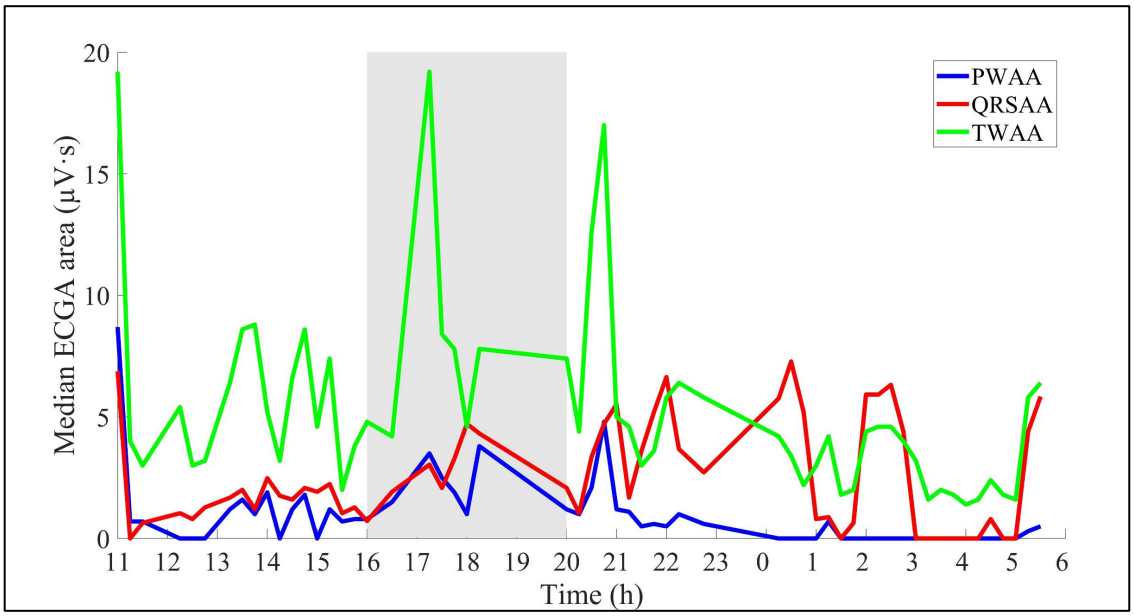

Figure 63. Median ECGA area trend over the whole recording and for lead V_6. Values were computed in intervals of 15 minutes. Grey area corresponds to HD.

CONCLUSIONS

The aim of this thesis was to validate an improved quantification method for ECGA, devoid of reciprocal influences in PWA, QRSA and TWA evaluation, on a HD patient, given the association of HD patients with SCD. Part of the aim was also to investigate the effects that HD may have on ECGA, in order to better understand if HD increases the risk of arrhythmias, comprehend if such risk mainly affects atrial or ventricular chambers and ultimately understand the relationship among PWA, QRSA and TWA.

A continuous 24-hour Holter recording performed on a HD patient was therefore processed and analyzed by means of the improved quantification method based on the popular HRAMF. The recording was then divided into four macro-time periods, in order to perform statistical analysis.

Results showed that, in several cases, TWA was the prevalent alternans, although also QRSA showed the highest amplitude values during and after HD. In fact, while TWA decreased after treatment, QRSA values seemed to increase. TWA decreasing trend, in accordance with findings in literature, suggests that HD treatment may be effective on cardiac electrical activity, rebalancing ionic concentrations in the body. Moreover, TWA being the prevalent alternans, together with QRSA increase, seems to point out that HD mainly affects ventricular electrical activity. As PWA values were particularly small and decreased to zero after treatment, atrial problems might be excluded.

Statistical analysis performed on PWA, QRSA and TWA for the different time periods as well as across the whole recording showed that there were statistical differences among the three types of alternans in almost all cases. In addition, PWA, QRSA and TWA poorly correlated with each other, showing that the improved ECGA quantification method may indeed independently measure PWA, QRSA and TWA, limiting reciprocal influences. Weak, but nonetheless not null correlations could be due to physiological phenomena, mainly ionic concentrations affecting cardiac APs and, as a consequence, ECG waves: changes physiologically happening at the level of one wave may in fact introduce changes at the level of the other ECG waves.

As this study was limited to a single HD patient, future studies on larger HD population, planned according to the availability of data, should be performed to further confirm and

generalize the findings of this thesis. Generalized results could contribute to the attainment of a more complete classification of SCD risk in subjects undergoing HD. As ECGA, seen as an expression of PWA, QRSA and TWA, gives a complete overview of electrical alternans happening at the level of the atria and/or ventricles, its analysis in HD patients may allow to promptly identify, locate and treat cardiac pathologies that could be a direct consequence of HD treatment.

REFERENCES

[1] Genovesi S, Boriani G, Covic A, Vernooij RWM, Combe C, Burlacu A, et al. Sudden cardiac death in dialysis patients: different causes and management strategies. Nephrol Dial Transplant (2019);1-10.

[2] Marcantoni I, Calabrese D, Chiriatti G, Melchionda R, Pampianco B, et al. Electrocardiographic Alternans: A new Approach. 15th MEDICON 2019, IFMBE Proc (2020);76:159-66.

[3] Saladin KS. Anatomia Umana. Piccin Nuova Libraria. 2011. Third edition.

[4] Stanfield CL. Principles of Human Physiology. Pearson. 2013. Fifth edition.

[5] Widmaier EP, Raff H, Strang KT. Vander's Human Physiology: The Mechanisms of Body Function. McGraw Hill. 2016. Fourteenth edition.

[6] Malmivuo J, Plonsey R. Bioelectromagnetism - Principles and Applications of Bioelectric and Biomagnetic Fields. Oxford University Press, New York. 1995.

[7] Klabunde RE. Cardiovascular Physiology Concepts. Wolters Kluwer / Lippincott, Williams & Wilkins. 2011. 2nd Edition.

[8] Waller AD. A demonstration on man of electromotive changes accompanying the heart's beat. J Physiol (1887);8:229-34.

[9] Einthoven W. Weiteres über das Elektrokardiogram. Pflüger Arch ges Physiol (1908);122:517-48.

[10] Wilson FN, Johnston FD, Macleod AG, Barker PS. Electrocardiograms that represent the potential variations of a single electrode. Am Heart J (1934);9:447-71.

[11] Goldberger E. The aVL, aVR, and aVF leads; A simplification of standard lead electrocardiography. Am Heart J (1942);24:378-96.

[12] Wilson FN, Johnston FD, Rosenbaum FF, Erlanger H, Kossmann CE, Hecht H, et al. The precordial electrocardiogram. Am Heart J (1944);27:19-85.

[13] Mason R, Likar L. A new system of multiple leads exercise electrocardiography. Am Heart J (1966);71(2):196-205.

[14] Merchant FM, Sayadi O, Moazzami K, Puppala D, Armoundas AA. T-wave Alternans as an Arrhythmic Risk Stratifier: State of the Art. Curr Cardiol Rep. (2014);15(9):1-18.

[15] Hering HE. Das Wesen des Herzalternans. Munchen. Med. Wchenshr (1908);4:1417–21.

[16] Verrier R, Klingenheben T, Malik M, El-Sherif N, Exner D, Hohnloser S, Ikeda T, et al. Microvolt T-wave alternans: physiological basis, methods of measurement, and clinical utility – consensus guideline by International society for Holter and Noninvasive Electrocardiography. J Am Coll Cardiol (2011); 58: 1309-24.

[17] Marcantoni I, Cerquetti V, Cotechini V, Lattanzi M, Sbrollini A, et al. T-Wave Alternans in Partial Epileptic Patients. Comput Cardiol (2018);45:1-4.

[18] Burattini L, Bini S, Burattini R. Repolarization alternans heterogeneity in healthy subjects and acute myocardial infarction patients. Med Eng Phys (2012);34(3):305-12.

[19] Burattini L, Man S, Swenne CA. The Power of Exercise-Induced T-wave Alternans to Predict Ventricular Arrhythmias in Patients with Implanted Cardiac Defibrillator. J Healthc Eng (2013);4(2):167-84.

[20] Marcantoni I, Vagni M, Agostinelli A, Sbrollini A, Morettini M, Burattini L, et al. T-Wave Alternans Identification in Direct Fetal Electrocardiography. Comput Cardiol (2017);44:1-4.

[21] Narayan S. T-wave alternans testing for ventricular arrhythmias. Prog Cardiovasc Dis (2008);51(2):118-27.

[22] Burattini L, Man S, Fioretti S, Di Nardo F, Swenne CA. Heart Rate-Dependent Hysteresis of T-Wave Alternans in Primary Prevention ICD Patients. Ann Noninvasive Electrocardiol (2016);21(5):460-9.

[23] Smith JM, Clancy EA, Valeri CR, Ruskin JN, Cohen RJ. Electrical alternans and cardiac electrical instability. Circulation (1988);77(1):110-21.

[24] Rosembaum DS, Jackson LE, Smith JM, Garan H, Ruskin JN, Cohen RJ. Electrical Alternans and Vulnerability to Ventricular Arrhythmias. N Engl J Med (1994);330:235-41.

[25] Bini S, Burattini L. Quantitative characterization of repolarization alternans in terms of amplitude and location: what information from different methods. Biomed Signal Process Control (2013);8:675-81.

[26] Nearing BD, Huang AH, Verrier RL. Dynamic tracking of cardiac vulnerability by complex demodulation of the T wave. Science (1991);252:437-40.

[27] Nearing BD, Verrier RL. Modified moving average analysis of T-wave alternans to predict ventricular fibrillation with high accuracy. J Appl Physiol (2002); 92(2):541-49.

[28] Martínez JP, Olmos S, Wagner G, Laguna P. Characterization of alternans during ischemia: time-course and spatial analysis. IEEE Transactions on Biomedical Engineering (2006); 53:701-11.

[29] Burattini L, Zareba W, Burattini R. Automatic detection of microvolt T-wave alternans in holter recordings: effect of baseline wandering. Biomed Signal Process Control (2006);1:162-8.

[30] Burattini L, Zareba W, Burattini R. Adaptive Match Filter Based Method for Time vs. Amplitude Characterization of Microvolt ECG T-Wave Alternans. Ann Biomed Eng (2008);36(9):1558-64.

[31] Burattini L, Ottaviano G, Di Nardo F, Fioretti S. Adaptive Match-Filtering: A Biomedical Application to Identify T-Wave Alternans. Natural Science (2014);6:709-18.

[32] Donato A, Oreto G, Schamroth L. P wave alternans. Am Heart J (1988);116(3):875-7.

[33] Lenis G, Pilia N, Oesterlein T, Luik A, Schmitt C, Dössel O. P wave detection and delineation in the ECG based on the phase free stationary wavelet transform and using intracardiac atrial electrograms as reference. Biomed Eng Biomed (2016);61(1):37-56.

[34] Tsiaousis G, Fragakis N. P-wave alternans in a patient with hyponatremia. Hellenic J Cardiol (2016);57(3):188-90.

[35] Siniorakis E, Arvanitakis S, Tzevelekos P, Giannakopoulos N, Limberi S. P-wave alternans predicting imminent atrial flutter. Cardiol J (2017);24(6):706-7.

[36] Pipitone S, Giudice G, Giuffrè M, Sperandeo V. Extreme Pulsus Alternans with P Wave Alternans in a Child. Pediatr Cardiol (2002);23:557-61.

[37] Maury P, Metzger J. Alternans in QRS amplitude during ventricular tachycardia. Pacing Clin Electrophysiol (2002);25:142-50.

[38] Christov I, Bortolan G, Simova I, Katova T. T Wave and QRS Complex Alternans During Standard Diagnostic Stress ECG Test. Comput Cardiol (2010);37:1039-42.

[39] Christov I, Bortolan G, Simova I, Katova T. T Wave and QRS Complex Alternans During Stress ECG Testing According to the Presence or Absence of Diabetes Mellitus. J Endocrinol Metab (2012);2(1):32-8.

[40] Jolliffe IT, Cadima J. Principal component analysis: a review and recent developments. Phil Trans R Soc A (2016);374:1-16.

[41] Suszko A, Nayyar S, Labos C, Nanthakumar K, Pinter A, Crystal E, at al. Microvolt QRS Alternans Without Microvolt T-Wave Alternans in Human Cardiomyopathy: A Novel Risk Marker of Late Ventricular Arrhythmias. J Am Heart Assoc (2020);9(17):1-15.

[42] Marcantoni I, Di Menna A, Rossini F, Turco F, Morettini M, et al. Electrocardiographic Alternans in Myocardial Bridge: A Case Report. Comput Cardiol (2020).

[43] El-Sherif N, Turitto G. Electrolyte disorders and arrhythmogenesis. Cardiol J (2011);18(3):233-45.

[44] Kestenbaum B, Rudser KD, Shlipak MG, Fried LF, Newman AB, Katz R, et al. Kidney Function, Electrocardiographic Findings, and Cardiovascular Events among Older Adults. Clin J Am Soc Nephrol (2007);2:501-8.

[45] Shafi S, Saleem M, Anjum R, Abdullah W, Shafi T. ECG Abnormalities in patients with Chronic Kidney Disease. J Ayub Med Coll Abbottabad (2017);29(1):61-4.

[46] Karmacharya P, Poudel DR, Pathak R, Rettew A, Alweis R. Acute hyperkalemia leading to flaccid paralysis: a review of hyperkalemic manifestations. J Community Hosp Intern Med Perspect (2015);5:1-4.

[47] Morrisey M. Willem J Kolff (1911-2009): physician, inventor and pioneer: father of artificial organs. J Med Biogr (2012);29:136-8.

[48] Friedman EA. Willem Johan "Pim" Kolff. Dial Transplant (2009);38:180-2.

[49] Kurkus J. Nils Alwall – one of the precursors of dialysis treatment. G Ital Nephrol (2018);35:38-43.

[50] Chisholm GD. The Scribner Arteriovenous Fistula for Haemodialysis. Br Med J (1961);2(5243):30-3.

[51] Quinton W, Dillard D, Scribner BH. Cannulation of blood vessels for prolonged hemodialysis. Trans Am Soc Artif Intern Organs (1960);10(6):104–13.

[52] Luyckx VA, Tonelli M, Stanifer JW. The global burden of kidney disease and the sustainable development goals. Bull World Health Organ (2018);96:414-22C.

[53] Cozzolino M, Mangano M, Stucchi A, Ciceri P, Conte F, et al. Cardiovascular disease in dialysis patients. Nephrol Dial Transplant (2018);33:iii28-34.

[54] Geberth S, Nowack R. Praxis der Dialyse. Springer. 2014.

[55] Polaschegg HD. Machines for Hemodialysis. Cardiovascular Disorders in Hemodialysis. Contrib Nephrol (2005);149:18-26.

[56] Locatelli F, Cavalli A, Manzoni C, Portoriero G. The Membrane Permeability Outcome study. Contrib Nephrol (2011);175:81-92.

[57] Cruz Andreoli MC, Totoli C. Peritoneal Dialysis. Rev Assoc Med Bras (2020);66(1):37-44.

[58] Astan R, Akpinar I, Karan A, Kacmaz F, Sokmen E, et al. The Effect of Hemodialysis on Electrocardiographic Parameters. Ann Noninvasive Electrocardiol (2015);20(3):253-7.

[59] Sun CY, Sung JM, Wang JD, Li CY, Kuo YT, et al. A comparison of the risk of congestive heart failure-related hospitalizations in patients receiving hemodialysis and peritoneal dialysis – A retrospective propensity score-matched study. PLOS ONE (2019);14(10):1-14.

[60] Ohnishi T, Kimachi M, Fukuma S, Akizawa T, Fukuhara S. Postdiaysis Hypokalemia and All-Cause Mortality in Patients Undergoing Maintenance Hemodialysis. Clin J Am Soc Nephrol (2019);14(6):873-81.

[61] Fuenmayor AJ, Vasquez CJ, Fuenmayor AM, Winterdaal DM, Rodriguez D. Hemodialysis changes the QRS amplitude in the electrocardiogram. Int J Cardiol (1993);41(2):141-5.

[62] Ojanen S, Kööbi Tiit, Korhonen P, Mustonen J, Pasternack A. QRS Amplitude and Volume Changes during Hemodialysis. Am J Nephrol (1999);19:423-7.

[63] Szabó Z, Kakuk G, Fülöp T, Mátyus J, Balla J, et al. Effects of haemodialysis on maximum P wave duration and P wave dispersion. Nephrol Dial Transplant (2002);17:1634-8.

[64] Tezcan UK, Amasyali B, Ilknur C, Aytemir K, Köse S, et al. Increased P wave dispersion and maximum P wave duration after hemodialysis. Ann Noninvasive Electrocardiol (2004);9(1):34-8.

[65] Madias JE. Increases in P-Wave Duration and Dispersion After Hemodialysis Are Totally (or Partially) Due to the Procedure-Induced Alleviation of the Body Fluid Overload: A Hypothesis with Strong Experimental Support. Ann Noninvasive Electrocardiol (2005);10(2):129-33.

[66] Drighil A, Madias JE, Yazidi A, Bennani M, Bennis A, et al. P-wave and QRS complex measurements in patients undergoing hemodialysis. J Electrocardiol (2008);41:60.e1-7.

[67] Jebali H, Ghabi H, Mami I, Fatma L, Smaoui W, et al. Evaluation of electrocardiographic findings before and after hemodialysis session. Saudi J Kidney Dis Transpl (2020);31(1):639-46.

[68] Friedman AN, Groh WJ, Das M. A pilot study in hemodialysis of an electrophysiological tool to measure sudden cardiac death risk. Clin Nephrol (2007);68(3):159-64.

[69] Miyaji K, Abe K, Abe K, Kondo N, Suzuki H, et al. Cardiac Pacing Suppressed Macroscopic T Wave Alternans in a Patient with Heart Failure Caused by Non-ischemic Cardiomyopathy. J Arrhythmia (2008);24(4):224-7.

[70] Andrade J, Aymong E, Tung S. Macrovolt T-Wave Alternans. Clin Cardiol (2008);33(2):E81.

[71] Kouidi EJ, Grekas DM, Deligiannis AP. Effects of Exercise Training on Noninvasive Cardiac Measures in Patients Undergoing Long-term Hemodialysis: A Randomized Controlled Trial. Am J Kidney Dis (2009);54(3):511-21.

[72] Patel RK, Mark PB, Halliday C, Steedman T, Dargie HJ, et al. Microvolt T-Wave Alternans in End-Stage Renal Disease Patients – Associations with Uremic Cardiomyopathy. Clin J Am Soc Nephrol (2011);6:519-27.

[73] Secemsky EA, Verrier RL, Cooke G, Ghossein C, Subacius H, et al. High prevalence of cardiac autonomic dysfunction and T-wave alternans in dialysis patients. Heart Rhythm (2011);8:592-8.

[74] Green D, Batchvarov V, Wijesekara C, Kalra P, Camm A. Dialysis-Dependent Changes in Ventricular Repolarization. PACE (2012);35:703-10.

[75] Simova II, Bortolan G, Kambova LG, Christov II, Katova TM. Episodes of T-Wave and QRS Complex Alternans in Haemodialysis Patients. EC Cardiology (2015);2(1):60-7.

[76] Kaplan RM, Herzog CA, Larive B, Subacius H, Nearing BD, et al. T-Wave Alternans, Heart Rate Turbulence, and Ventricular Ectopy in Standard versus Daily Hemodialysis: Results from the FHN Daily Trial. Ann Noninvasive Electrocardiol (2016);21(6):566-71.

[77] Leoni C, Marcantoni I, Sbrollini A, Morettini M, Burattini L. TWA Identifier for Cardiac Risk Self-Monitoring during Hemodialysis: A Case Report. IEEE ISCT (2019);143-6.

[78] Marcantoni I, Di Monte J, Leoni C, Mansour Z, Sbrollini A, et al. Electrocardiographic Alternans in Hemodialysis: A Case Report. GNB (2020);1-4.

[79] Burattini L, Zareba W, Burattini R. Assessment of physiological amplitude, duration, and magnitude of ECG T-wave alternans. Ann Noninvasive Electrocardiol (2009);14:366-74.

[80] Burattini L, Zareba W, Burattini R. Identification of gender-related normality regions for T-wave alternans. Ann Noninvasive Electrocardiol (2010);15:328-36.

[81] Qu Z, Xie Y, Garfinkel A, Weiss JN. T-wave alternans and arrhythmogenesis in cardiac diseases. Front Physiol (2010);1(154):1-15.

[82] Burattini L, Man S, Burattini R, Swenne CA. Comparison of Standard versus Orthogonal ECG Leads for T-Wave Alternans Identification. Ann Noninvasive Electrocardiol (2012);17:130-40.